NTNU

Norwegian University of
Science and Technology

Programmable Biopolymers for theranostic applications.

Haris Ud Din

Biotechnology

Submission date: June 2016

Supervisor: Berit Løkensgard Strand, IBT

Co-supervisor: Wilhelm Robert Glomm, IKP
Sulalit Bandhyopadhyay, IBT
Birgitte Hjelmeland McDonagh, IKP

Norwegian University of Science and Technology
Department of Biotechnology

Abstract

Biopolymers hold great potential in drug delivery and tissue engineering applications. Alginates, a natural polysaccharide derived from brown algae, possess unique properties in terms of gel formation and their interaction with biological systems. Their physical and chemical properties can be tuned for desired functionalities for applications ranging from food to medicine. Alginate based systems can be used for targeted drug delivery. Targeted drug delivery and release of drug at the diseased site has become increasingly important to have effective therapeutic effect and limited toxicity. Alginates can be incorporated within nanoparticles (NPs) to avail of the functions from both the counterparts – gelling properties from alginates and drug delivery and imaging applications from the multifunctional NPs. NPs are considered as an effective tool in nanomedicine due to their small size and unique optical properties. These multifunctional NP/alginate hybrids can be exploited to perform the desired theranostic function and revolutionize the field of medicine.

In this work, alginate gelation has been investigated in very dilute concentrations in the aqueous phase. $CaCl_2$ was used as cross linker to facilitate binding of alginate α-L-guluronic (G) blocks to form a three dimensional gel network, especially at higher concentrations of $CaCl_2$. Three different gelling architectures have been investigated after conducting a preliminary set of gelling experiments. These have been hypothesized as micro-aggregate, intermediate and gel phases respectively that show increasing fraction of gelled networks and are obtained with an increasing mole ratio of calcium ions to alginate. $CaCl_2$ was observed to be the dominant factor in gelation and incorporation studies of alginate.

With an attempt to understand the role of surface properties of NPs on alginate gelling, three different Fe@Au NPs were synthesized. Characteristic LSPR peak for Fe@Au NPs was obtained at 526 nm and with an average hydrodynamic size of 74 ± 2.7 nm. Successful coating of the NPs with PEG and Poly Lysine (PL) were confirmed by an increase in hydrodynamic sizes of Fe@Au_PEG and Fe@Au_PL to 96 ± 1.3 nm and 124 ± 4.2 nm respectively. Fe@Au and

Fe@Au_PEG NPs showed zeta potentials -45±0.8 mV and -26 ± 0.4 mV respectively, while Fe@Au_PL NPs were cationic with a zeta potential of and 27 ± 0.2 mV.

Interaction and binding of alginates with Fe@Au, Fe@Au_PEG, Fe@Au_PL was also studied. The physicochemical properties of these systems were mapped using UV-Vis spectroscopy, spectrofluorometry, viscometery, dynamic light scattering (DLS), zeta potential measurement & S(T)EM among other techniques. Higher concentration of the NPs led to higher incorporation inside the alginate networks. However, NP coating did not influence the gelation characteristics of the networks, and, thus, Fe@Au NPs was only used for the loading and release parts of the study.

Fluorescein sodium salt was used as a model dye both for supporting the hypothesized gel architectures, and for understanding loading and release from NP/alginate systems. Three methods were used to load the dye to the system. The difference between these methods relied on the relative order of forming dye-loaded NPs or alginates and incorporation of NPs into alginate networks.

Results have shown that Method 1, wherein, the dye was first loaded onto the Fe@Au NPs followed by incorporation of dye loaded NPs into the alginate networks, gave the highest loading and incorporation efficiency. Loading efficiency of the dye onto the Fe@Au NPs was 61 % whereas incorporation percentage of dye in the gel network was found to be 70 % for the gelling condition. Other loading methods also showed good loading and incorporation percentages significantly in gelling phase of alginate where dimerized G Block content are in excess. However, method 1 was chosen for carrying out further release experiments, since it gave highest loading for all the three different gelling architectures. Release of dye was investigated at laboratory conditions by simple diffusion method based on concentration gradient.

Consistent release was observed in gelling condition of 1 mg/ml Fe@Au dyed/alginate system with 27 % release of the dye after 20 hours. The release is estimated to be primarily diffusion-based. Other solutions show very abrupt release behavior which might be due to the measurement techniques used or due to the release setup used during the study. These NP-alginate systems have shown promising results for delivery of model dye, which could be further extended to study the release of specific drugs. Release can also be modulated using pH or temperature to combine diffusion with stimuli related response of these alginate-NP systems.

Acknowledgement:

First of all, I want to thank Almighty, for giving me strength and courage to pursue this work. I want to thank my supervisors Dr. Wilhelm. R. Glomm & Dr. Berit.L. Strand for their advice and continues support throughout the course of the project. You people truly shaped me by helping me developing my research skills and confidence in general.

Then I would like to say thanks to my co-supervisor Sulalit Bandhyopadhyay for his motivation, encouragement at all levels of the project. Whether it is experimental tasks or analysis of data he was there to help. He was the backbone of project who helped me shaping my research and report writing skills. He is the real gentleman and I have learnt a lot from him both professionally and personally.

I would like to say thanks to my friends in Trondheim for their support throughout my stay in this beautiful city. My stay was a memorable experience and I am going to cherish it for a long long time. Special thanks to Anuvansh Sharma and Awais Alvi for their support in this master project.

Also I want to thank my beautiful parents for their love and support. Ami and Abu. It's only because of you what I am today.

And last but not the least, a big thanks to my lovely Noor Fatima. Chaachoo loves you. Without you this world was a dark place. You light it up. Welcome!

Table of Contents

List of Figures:

1 Introduction:

With the aim to understand alginate based system and their applications, the introduction is outlined as follows. Firstly, biopolymers will be discussed with special focus on alginate. Thereafter nanomaterials and their properties leading to their end use will be outlined. Finally therapeutic applications of alginates and nanomaterials will be discussed in subsequent sections.

1.1 Polymers:

Polymers are large macromolecules which are built up of small units or monomers. They can be characterized by their type of chains, arrangements, shape and wide range of properties they possess[1]. In general, there are two main types of polymers based on how they are obtained; biopolymers and synthetic.

1.1.1 Synthetic Polymers:

The synthetic polymers are artificial polymers which are synthesized artificially using biomolecules present in nature. Both synthetic polymers & natural polymers are used in daily life. Plastics, teflon, epoxy polyesters are some synthetic polymers manufactured at industrial level. Polymers can be synthesized using monomers in the laboratory e.g. poly lactic acid (PLA) and fossil resources can also be used to synthesize polymers like polycaprolactone (PCL).

1.1.2 Biopolymers:

Biopolymers are polymers which are naturally occurring and produced by certain organisms [2]. Some naturally occurring biopolymers are cellulose, silk, wool, DNA etc. Biopolymers are different from synthesized polymers in their structure. Biopolymers of a specific type (protein) usually have well defined structures. In contrast, the synthetic polymers exhibit polydispersity and have random structures [3]. Polysaccharides hold special importance in drug delivery applications as they are highly biocompatible and most of them are hydrophilic in nature [4].

Polysaccharides are composed of monomeric units and naturally they have algal origin (e.g. alginates), plant origin (pectin), microbial origin (dextrin), and animal origin (e.g. chitosan).These biopolymers are usually stable, non-toxic, biodegradable and hydrophilic in nature.

Polysaccharides can be modified into its derivatives as they contain derivable carboxyl, hydroxyl and amino groups on their molecular chains [5]. Some of the common biopolymers are described below.

1.1.2.1 Starch:

Starch is the polysaccharide linked with glucose monomers by α (1, 4) linkages and found in plants It can be referred as house of the plant energy stored in them. Starch is available as linear amylose and branched amylopectin polymers as shown in Fig.1. Starch grafts can be used in biomedical engineering but they are not very strong on their own however they can be chemically engineered to increase their mechanical strength. Starch is biocompatible, contains natural D- glucose and it can be very important in tissue regenerative science due to its non-toxicity[6].

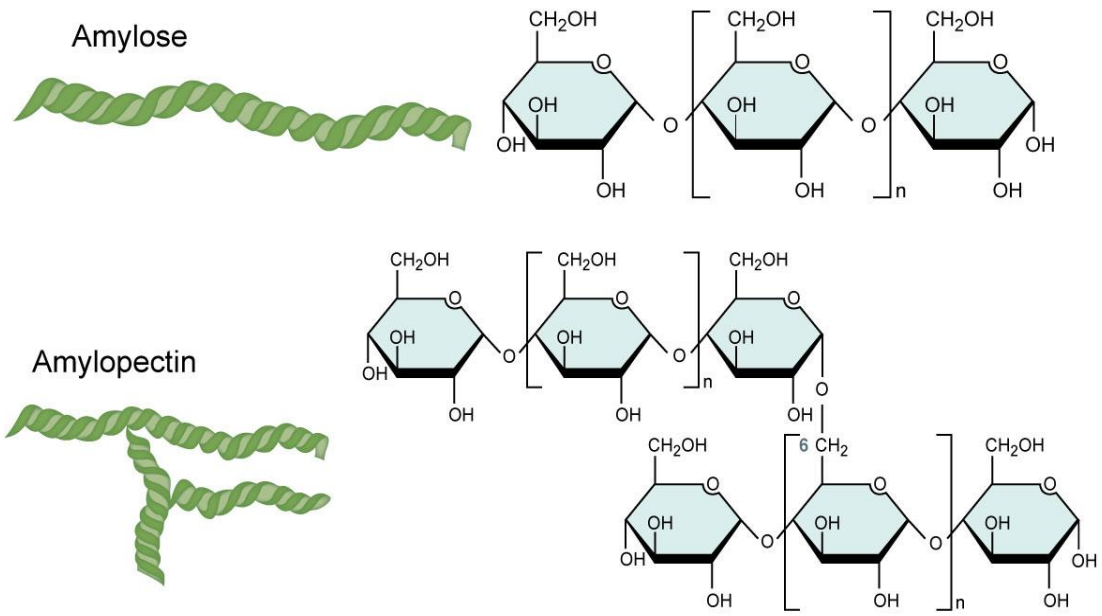

Figure 1: Structure of Starch. Amylose & Amylopectin[7].

1.1.2.2 Cellulose:

Cellulose is the most abundant naturally occurring polysaccharide consisting of many D-glucose β, 1-4 linked monomers forming a linear chain (Fig.2). It is found in cell walls of green plants and certain algae. Some bacteria also produce biofilms containing cellulose. Cellulose fibers are extensively used in the textile industry and exploited to form several useful products like manufacturing paper and textiles [8].

Biomaterials made from cellulose have been used in bioengineering techniques e.g. construction of membranes for hemodialysis, for biosensors by production of enzyme carriers, structuring the scaffolds for various tissue type regeneration applications. Although these applications are in use to some extent, but it has been investigated in most of the studies that cellulose based materials can provoke inflammatory and toxic responses [6].

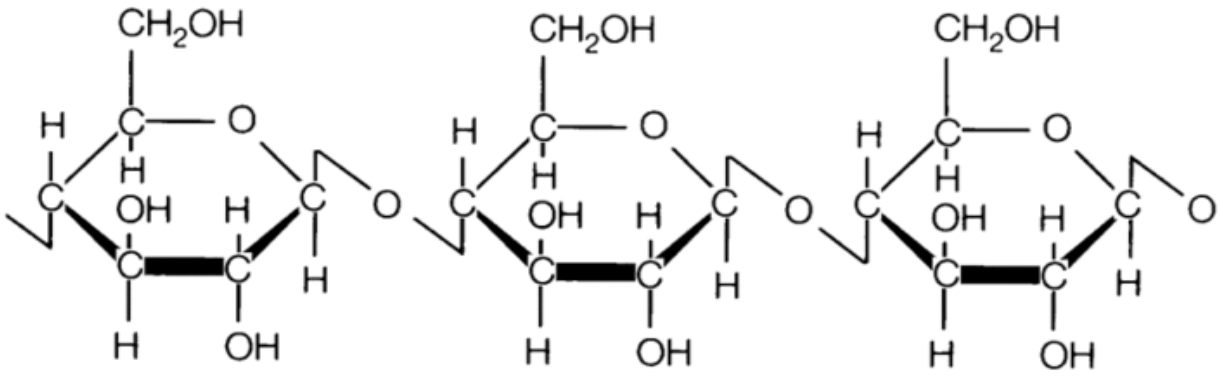

Figure 2: Structure of Cellulose[9].

1.1.2.3 Chitosan:

Chitosan is a linear polysaccharide containing units of D-glucosamine linked with β-1, 4-glycosidic linkages and unusually positioned N- acetyl-glucosamine units. Chitosan is actually derived from deacetylation of chitin. Chitin and chitosan are structural components of many crustaceans found in fresh water and open oceans [10]

Chitosan is a cationic polymer having the ability to bind with other negatively charged polymers e.g. alginates and have been used in biomedical applications. It usually forms mechanically strong gels in high pH and charge density is directly related to pH[11]. This property makes it a unique polymer to study in systems exploiting controlled release of drug [12].

Chitosan is a candidate of research in bioengineering and tissue regeneration of diseased tissues. It is water insoluble and does not easily biodegrade in its highly crystalline phase. Chitosan is relatively biocompatible and investigations have shown that they do not provoke immune responses like fibrous encapsulation,but may cause leukocyte infiltration in acute stage of implant induced infection [6].

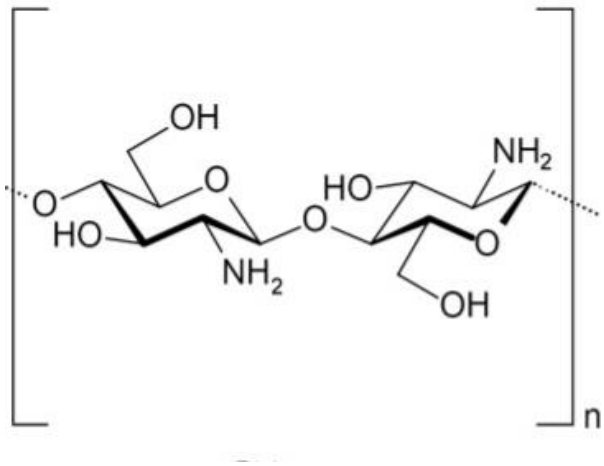

Figure 3: Structure of Chitosan[13].

1.1.2.4 Alginates:

Alginates are water soluble biopolymers composed of alternating sequences of α-L-guluronic(G block) and β-D-mannuronic acid (M block) polysaccharides which are linear and unbranched. They are naturally occurring water soluble polysaccharides obtained from brown seaweed and possess wide range of applications in biomedical engineering due to their biodegradability, and gelling properties in presence of divalent cations e.g. Ca^{2+} [14].

Alginates have been extensively used primarily as food additives but their potential in drug delivery and tissue engineering has made them important candidates for research due to their lack of toxicity and biocompatibility. In recent years, the synthesis of tunable alginates has gained huge interest in research community[15].As alginates are one of the main component of this study, detailed description of their properties and applications will be outlined in the subsequent sections.

1.1.3 Physicochemical Properties of Alginates:

1.1.3.1 Structure of Alginates:

The structure of alginates and their properties are widely studied in biomedicine. Alginates are anionic polysaccharides which are obtained from Brown algae e.g. *Laminaria hyperborea* and they are found in marine waters. It was Stanford who first characterized algic acid and extracted it with sodium carbonate and then at low pH alginate precipitated. The arrangement of G block, M block and alternating regions is variable within the structure of alginate and depends on the source. A diamond home shape will be formed[16] when two G blocks are aligned side by side which is a unique property employed in gelling of polymers. The blocks can be either similar or alternating (e.g. MMMMMM GGGGGG GMGMGM). Such arrangements, length and molecular weights give information of their behavior when they are used in nanostructures and also reveal other physical properties like size, charge and so on.[17] [18]. Alginate properties greatly influence the resulting gel form with the addition of divalent cations.

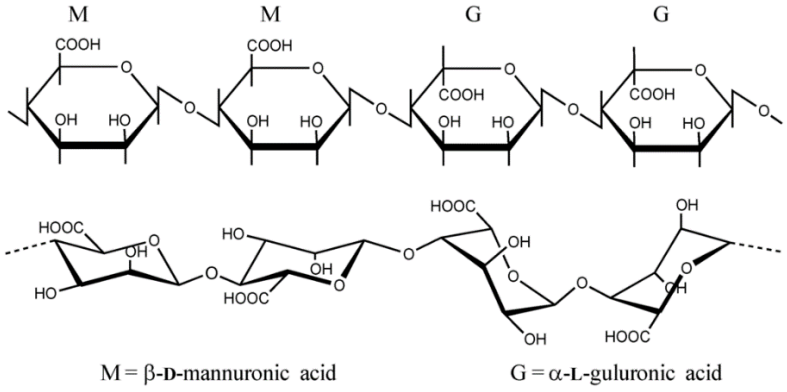

Figure 4 Structural conformations of Alginate: M- blocks & G-blocks [18]

1.1.3.2 Gelling of Alginates:

Alginates are used as hydrogels for biomedical applications like wound healing, drug delivery and tissue engineering [15]. Hydrogels are considered to be biocompatible as they are similar to the macromolecules of the human body. Hydrogels are three dimensional cross linked networks composed of hydrophilic polymers with high water content. By cross-linking these polymers chemically or physically we can perform gelling of alginates and physico-chemical properties of such hydrogels are highly dependent on cross- link type. [19].

1.1.3.2.1 Cross linking through ions:

In order to form hydrogels, divalent cations such as Ca^{2+} are used as cross linking agents in aqueous alginate solution. These ions only bind to the G-blocks of the alginate polymers which in turn bind to the adjacent G block of the polymer resulting in gelling of the alginate. This process is termed as egg box model of cross linking [20].On the other hand, M- blocks give relatively fragile gels due to their flatter structure[21].

Calcium chloride is the commonly used agent to cross link alginates, but, due to its high solubility in solutions, fast and poorly controlled gelation occurs. To perform slow and more controlled gelation of alginates, a buffer containing phosphate can be used. The phosphate group in buffer (sodium hexa-metaphosphate) competes with the carboxylate group of polymer cross linked with calcium ions resulting in gelation [22].

1.1.3.2.2 Gelation through heat

Thermo sensitive hydrogels are immensely studied for drug delivery applications. Swelling properties can be tuned by applying heat to the system which is important in controlling release of drug from hydrogels [23]. Alginates are not naturally thermo-sensitive but there are few systems which are being used by researchers to study gelation by using heat. PNIPAm is a highly exploited stimuli responsive hydrogel and gelation in PNIPAm can be controlled by heat [24].

In a study, Calcium ions loaded lipid vesicles have been used to release ions into the fluid suspension of sodium alginate. The liposomes were used to prevent the alginate gelation by separating intra-vesicular calcium ions from extra vesicular sodium alginate. Increasing the temperature of the fluid liposome and alginate mixture to 37^{o}C resulted in release of calcium ions forming alginate gels. Gelation time at body temperature was found to be dependent on the liposome to alginate ratio[25].

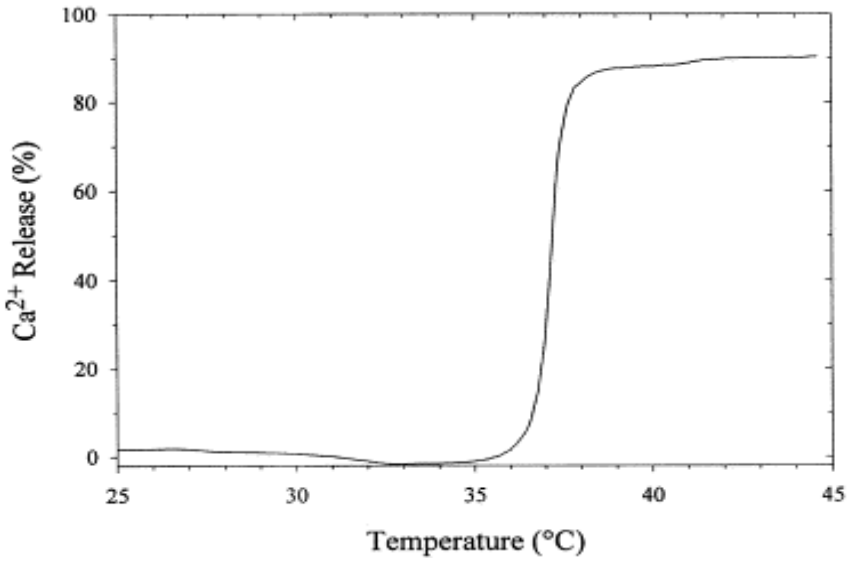

Figure 5: Heat triggered release of calcium ions from liposomes[26].

1.1.3.2.3 Covalent cross linking:

In order to improve the physical properties of hydrogels, covalent cross linking in gels has been widely investigated. Pressure is applied on cross linked alginate gels which are ionically linked causing cross links to dissociate. This removes water from the gel resulting in plastic deformation. Covalent cross linking of alginates with PEG (polyethylene glycol) having different molecular weights has been studied to prepare gels with greater mechanical integrity. PEG is widely used as cross linker to study the properties of hydrogels. It is very favorable to use multi-functional cross linking molecules than bi functional cross linkers in order to improve mechanical strength and improved control over degradation rates of the polymer [27].

1.1.3.2.4 Cross linking through light:

There is very exciting new approach for cross linking gels *in situ* by using light in mild reaction conditions. Researchers have developed techniques to gel alginate by introducing U.V light and lasers. In a study, alginate gels were formed by mixing alginate with calcium carbonate which serves as calcium ion source. In this system, a photo-acid generator (PAG) was photolyzed using ultra violet radiations to release the calcium ions to cause alginate gelation. It was found that gel formation time was inversely related to the intensity of U.V radiations[28].

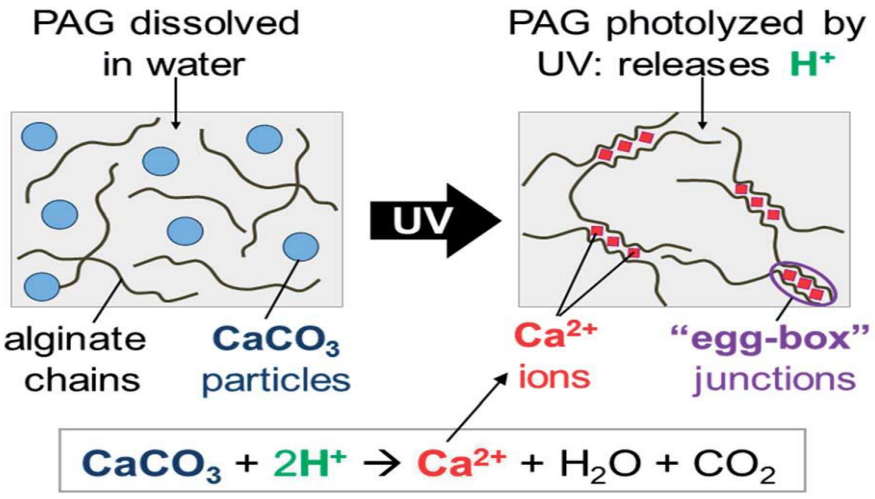

Figure 6: U.V induced ionic cross linked gelation of alginate[28].

1.1.3.3 Solubility of Alginates in water:

The size and type of particles of alginate powder greatly influence the solubility of alginates in water. Upon hydration, alginate particles become sticky which results in formation of aggregates. Depending on the type of alginate powder in use, fine and coarse particles affect solubility rates. Even though alginate dissolution in water is slow, but use of coarse particles is better because they disperse in water and do not form clumps. Fine particles have good solubility but they stick to each

other more readily in water. It is desirable to add alginate slowly and stir the water forcibly on adding the alginate for better mixture[29]. In higher concentrations of alginate, it passes through various phases from viscous fluid to solid paste and then it becomes increasingly difficult to disperse more alginate into the solution [30].

It becomes tricky to dissolve alginates in water when water contains chemicals that compete for water needed to hydrate the alginate. Salts, sugars, proteins or other substances like alcohols and proteins present in water will increase the time required to dissolve alginate. These compounds can be added afterwards when alginate dissolves completely in water, if desired [14, 30].

1.1.3.4 Modifications of Alginates:

Alginates can be modified for many applications due to their gelling and encapsulation properties. There are many studies in which researchers have chemically modified alginates for drug delivery applications[31]. Alginate modification is done in order to understand drug loading and release models. In a study, octylamine was used to modify alginate to increase hydrophobicity and drug release studies were carried out by comparing release from unmodified alginates [32]. Modified alginate NPs have also been investigated as carriers of various drugs like rifampicin, isoniazid and so on [33].

Alginate modification has also proved to be helpful in diagnosis. In this context, researchers have modified alginate/chitosan hybrid NP systems in order to detect cancerous cells in the body assisting in endoscopy. Cancerous cells show upregulation in folic acid receptors and researchers have used 5-aminolevulinic acid which is recognized by folic acid receptors. To detect the cancerous cells, alginate NPs containing fluorescent dye were modified with 5-aminolevulinic acid to recognize overexpressed folic acid receptors on cancerous cells [34]. Arginylglycylaspartic acid (RGD) modified alginate has been used for cellular delivery in different type of cells like endothelial and mesenchymal stem cells[35],[36]. Certain growth and bio active molecules can be incorporated in alginate gels e.g. VEGF (Vascular endothelial growth factor) loaded in alginate gel can promote angiogenesis (formation of blood vessels) in engineered tissues[37].

1.1.3.5 Biocompatibility:

Biocompatibility is the most used term in biomaterial science and it is defined as the ability of a material to perform with an appropriate host response in a specific application [38]. Alginate's biocompatibility has been studied to demonstrate the potential immune responses against the implanted alginate hydrogel. Alginate is usually biocompatible and it has been found that purification of alginate during its extraction is a necessary step to reduce the chances of any impurity to cause adverse effects in host. Potential impurities can be in the form of any heavy metals or toxins which can contaminate alginates. Bacterial and fungal growth in alginates can be possible because of impurities present in commercial alginates[39].Contaminants like nitrogen and phosphorus may support bacterial growth in alginates although they are present in very small amounts. Microorganism's contamination results in loss of viscosity and may cause depolymerization. It can be very disadvantageous for alginate based products. Hence preservatives like sorbic acid, benzoic acid or methyl esters etc. can be added to preserve the alginates[30]. It has also been found that high M-alginates may provoke innate immunity through CD14 and TLR (Toll like receptors)[40].

There is no evident antibody response in animals against the purified G-beads. Raw M- and G-alginates may contain impurities but the difference in their impurity content with respect to their composition must be taken into consideration [41].

1.1.4 Applications of alginates in Biomedicine:

1.1.4.1 Drug Delivery Applications:

Alginate is the most common natural polymer which is extensively used in biomedicine mostly due to its gelation property. In recent years, researchers have shown greater interest to exploit alginates for theranostic applications[15].

1.1.4.1.1 Biomolecules and drug delivery:

Alginate beads are in use for controlled release studies. Biomolecules, such as proteins to be delivered are encapsulated in alginate beads. These are released from the system either by inherent porosity of alginate or by the degradation of the gel network. The size of these pores determines the release of specific proteins from the network. Pore size ranges from 5nm to 200 nm[42]. Charge is also important as positively charged proteins can interfere with the calcium ions to bind with the carboxylic acid groups of the alginate gel. Hence additives like Poly-acrylic acid can be added to protect the polymer network from collapsing. Flexibility of such networks is also important. It has been observed that flexibility of the alginate matrices is associated with higher release rates of proteins [43].

In order to get efficient encapsulation of the proteins, gelling conditions, pore sizes, water content and flexibility of alginates beads need to be tuned for controlled release. There are studies in which alginates have also been used to encapsulate and deliver DNA molecules in gene therapy [43].

1.1.4.1.2 Formulations of small drugs delivery:

Alginate gels have porous structure at nanoscale (5nm), hence, small drugs can diffuse out. Partially oxidized gels have been in use to make formulations for localized administration. Alginate gels are now employed to treat acid indigestion and inflammation of oesophagus. The alginates provide foamy cushions which act as barriers against the stomach acids.

In a recent study, a preparation of sodium alginate combined with calcium has been developed to counter the *Helicobacter pylori* which is bacterium responsible for causing ulcers in stomach. Alginate with loaded formulation to fight against bacterium. On reaching the infected area, itspreads itself in stomach wall. Gel forms,which keeps stomach wall protected from being more ulcerated and drug is released to fight the bacterium present in the stomach [15] [44].

1.1.4.2 Regeneration of tissues/Organs:

Alginates can be employed in many tissue regenerating strategies. Alginates can be modified according to the function it will perform *in vivo*[17].

1.1.4.2.1 Vascularization:

Engineering new blood vessels is very important in tissue engineering in order to transport nutrients and oxygen to the implanted tissues. Alginate hydrogels have a great role in delivering growth factors and active molecules to the newly engineered tissues and it has been an active field of research in tissue engineering in recent years [45] .

VEGF (vascular endothelial growth factor) is an angiogenesis promoting factor which must be delivered to the tissues to grow new blood vessels. VEGF can be incorporated in alginate hydrogels and it diffuses out of the gel by mechanical methods. It has been seen that VEGF delivery with an alginate hydrogel has greater activity in vascularizing tissues than the delivery of VEGF without a hydrogel. Such delivery of active biomolecules needs to be targeted precisely to prevent VEGF from inducing angiogenesis in non-targeted cells [37].

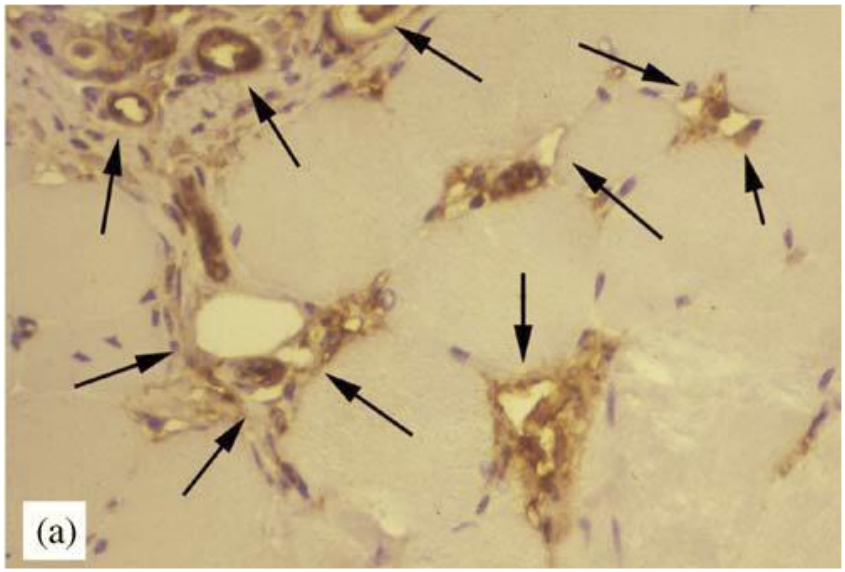

Figure 7: VEGF release from alginate scaffolds resulting in angiogenesis. Alginate is mechanically stimulated. Arrows showing vascularization in muscle tissue around implanted gel [37].

1.1.4.2.2 Cartilage & Bone repairing:

With advancement in tissue engineering, cartilage and bone regeneration have also gained interest among researchers. Peptides (RGD) linked with alginates have a good influence to adhere to the chondrocytes. Such an implant in mice have shown promising results to engineer cartilage *in vivo* [46]. For bone regeneration, alginate has been under investigation for delivery of many osteogenic growth factors in mice *in vivo*. But it has been found that alginate has low mechanical properties to withstand bone regeneration and a higher control of alginate gel degradation in desirable to produce restriction free bone regeneration. Various studies have shown promising results in mice but need to be replicated in human as well which can be the way forward in osteogenesis [14].

In a recent study, chondrocytes suspension were used in an alginate solution and calcium sulphate. The chondrocytes obtained from a donor rabbit were allowed to grow in the alginate solution and then calcium sulphate was added. The resultant mixture was introduced into the defective part of the cartilage to check the regenerative activity. The cartilage repairing using alginate in chondrocytes suspensions proved to be promising in experimental animals, but its efficiency must be evaluated in higher animals having the same joints/cartilage makeup as humans [47].

1.1.4.3 Dressings for wound healing:

Alginate dressings are made by reacting calcium with alginic acid salts. They occur in the form of porous sheets which are frozen and dried. They are also used as flexible fibers in wound healing. Alginate dressings can be used to moderate severe oozing wounds by making strong protective hydrophilic film which prevents the wound secretions and also limits the pathogenic contamination. These calcium alginate dressings are biodegradable and can be rinsed away after use by saline solution. [48].

1.1.4.4 Cell encapsulation & cell culture:

Due to the biocompatibility of alginates with host and also with the bodily cells, cell encapsulation is widely used in tissue engineering. Cells are encapsulated in the alginate capsules and transported to the sites inside the body to check bioactivity. Mouse 3T3 fibroblast and Human embryonic kidney cell lines (HEK293) have been shown to encapsulate in alginate beads (Fig.8) [49].Mechanical integrity and flexibility of alginates in cell encapsulation studies is important to ensure prolonged delivery. Engineering such alginate beads protects the encapsulated cell from host immune responses and delivers the desired biomolecules to the targeted area [50].

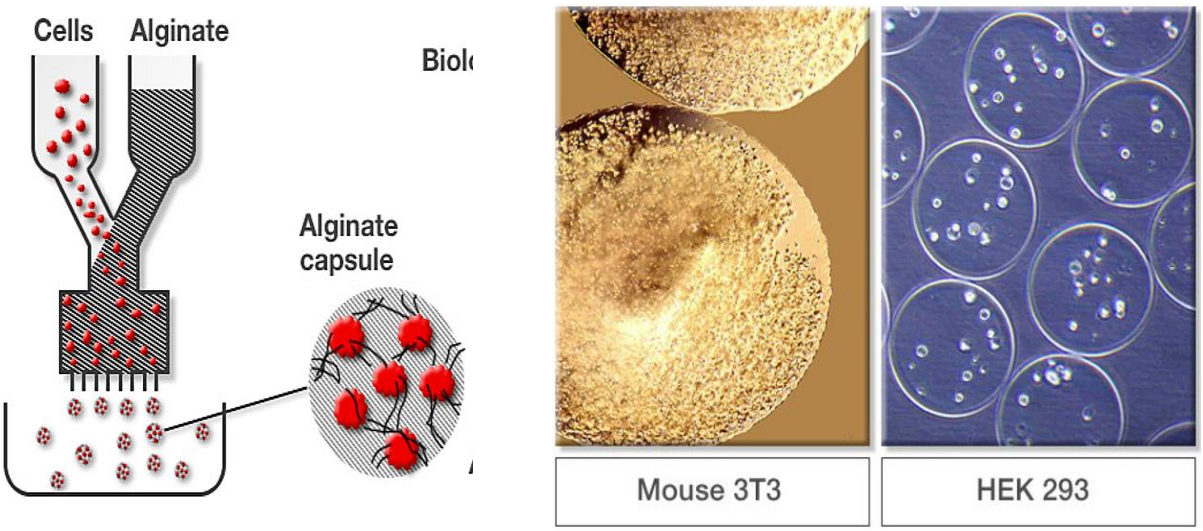

Figure 8: Cell encapsulation: Mouse 3T3 fibroblast cell line and Human Embryonic Kidney (HEK293) cell lines encapsulated in alginate beads[49].

1.2 Nanomaterials:

Nanotechnology is the emerging science which deals with the production, functionalization and designing structures or systems at nano-meter scale. There are many benefits in use of nano-materials in many different fields, but use of nanoparticles (NPs) for diagnosing & treating vital

diseases like Hepatitis, cardiovascular disease, cancer or Parkinson's disease is very promising. Drug delivery, imaging, tissue regeneration are few exciting interest topics among researchers. One of the most commonly used NPs among research community is gold NPs [51].

The current research focuses on manufacturing new formulations to increase the understanding of diagnostics and treatment of viral diseases. There are many nano-based drugs which are already in the market and others are in the pipeline (Fig.9) [52].

There are many advantages of nano-approaches in medicine. Conventional medicine uses bulk material having larger molecules with high dosage and less probability to reach the diseased part of the body and thereby, have higher rates of possible adverse effects. But on the other hand, nano drugs having small size with required drug dosage, overcome physiological barriers and target the diseased site with precision without affecting healthy cells. [53].

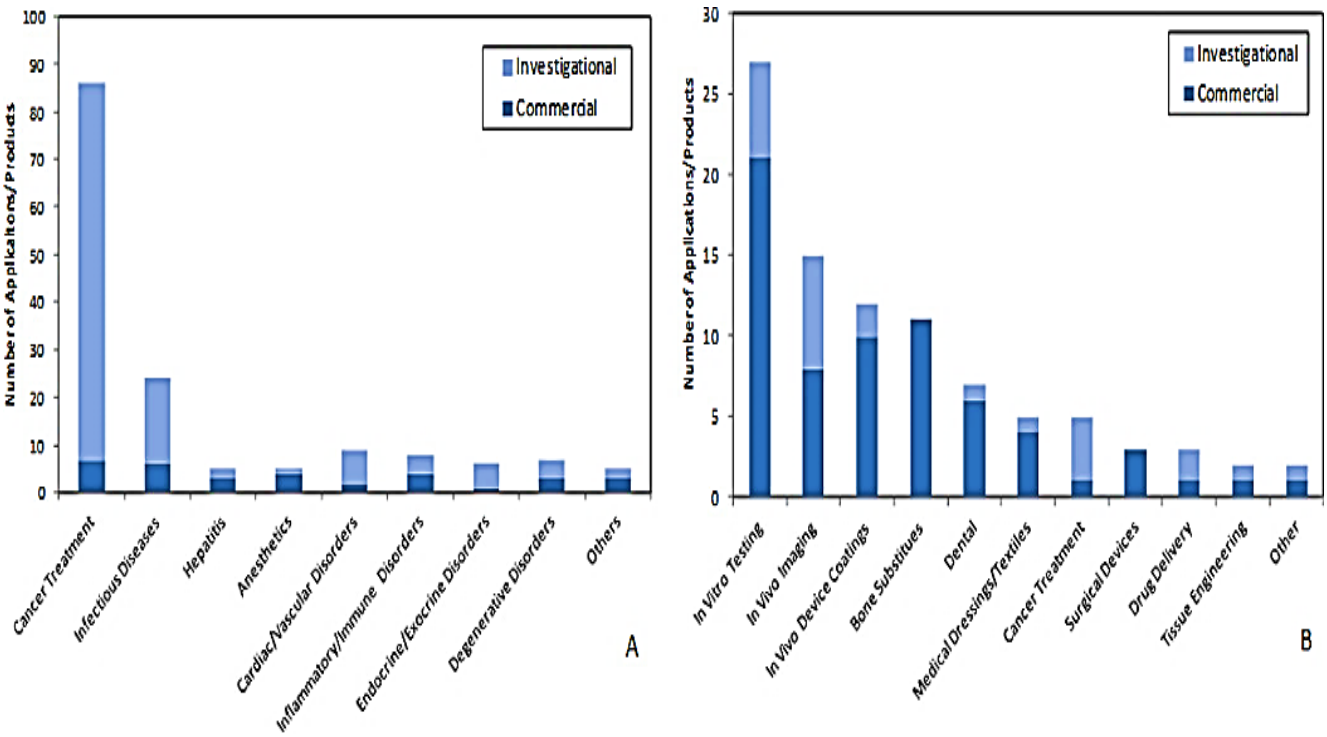

Figure 9:A: Commercial and investigational Nano drugs (Diagnostic and therapeutic) and (B) nano based devices.[54].

1.2.1 Nanoparticles (NPs):

NPs are defined as particles which range from 1 nanometer (nm) to 100 nm in three dimensions. Such small size is very important from a reactivity viewpoint since these have higher surface area to volume ratios, compared to materials having larger sizes [55]. Due to their smaller size, quantum effect comes into play [56].

Nanomedicine is considered to be the future of medical science. Many of the physiological processes of the body occurs at the nano scale; e.g. haemoglobin, an iron carrier protein in the red blood cells have a diameter of 5 nm [57]. Nano based drugs have been found to be helpful in treating and diagnosing diseases utilizing their small size and inert nature. There have been very exciting studies in where NPs are used as theranostic agents. One such innovative example is Bio barcode assay, developed by exploiting gold NPs to detect prostate specific antigens in the blood stream. It is a sensitive method and can detect samples of low molecular weights [58].

In another study. scientists have found a way to clear clots inside the blood vessels, which is a major cause of heart attack and stroke. They have developed shear-activated nano-therapeutics (SA-NTs) which carries drug to the clot and clears it within a short span of time, as shown in (Fig.10).The major advantage of such therapy is to reduce effective dose required to clear clot by conventional methods [59].

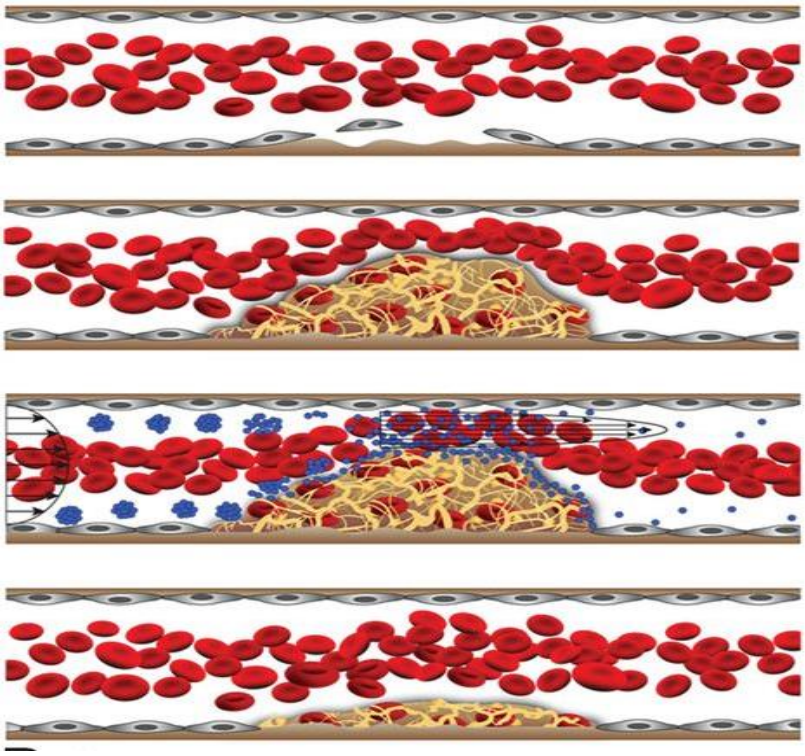

Figure 10: Scheme of SA-NTs (shown in Blue) targeting clot in blood vessel [59].

Over the last few years, researchers have faced many challenges in exploiting drug delivery systems. Internalization of such systems inside the cell and how to make it escape from the endosomal activity is certainly an issue. But scientists are trying to overcome this challenge of nano-bio interface by using different methods. It has been found in a study that modification of gold NPs by a 'RME peptide' (receptor mediated endocytosis) actually helps NPs escape from the endosome. Such modifications of NP systems have great potential in bio-imaging and drug delivery applications[60].

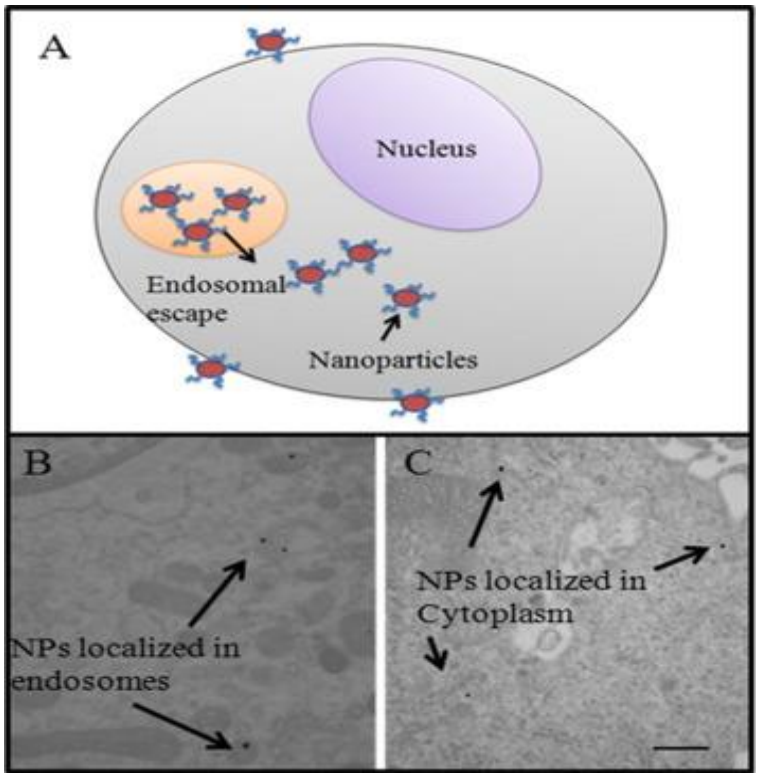

Figure 11: Schematic diagram showing Peptide coated gold NPs escaping endosome[60].

1.2.2 Properties of NPs:

NP properties can be tuned to use them for different applications like drug delivery and bio-imaging. Polymeric and inorganic NPs are the major classes of NPs based on their composition. NPs can be functionalized with a range of therapeutic and diagnostic (theranostics) agents depending upon the function. Their optical and magnetic properties are important to control and hence effect the delivery of the nano-carriers to the target. There are many multifunctional NPs which can be produced, possessing targeting and bio-imaging functionalities [61].

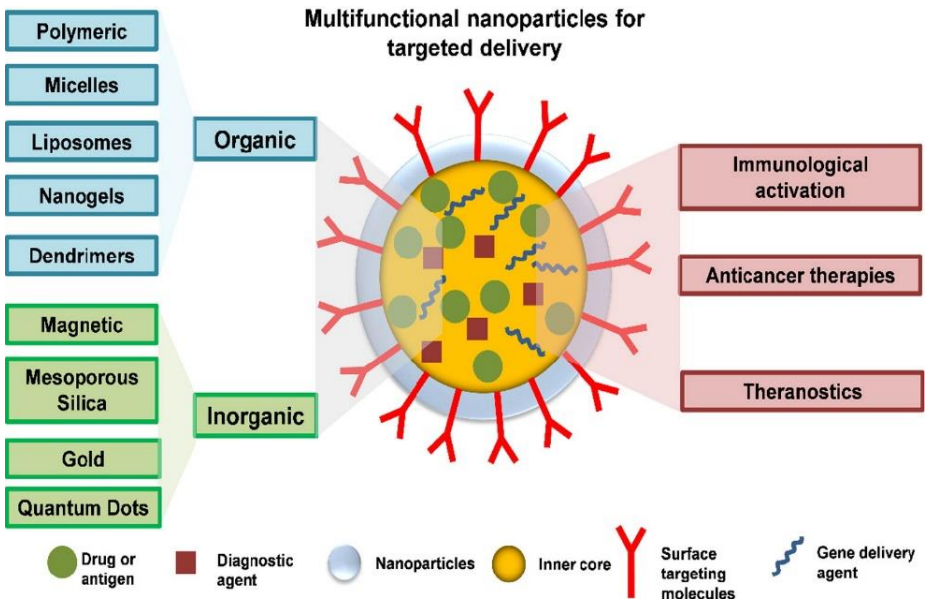

Figure 12: Multifunctional NP for biomedical applications [61].

1.2.2.1 Localized surface Plasmon Resonance (LSPR):

Optical properties of metallic NPs can be exploited for several biomedical applications like diagnostic imaging, bio-sensing and targeted therapies. Plasmonic NPs are different from other nano-based biomaterials because these NPs shows unique surface plasmon resonance (SPR) which can be employed in many biological applications [62].

LSPR is an optical phenomenon widely seen in metallic NPs like gold, silver and so on. When an incoming electromagnetic wave is incident upon a metallic surface, the free electrons of the metal are set into resonance when the incoming wave's frequency matches the frequency of oscillation of the electrons. This phenomenon is called SPR and for nanoparticles, this is confined to a small space, hence the term localized SPR. The position of the LSPR band depends on the size, shape of the NPs and the properties of the medium[63]. Au and Ag NPs exhibit LSPR in the visible region of the spectrum. It has been found that Ag shows the sharpest bands of LSPR oscillations but due to chemical inertness Au is preferred to be applicable in many biomedical applications like bio-sensing, imaging and nano-therapeutics[64]. Spherical Au NPs exhibit LSPR at 520nm in the visible spectra of light[65]. It is an important optical property of gold NPs. They can be used in

many biomedical applications due to their versatility in diagnosing, imaging and treating vital diseases like Parkinson's disease or cancer[66].

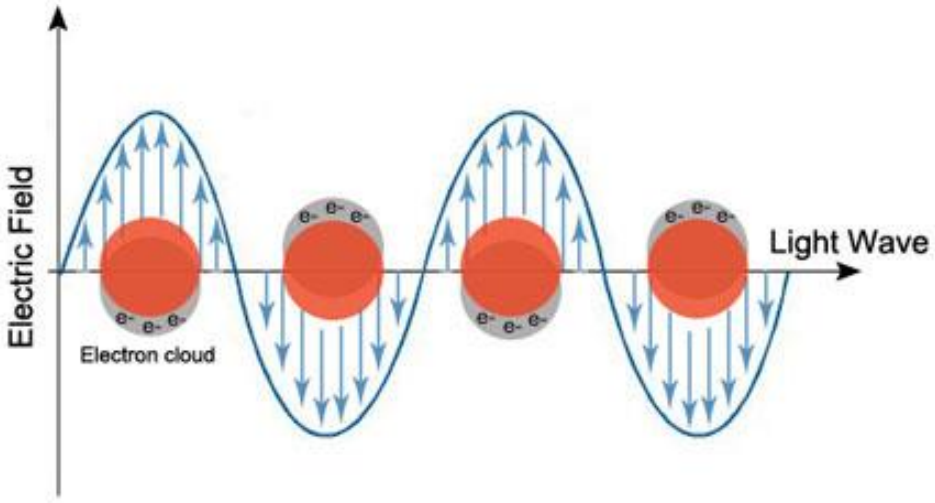

Figure 13: LSPR: Oscillations of Gold NPs surface electrons due to incident light wave[67].

Gold NPs can be conjugated directly via bonding with the active molecules and can carry low amount of drug to the target site which is desirable to decrease the dose related side effects. For example, in a study, methotrexate (MTX) binding with gold NPs was investigated. MTX is an analogue of folic acid and a cytotoxic anti-tumor drug. The system was incubated overnight after mixing the drug with the particles. MTX-AuNP mixture were introduced in tumor cell lines. It was found out that drug conjugated with gold NPs has seven times more cytotoxic efficacy than the methotrexate alone [68].

Surface chemistry of gold NPs surface chemistry is important for their applications in drug delivery and imaging. Attaching desired targeting ligands or drug conjugates is done by modifying the surface of gold NPs. Biomimetic modification of particle surfaces is also a prerequisite for biocompatibility and hence it can be achieved by biodegradable and biocompatible polymers. PEG coated gold NPs for tumor targeting is one example.[69].

1.2.2.2 Fluorescence quenching & Enhancement by gold NPs:

In recent years, gold NPs have attracted researchers due to their unique properties. When any fluorescent molecule is placed in close proximity of gold NPs, quenching and/or enhancement of fluorescence intensity takes place[70].Energy transfer by/to gold is dependent on shape, size, coating, and distance from fluorescent molecule and wavelength of incident & emitting light. This phenomenon is called resonant energy transfer (RET) [71, 72].

1.2.2.3 Superparamagnetism:

When external magnetic field is applied, the collective magnetic dipoles of all the atoms align in a single preferable direction. This can be referred as uniaxial anisotropy of the NPs along single axis [73]. Upon removal of magnetic field, high thermal energy randomly flips the direction of magnetization of NPs. This is the paramagnetic effect. Whereas in super paramagnetism, magnetic effect is observed in which all the spins co-linearize to each other as shown in Fig 14. But thermal energy is not enough to keep them magnetized in the same direction. Hence the material shows superparamagnetism with constant change in their spins. In superparamagnetism, the magnetic susceptibility of NPs is much larger than that of a paramagnetic effect under applied magnetic field. In normal conditions, any ferromagnetic material can act as paramagnetic at a certain temperature that is higher than the Curie temperature. In superparamagnetism, the transition from paramagnetic to supermagnetic phase happens below the Curie temperature[74],[75].

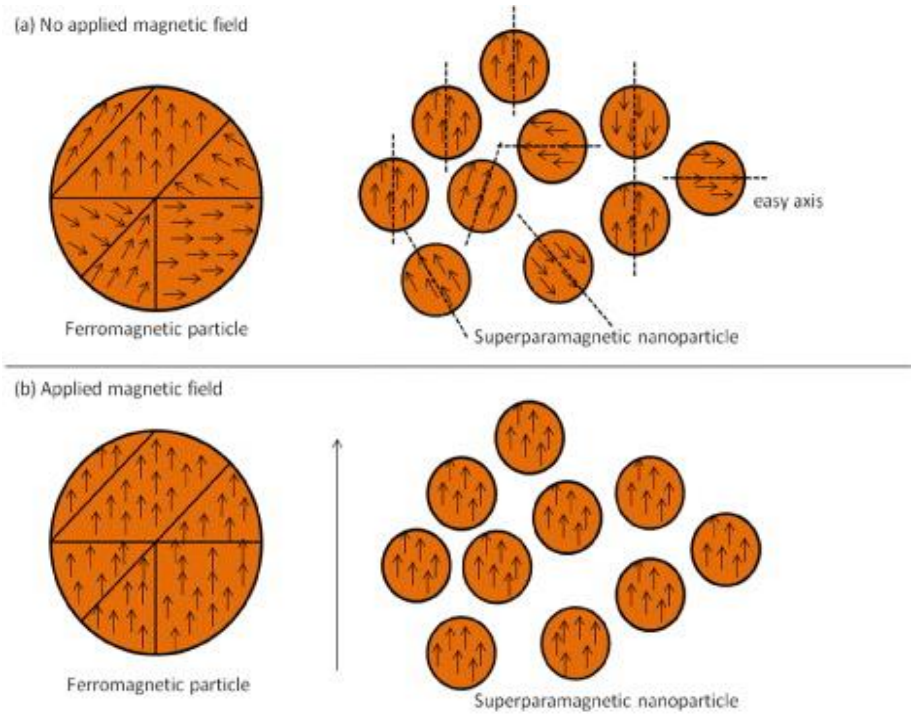

Figure 14: Supermagnetism in ferromagnetic NPs[74].

1.3 NPs based on composition:

1.3.1 Inorganic NPs:

Inorganic NPs have gained immense attention of researchers due to their synthesis and modification attributes for imaging and targeted therapies. Multifunctional inorganic NPs can be modified depending on type of function they are going to perform [76]. Following are some methods to synthesize inorganic NPs.

1.3.1.1 Synthesis of Inorganic NPs:

There are different strategies to synthesize inorganic NPs depending on the end use of the particles[77]. Solution based synthesis, sol-gel method, micro-emulsions, electro-templating, microwave based synthesis are some synthesis methods described here.

1.3.1.1.1 Solution based synthetic route:

The synthesis of inorganic NPs is done in solutions by the reduction of metal precursor. Commonly used metal precursors are composed of inorganic salts and metal complexes like $HAuCl_4$, Ni, Ag, Fe etc. In order to generate the respective NPs from these compounds, reducing agents like sodium hydroxide, tri sodium citrate, sodium borohydride, sodium carbonate are used. [78].

The strength of reducing agents has important role in controlling particle size and reaction rates. Smaller size of resulting NPs is directly proportional to the strength of reducing agent. Stronger the reducing agent's reduction ability, higher will be the supersaturation which results in great number of small nuclei[79].

Agglomeration of the resulting NPs is the common problem in solution based synthesis. In several situations, an organic capping substance is used to prevent these particles from agglomerating with each other. In some cases, these organic capping materials can also be used as reducing agents. [80].Steric stabilization is provided by using stabilizing agents in order to stabilize them. Consequently, a steric repulsion is created which is between the capping molecules absorbed on the approaching particles which keeps them apart[81].

Polymers are mostly used as stabilizers. Common stabilizing agents are sodium polyacrylate or polyvinyle ethers [82]. Stabilization is highly dependent on type of polymer used, aqueous conditions, surface charge of NPs and temperature[79]. Polymer binding with the surface of NPs has added advantage of encapsulating biologically active molecules which shows the versatility of these systems in biomedical applications. [79].

1.3.1.1.2 Sol-Gel:

Sol gel method is commonly used in order to synthesize metal oxide NPs. This method consists of hydrolysis and condensation of metal precursors like metal alkoxides. Continued condensation and polymerization results in a gel having 3D metal oxide network. This method can be employed in aqueous media where oxygen is provided by the water molecules, whereas, in non-aqueous media water is provided by the organic solvents in use for example, ethers or aldehydes.[77]. Fig. 15 shows the detailed scheme of the method.

To obtain small particles, hydrolysis is done in a slow and controlled manner[83].NPs are extracted by drying the gel by removing the solvent. Hydrolysis and condensation can be continued to form ceramic materials if desired[84].Precipitation can also be done to form ceramic powders.

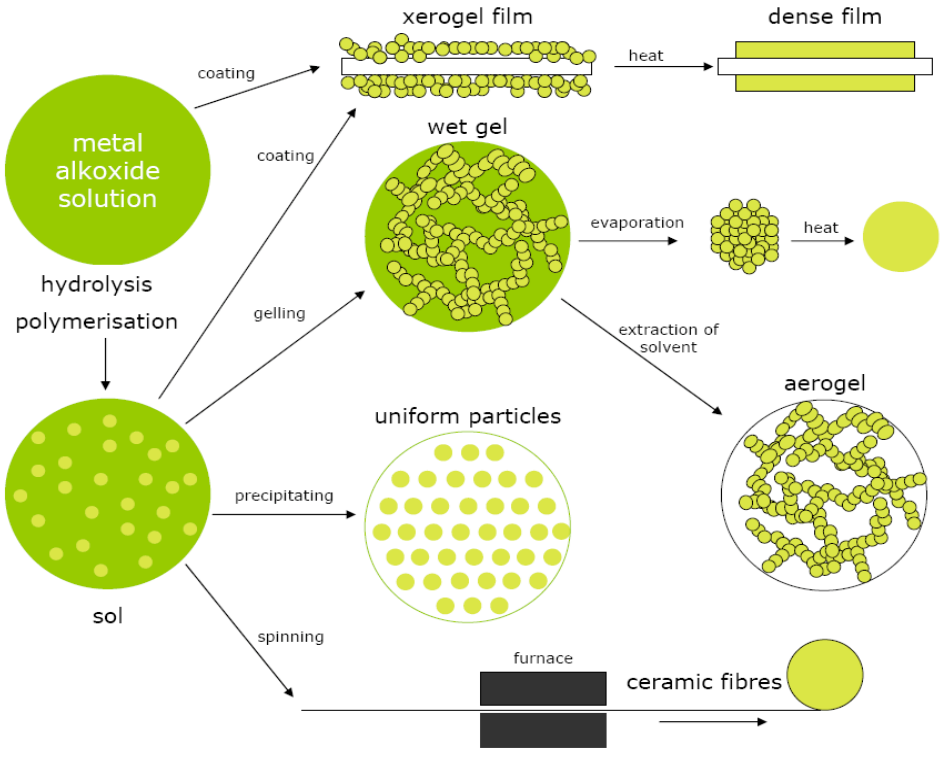

Figure 15: Schematic representation of Sol-gel method[85].

1.3.1.1.3 Micro-emulsion based synthesis:

Microemulsions can be referred to as nanoreactors to synthesize NPs. They are stable, isotropic mixtures of two immiscible liquids with a surfactant[86]. Surfactant molecules stabilize the two liquids. Water to surfactant ratio is important to consider in order to calculate the size of micelles in use and the size of resulting NPs. In case of water in oil (w/o) microemulsions system,one having metal precursor and other having reducing agent are allowed to mix[87]. The random Brownian motion of the micelles occurs which causes collision. The continuous collision results in mixture of two contents and it leads to the formation of NPs[88].

In w/o system, solubilization of hydrophilic compounds occurs, whereas in oil in water (o/w) emulsions, solubilization of organic compounds occurs. It is a very common method of producing NPs where proper amount of reactants are mixed[77]. NPs can be obtained from the system by using solvents like ethanol and followed by centrifugation[89]. Fig 16 shows the general scheme of the method.

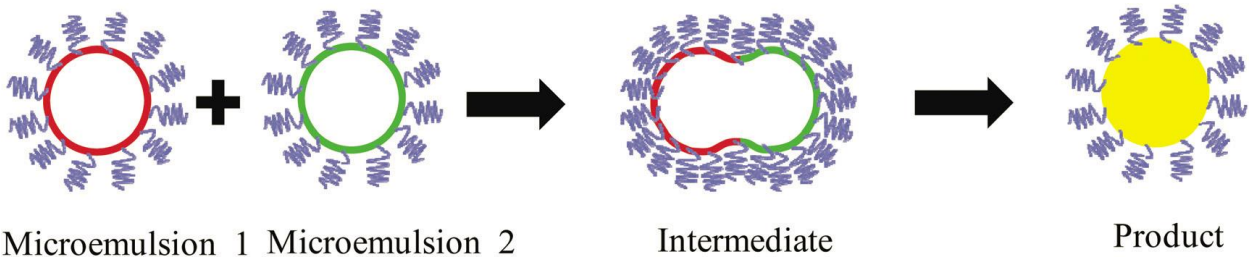

Figure 16: Scheme showing two microemulsions solutions mixing to form NPs[77].

1.3.1.1.4 Microwave based synthesis:

Microwave based synthesis is a very straight forward method to synthesize inorganic NPs. Magnetron is used to produce microwaves. Reactants soak up this energy and consequently produce heat in the system. This degrades the precursors and produce supersaturated solutions.

Nucleation is done in order to synthesize desired nano structures. Gold NPs have been prepared having different shapes using microwaves from Chlorauric acid in HCl as gold precursors[77].

1.3.1.1.5 Electro-templating:

Electrolysis is done by using desired metal as anode and the cathode is employed as an inert electrode. In a system, solution of a stabilizer is electrolyzed. The cations from the metal anode move towards cathode which cause reduction, growth and stabilization of the metallic NPs as shown in Fig: 17. Electrochemical synthesis is also employed for preparation of metallic composites and production of NPs from polymers[81]. Electrochemical methods produce pure metallic NPs and particle size can also be controlled by tuning density of current [90].

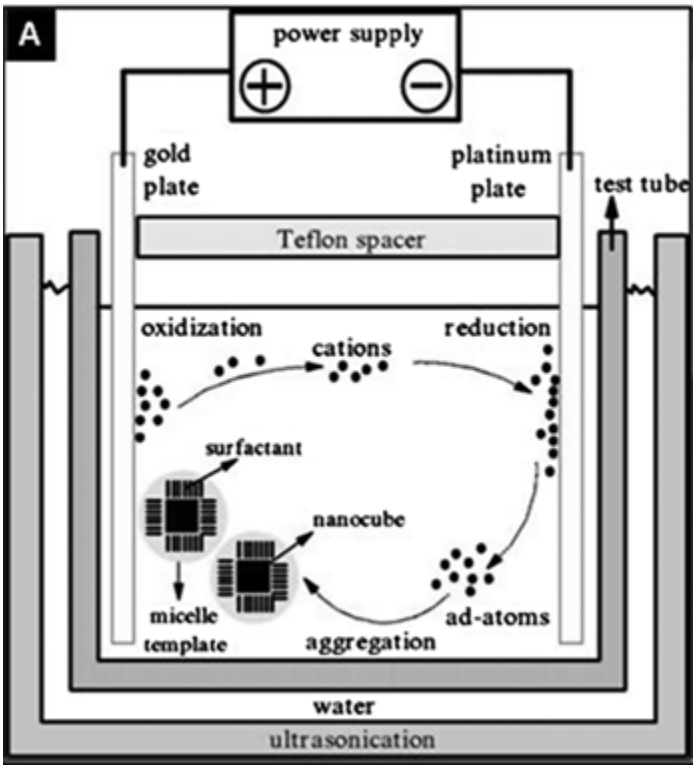

Figure 17: Electrotemplated synthesis of gold nanocubes [91].

It can be difficult to induce oxidation of metal at anode terminal, in that case, inorganic salts can be used as metal anode [90].

1.3.2 Polymeric NPs:

Another category of NPs studied within the scope of this work is polymeric NPs. They are made up of the organic compounds like lipids and polymers with a diameter range from 10 nm to 1 micrometer. In nanotechnology, these polymeric organic NPs are less exploited than inorganic NPs. But organic NPs have a great potential in nanomedicine, as they have the ability to encapsulate the active biomolecules. They are in use in many biomedical applications. Dendrimers, liposomes or micelles are few examples of organic NPs[92].

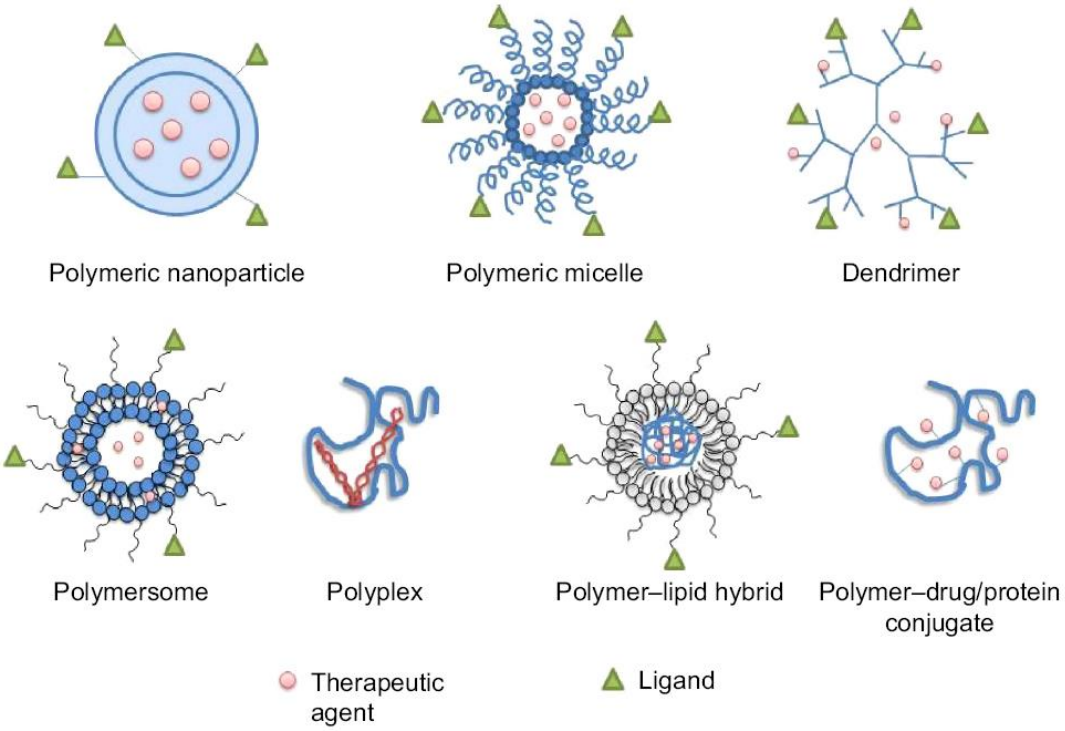

Figure 18: Different types of polymeric NPs [93].

Polymeric NPs are made from using natural or synthetic polymers. Synthetic polymers (PGA, PLA etc.) usually are considered as polymers made in highly purified environments, but they must be biodegradable and nontoxic. Natural polymers (Chitosan, Alginate etc.) are extensively exploited in drug delivery applications for their biocompatibility and nontoxicity. It is important to select the right synthesis process of polymeric NPs for the specific drug (hydrophobic or hydrophilic) with a defined route of administration [12].

1.3.2.1 Polymeric Micelles:

Polymeric micelles are extensively used in drug delivery systems due to their encapsulating ability of many active biomolecules. They are self-assembled NPs which are prepared in aqueous solutions having amphiphilic block copolymers. These core shell structures have a hollow hydrophobic core which is vital for delivery of drugs which are insoluble in water. The core is surrounded by hydrophilic polymer chains which stabilizes the inner core[94].

1.3.2.2 Liposomes:

Liposomes are spherical NPs having lipid bilayer membrane and an internal hollow core. Liposomes are comparatively larger than the commonly used NPs (90nm-150nm). Liposomes carry important active molecules like certain antibodies and antigens and act as ligands. The most prominent feature of liposomes is that their composition complements the phospholipids of human cell membrane which can be beneficial in targeted drug delivery applications. Liposomes have higher retention time and good targeting abilities than other NPs. They can carry both hydrophilic and hydrophobic drugs in its hollow core. One can tune liposomes and exploit disease conditions by functionalizing them as pH or temperature responsive, which is necessary in controlled release of the drug from the core[53].

1.3.2.3 Dendrimers:

Dendrimers are versatile polymeric nanomaterials having a tree like three dimensional branched structure with improved functionalities. They have inner core and branched moieties which can be exploited in many drug delivery applications. Because of their structure, they can be linked with different substances (hydrophobic or hydrophilic) with different functional groups which make them a multifunctional nano-carrier of drugs and imaging molecules[95].

Dendrimers can be synthesized by branching monomers leading to a branched structure with a central core. The branches can be functionalized. They are synthesized by two different methods; divergent and convergent polymerization. By divergent polymerization method, assembly of monomers starts from the initiator central core, while in convergent polymerization the periphery branching units lead to form a complete branched dendrimer structure, as shown in Fig (19.a,b) [96].

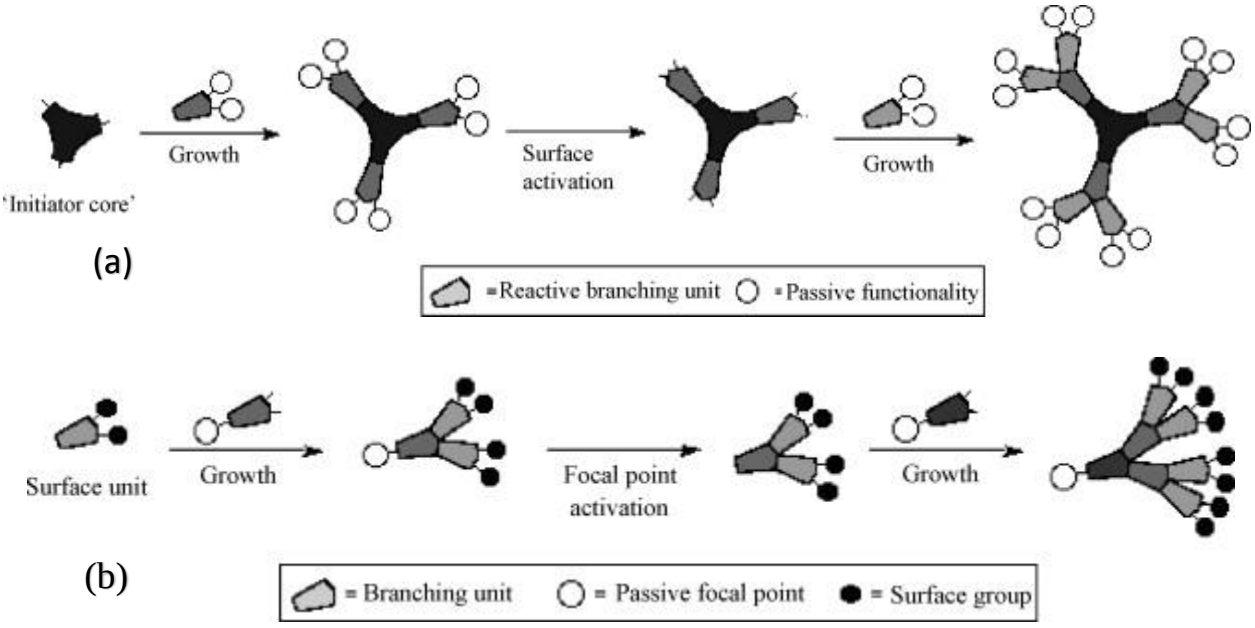

Figure 19: a) Divergent polymerization). b) Convergent polymerization [96].

Dendrimers are used widely in biomedical applications like drug delivery and gene delivery. In gene delivery conjugation of DNA/RNA can be done to induce gene expression when this system is targeted inside the defected cell as shown in Fig. 20 [97]. Different drugs and imaging molecules can be incorporated in branched structure of dendrimer. Physical and chemical interaction of drugs with the dendrimer is important to strategize the incorporation of active compounds. Chemically, modification of drug dendrimer interaction is achieved by using functional groups. PEG can be used to covalently cross link drugs with the dendrimers. Biodegradable chemicals like esters can also be used as cross linkers [98].

The current drawback known is to control the toxicity related issues linked with the exploitation of dendrimers. Dendrimers are cationic nanostructures and they can react with the anionic membranes of the body which disrupts the cell integrity and may cause cells to burst and die[98].

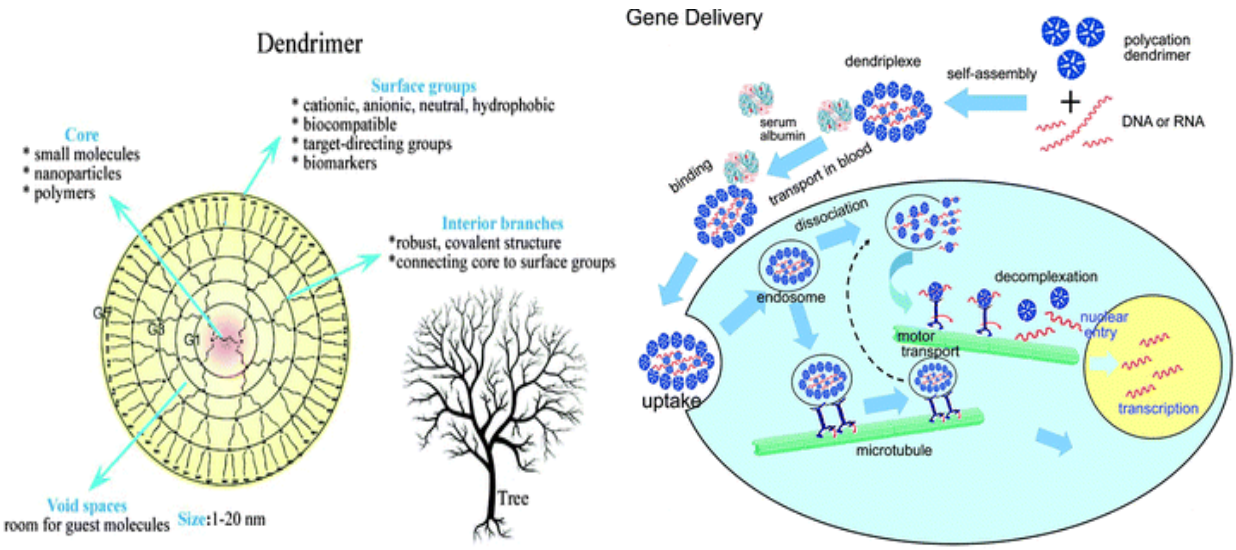

Figure 20: Structure of dendrimer and dendrimers as gene delivery vectors[97].

1.3.3 Stimuli responsive nanomaterials:

Stimuli sensitive nanomaterials offer a wide range of physicochemical properties in response to changes in the environment that provide important functions in various biomedical applications [99]. A multifunctional stimuli sensitive particle may have a core and a polymeric shell around the core which can swell and collapse. It can be functionalized with recognition ligands, diagnostic contrast agent or drug for targeted delivery. These intelligent hybrid structures can detect changes in the environment and respond to internal stimuli like pH, redox potential or respond to external stimuli like temperature & light and thereby can act accordingly[100].A general stimuli responsive delivery scheme is shown in Fig.21.

Figure 21: Stimuli dependent release of drug from nanocarriers[101].

1.3.3.1 pH sensitive NPs:

pH microenvironment of diseased sites of the body can be employed among other environmental stimuli. pH responsive nanocarriers can target organs, tissue/cells and sub-cellular organelles depending upon the respective differences in pH of healthy and diseased site[102]. Based on site specific targeting, three different strategies are shown in Fig. 22.

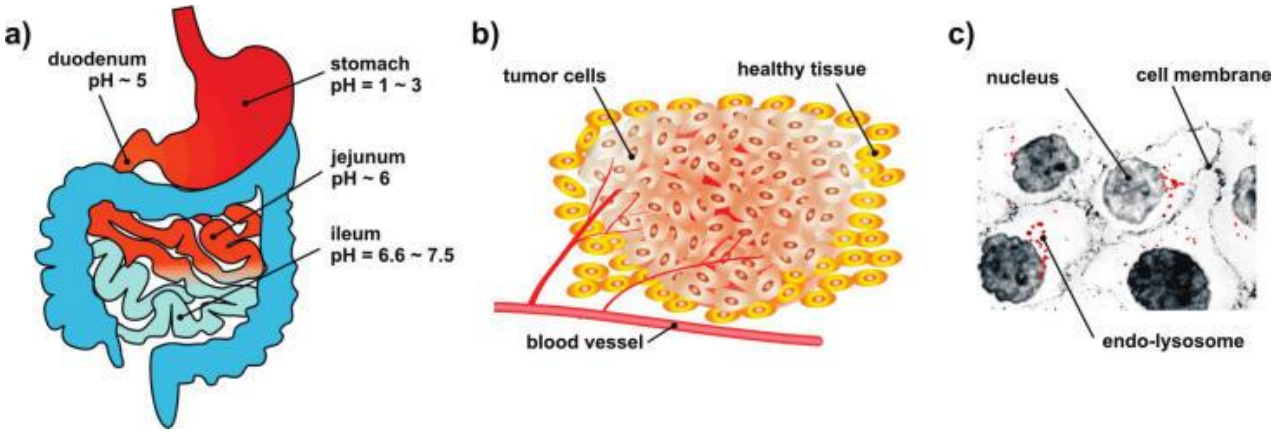

Figure 22: pH sensitive targeting at a)Organ ,b)Tissue, c) sub-cellular levels[102].

There are different pH levels in different parts of the body. At organ level, for example gastrointestinal tract (GIT), each segment has specific pH required for food digestion. The stomach lumen pH is most acidic (1-3). But when food goes down further to duodenum, pH is neutralized (6-7) due to alkaline conditions. Oral drug delivery exploits, such organs at different pH levels .It is a convenient and less expensive way for orally administered drugs. It is also possible that due to strong acidity of the stomach juices and enzymatic activity, degradation of nano based drugs may occur leading to poor bioavailability of drugs. Recently, biodegradable polymers and ligands are designed in order to increase the drug retention in stomach[103]. In a study, Heparin-chitosan NPs were synthesized to treat a severe stomach infection caused by bacteria, *Helicobacter pylori.* Epithelium layer of stomach wall has acidic pH than total acidic environment of the stomach. Results have shown that this NP system was stable at pH 1.2-2.5 which protects the drug from gastric juices. On contact with the infected epithelium and mucus cells of the stomach (pH 7.4) deprotonation of chitosan caused NP collapse and release of heparin[104].

At tissue level, pH sensitive strategies are exploited mainly for cancers. Tumor cells grow very fast. Their metabolic rates are very high due to high oxygen and glucose consumption. When more energy is required for tumor cells by glycolysis, pH of the growing tumor tissue becomes more acidic. Hence, tumor microenvironment can be exploited by using pH sensitive nanocarriers e.g. liposomes. They are designed to degrade at acidic pH and release the drug at tumor sites[105].

After endocytosis, acidification of endosome occur, hence pH levels of endosome drops to less than 6[106]. Acidification can be harmful for therapeutic nanocarriers especially DNA, RNA or protein delivery. But endosomal acidification can also be used to elicit the escape of NP and release of payload into the cytoplasm. Protonation effect is responsible for rise in osmotic pressure inside the endosome. This phenomenon is referred to as Proton sponge effect[107]. pH responsive polymers have been used in many studies that buffer the endosomes for intracellular delivery of active substances[108]. Aryal et al. have synthesized polymer (PEG-PLA) conjugated with cisplatin in the polymer network to investigate drug release at low pH. *In vitro* results have shown that cytotoxicity of polymer conjugated cisplatin in cancerous cells increased as compared to free cisplatin. It was suggested that these NPs have good acid responsive drug release after nanocarrier is engulfed by the cells which is an effective method in tumor targeting strategies[109].

1.3.3.2 Temperature sensitive NPs:

Heat responsive nanocarriers are widely investigated in many drug delivery applications. A sudden change in temperature is employed when thermo-sensitive system with encapsulated drug reaches the target site. Such sudden response induces the drug to release. Mostly used nanoparticle systems are polymeric micelles and liposomes. Poly(N-isopropyl-acrylamide) pNIPAM is a typical polymer used for heat triggered release of active biomolecules[101].

In recent years, thermosensitive liposomes have been greatly employed. Doxorubicin (Dox), an anti-tumor drug, loaded in thermosensitive liposomes (ThermoDox) are now in the 2nd phase of clinical trials for treatment of breast cancers. Drug release is linked with initial temperature of hyperthermia (40-45^{o}C) which targets the leaky vasculature of the tumor microenvironment [110]. General scheme is shown in Fig. 23.

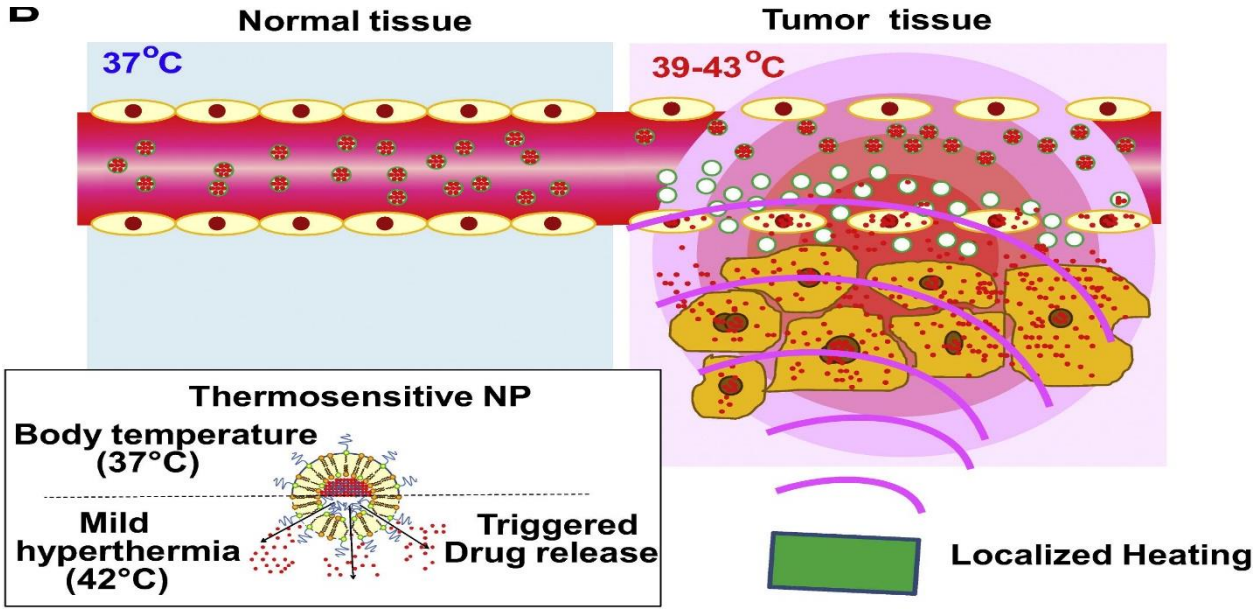

Figure 23: Thermo responsive liposome targeting tumor's leaky vasculature [110].

In another novel approach, researchers have loaded 5-Florouracil in pNIPAM hydrogel at room temperature. The hydrogel with loaded drug were put in a dialysis bag. Studies were performed using U.V spectrophotometer and drug release from this novel drug delivery system was monitored at 266 nm. It was found that increase in temperature from 25^{o}C to 37^{o}C released the drug at faster rate than by lowering the temperature to 10^{o}C from 25^{o}C. It was also suggested that by controlling heat responsiveness of the hydrogel and dialysis bag, release rates can be controlled [111].

1.3.3.3 Light sensitive NPs:

Photosensitive nanocarriers have been investigated for controlled release studies. Light is a good source for stimuli responsive systems since its penetration and intensity can be controlled accordingly. Nanocarriers can be irradiated with ultraviolet light to achieve drug release when required. The strategies can be tuned accordingly if there would be one time or repeatable release scenarios [101, 112].

In a study, near infra-red (NIR) light was used. NIR sensitive drug delivery system was inspired by DNA self-assembly method in which DNA template strands hybridize. Nanocarriers were composed of PEG coated gold nanorods (NRs) and complementary DNA nucleotides. One strand was made capture strand which was attached with gold NRs functionalized for NIR response. The other complementary strand was made as targeting strand with molecular ligands for targeting the required site. The CG (cytosine-guanosine) base pairs at both strands were used as binding sites for loading of DOX. DOX molecules were incorporated in the double stranded DNA strands consisting of both capture and targeting strands. In response to the irradiation, gold NRs become heated which results in DNA damage. Consequently, DOX molecules were released at the target site. It was found that tumor growth could be inhibited. Fig. 24 shows the schematic diagram of the method. It was also suggested that such systems can be finely tuned to control drug loading and release using DNA assembled nano based strategies [113].

Though, such drug delivery systems can be very useful in future but safety and biocompatibility of substances used in light responsive systems must be evaluated [23].

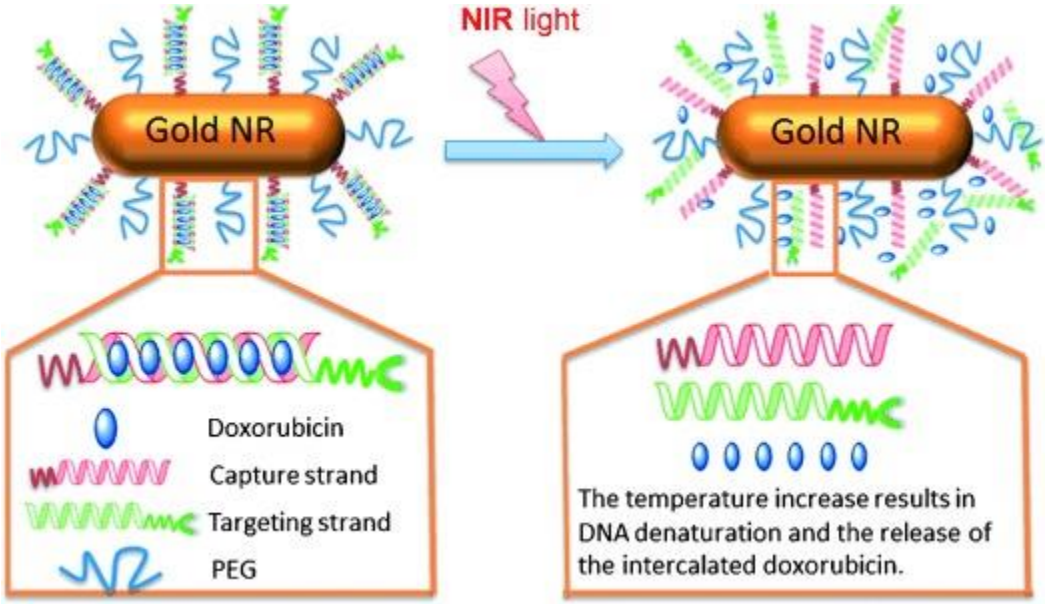

Figure 24: Photo-responsiveness, NIR light causing the strands to denaturate, releasing DOX [113].

1.3.4 Theranostic NP's:

Theranostic NPs possess both therapeutic and diagnostic capabilities whereby having dual function of diagnosing the disease and releasing the drug at the diseased site. The importance of such integrated drug delivery system is to enable researchers in the monitoring and management of vital diseases like cancer, diabetes, hepatitis etc. at relatively low cost. In cancer therapy, drug molecules and imaging contrast agents are added to the nano-carrier and delivered to the tumor site[114]. Fig: 25 (a) shows a scheme of a theranostic NP in action.

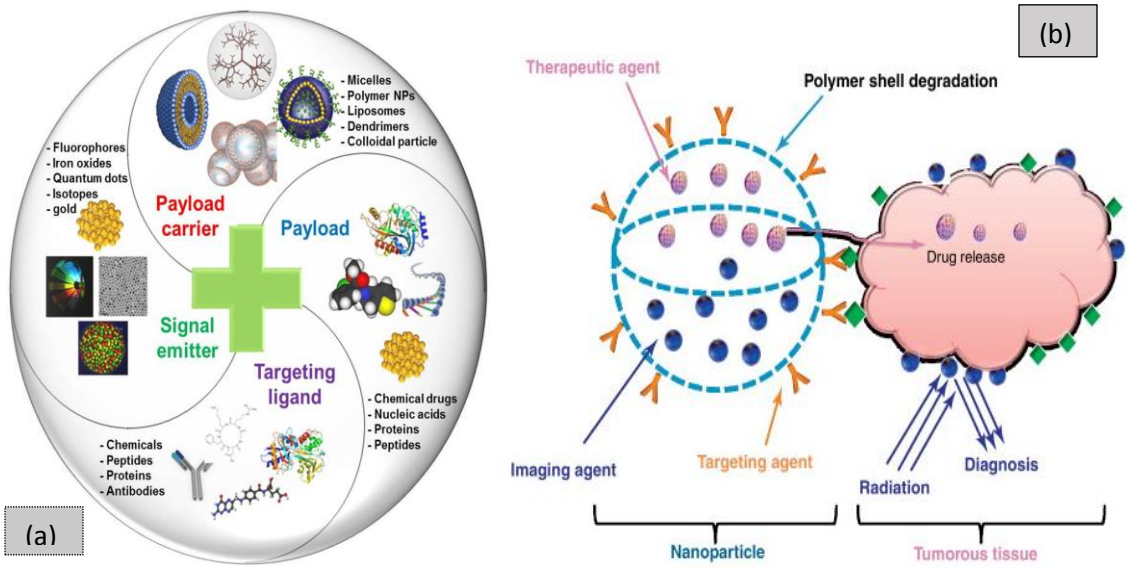

Figure 25: (a) Basic components of a theranostic NP. (b) Theranostic NP in action to diagnose and deliver drug to the tumor location[115].

Theranostic NPs have four basic components- therapeutic drug, a carrier, signal emitter and targeting ligand. The drug carrier can be polymeric NPs, liposomes etc. The signal emitter with diagnostic ability is required to emit signals on reaching the targeted anatomical site. The targeting ligands like proteins or antibodies are used specific to the diseased site, for example tumor site [115].

1.3.5 Applications:

In recent years there has been unrivalled development in the field of nanomedicine. Drug delivery and imaging applications of nano based systems have a great impact on the future of medicine. There is increasing anticipation in engineering such systems that effectively diagnose and cure vital diseases like cancer and Parkinson's disease [116].

1.3.5.1 Drug Delivery:

Drug delivery is the major application for NPs in the emerging field of nanomedicine. NPs possess unique properties like small size, surface functionality or ability to carry active molecules with them to accumulate the drugs in the diseased site[117].

1.3.5.2 Targeted & non-targeted drug delivery:

Drug delivery systems are based on targeting and non-targeting strategies. In non-targeting method, drugs are delivered to the body by conventional methods like bulk administration of drug. On the other hand, in targeted drug delivery, drugs are targeted to only diseased site without affecting healthy cells.Fig.26 shows two different targeting NPs with attached targeting ligands [118]. Targeted delivery do not completely depend on route of administration or method used. It is important in targeted delivery systems that how drugs will interact with the damaged cells. The prerequisites for a successful targeted delivery are biocompatibility of the nanocarrier system, strength of drug polymer conjugates and specificity to target the damaged cells only. Systemic and intracellular targeting strategies are mainly employed. In systemic drug delivery, localized triggered delivery and ligand-receptor interactions mediates the delivery of the drug. To target the drug inside the cells, for example to lysosomes, low pH can provide lysosomal escape of nanocarriers hence releasing the drug inside the cell[119]

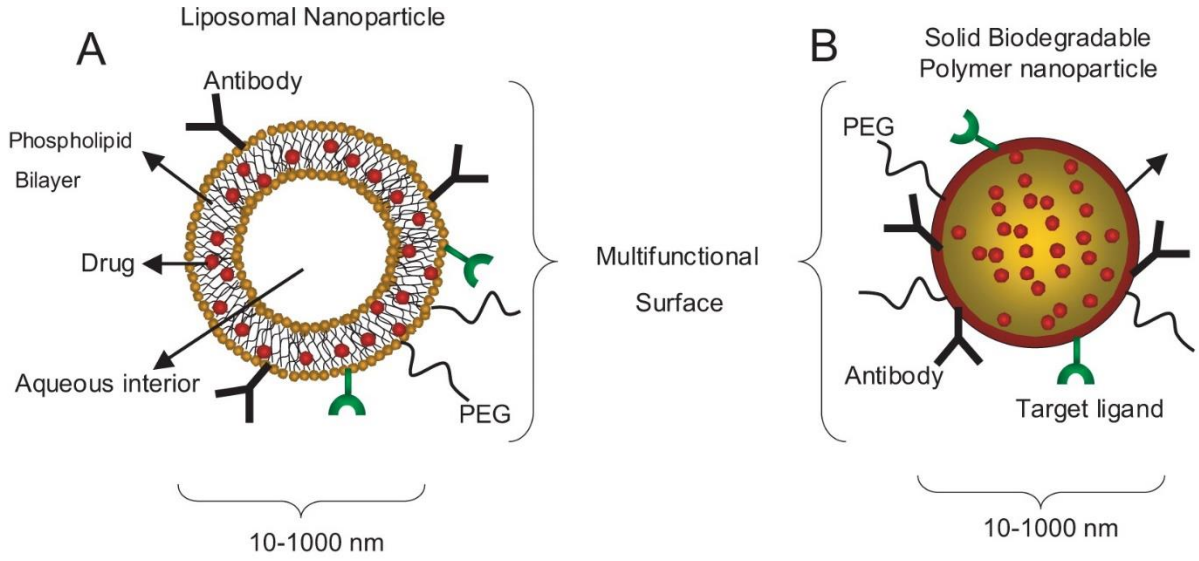

Figure 26: Two different targeting NP systems A) Liposomal NP, B) Polymeric NP[118].

Liposomes have better encapsulation capacity inside their core. Aqueous interior can provide space for encapsulation of hydrophilic drugs whereas hydrophobic drugs can be conjugated within the bilayer. PEG modification with its stealth nature can act as barrier which prevents interaction with circulation proteins. PEG increases liposomal retention time *in vivo*[120]. Although, liposomes are a potential targeting drug delivery vehicle but they yield poor release kinetics. Manufacturing such liposomes is also difficult at industrial scale. Storage of such lipid based drug delivery systems can be a challenge due to their lower stability[121]. On the other hand, biodegradable solid NPs offer wide range of functions in targeted drug delivery. Polymers offer biodegradability and biocompatibility features. It is possible to tune NP size and shape; polymer composition can also be varied in order to add drug release characteristics in nanocarriers. These NPs can provide constant doses for longer periods of time[118]. NPs can be designed with or without surface functional groups depending on type of application. Many polymers and polyesters like PGA, PLA are in use for targeted drug delivery applications due to their tunable degradation rate and biocompatibility [122]

1.3.5.3 Drug Route:

Size, shape and surface chemistry of drug delivery systems are important factors to consider when administrating the drug or imaging agent inside the human body. The bio distribution profiles of nanocarriers with known toxicities are prerequisites to design nano systems for drug delivery. There are many methods and routes to administer the nano based drugs depending on type of function and site targeted. Immune system activates when any biomaterial enters the human system. In ideal conditions, nanocarriers must be non -toxic, biodegradable and non-immunogenic. Polymers can act as good conjugation source for many drugs e.g. poly-glutamic acid (PGA), polyvinyl alcohol (PVA), or PEG. Polymeric NP systems provide biocompatible features for pharmacokinetics and pharmacodynamics of the drug [123]

A complete insight of anatomy and physiology is required when constructing nano systems for drug delivery and imaging applications. It is very important in tracking the injected drug carrier from its cellular uptake to elimination from human system. Fig.27 and 28 shows different methods of drug administration, uptake, metabolism and elimination mechanisms for nano based drug delivery systems[124].

1.3.5.3.1 Administration:

Most of the polymers are nanocarriers synthesized for delivery via intravenous (IV) route. It is efficient route of administration as therapeutic molecule can enter directly in the bloodstream. There are also many different formulations which are administered subcutaneously (SC) or intramuscularly (IM), for example, Peg-Intron®. These injections are used for slow and consistent release of drug, hence less periodic injections are used. In a study, administration of water soluble polymers PEG and PVA were investigated via different routes. It was found that elimination rate of intraperitoneal (IP) administered polymers is greater than IM and SC administered polymers. Oral and pulmonary routes have also been exploited for localized delivery. Liposomes and other polymeric NPs have been used. Low molecular weight of polymers has shown fast degradation. Route of administration, and nanocarriers system may vary depending on the disease, therapy and intended doses for longer or shorter periods[125].

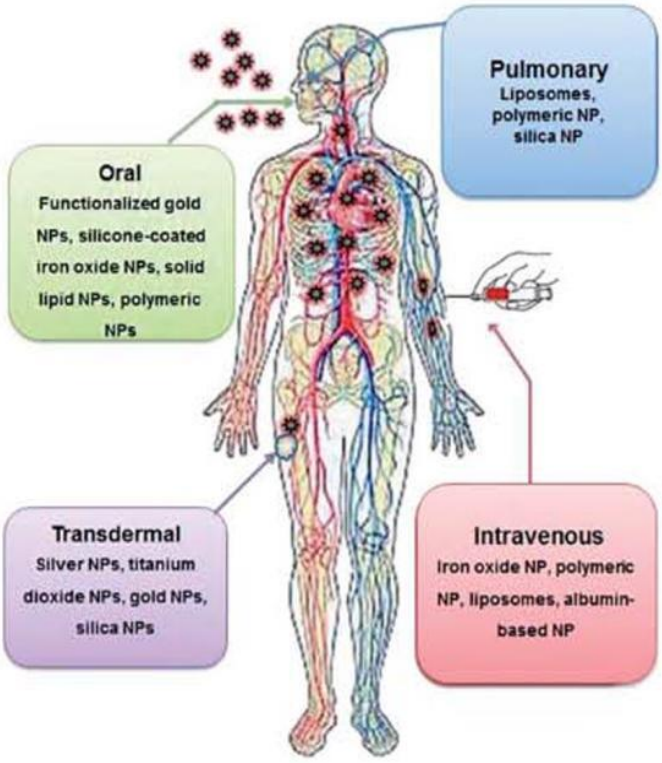

Figure 27: Significant routes for administering NPs [126].

1.3.5.3.2 Distribution

Physicochemical and mechanical properties of NPs play a key role in biodistribution, targeting, engulfment and biodegradation of the nanocarriers. Initially on entering the human system, interaction of NPs with immune cells and serum protiens occurs which determines the fate of distribution of nanocarriers [127]. Biodistribution of NPs is typically achieved by active & passive targeting.

1.3.5.3.2.1 Passive & active targeting:

The effective nanocarrier system has to target the damaged cells without affecting the healthy cells. For instance, in cancer, the microenvironment around tumor cells can be exploited to deliver the drug. This pathophysiological condition of tumor tissues allow drugs to accumulate and cause therapeutic effect. The drug polymer hybrid nanocarriers have longer circulation and retention

rates than the drugs with lower molecular weights. Normally, endothelial cells of blood vessels are more impenetrable to macromolecules. In pathological condition or tumors, disordered vasculature becomes responsible for permeability of larger molecules. This enhanced permeability of defective vasculature results in increased retention of macromolecules in tumor tissues. This type of targeting is called passive targeting. The anatomical difference of the tumors from healthy cells makes way for nanocarriers (up to 400nm) to pass through the vasculature. This phenomenon is called enhanced permeability & retention (EPR) effect[119] . Doxil works by passive targeting which is developed for cancers. It is a PEG coated liposome incorporated doxorubicin. It selectively targets the tumor cells and have better pharmacokinetics than conventional drugs of low molecular weights. Hence EPR effect is considered to be a landmark in developing anti-cancer drugs[128].

Active targeting is carried out by using proteins, conjugating ligands, antibodies or small molecules attached with nanocarrier system which actively targets the diseased site. These ligands will selectively bind to the specific receptors on surface of cells. Target cell binding depends on cell surface receptor expression, ligand receptor interaction and their surface chemistry. Ligand-receptor binding ensures entry of nanocarriers inside the cell. It is important for successful recognition that both receptor and ligand must be in closer (<0.5nm) proximity. Currently, nanodrugs are under investigation for selectively targeting and release of drugs from nanocarriers into the tumor cells [129].

1.3.5.3.3 Metabolism:

The system used for drug delivery needs to be degraded after performing its required thernaostic function. Polymers which are biodegradable degrade and need to be eliminated from the body immediately after performing their function. Their degradation is mostly imitated by the degradation of polymer backbone. Biopolymers like collagen degrades and are metabolized into amino acids or saccharides which become part of biochemical pathways of body. Chitosan is susceptible to lysozyme on acetylated residual hydrolysis. Dextran degrades when dextranases α-1-glucosidases. This enzyme is present in almost all the main organs of the body like liver, kidney

etc. Synthetic polymers degrade in similar fashion either hydrolytically or enzymatically e.g. PGA degrades into monomeric units of amino acids when lysosomal enzymes cleave bonding[130] .

1.3.5.3.4 Elimination:

Elimination of non-biodegradable polymers like PEG and other higher molecular weighted copolymers is a growing concern. Non degradable polymers go back to circulation via possibly defective lymphatic system of the diseased site. On reaching the glomerular filtrate of the kidney, they are eliminated if they are under the threshold of the glomerular. Molecular weight, size and shape of the nanocarrier are the factors which affect the rate of glomerular filtration and subsequently elimination from the body[131]. There is still considerable need to consider the potential risks while using higher molecular weight NP systems especially when periodic doses are to be administered[132].

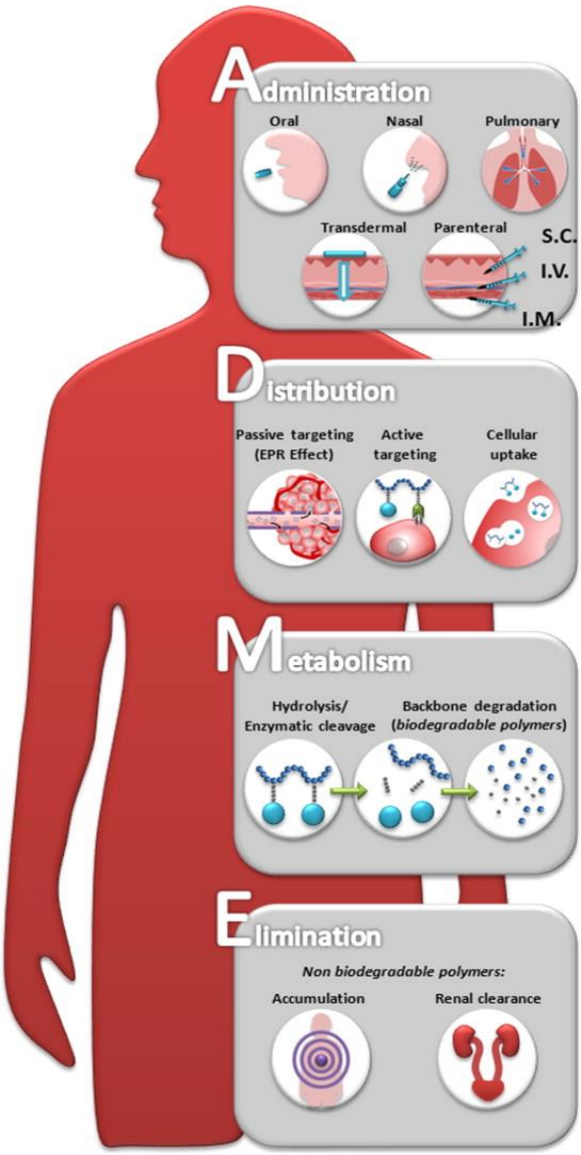

Figure 28: Journey of nanocarriers in human system showing administration routes, distribution, metabolism and elimination methods from the body [123]

1.3.5.4 Diagnostic Imaging:

NP based imaging techniques have influenced the modern diagnostic methods. Development of imaging moieties coupled with nanocarriers have great potential in diagnosis of diseases [133]. Molecular imaging is done to visualize the disease site in study where molecular probes are

constructed to characterize the processes at molecular or cellular level. There are many different NP systems (gold NPs, dendrimers, or polymeric NPs) which are used in order to image the desired site of the body. NP size, shape, surface charge needs to be considered while developing nano systems for imaging. Functionalization of nanocarriers can be done by using polymers like PEG which gives hydrophilic stealth characteristics. By using PEG, it is possible to enhance circulation time in blood because less adsorption of circulating serum proteins can be achieved. Similarly, anionic charged NPs can be used to increase the endocytosis of nanocarriers containing labelled probes required to imaging techniques[134]. NP based contrast agents are potentially good candidates for imaging which will help diagnosis of vital diseases like cancer, Parkinson's disease & hepatitis [135].

MRI has emerged as very potent tool in diagnostics. It is due to its higher efficiency of contrast, penetration and high resolution imaging capability in soft tissues of the body. It is based on signal intensities received and is dependent on the relaxation times T1 and T2. T1 is spin-lattice relaxation of in vivo water protons of the concerned diseased site. T2 provide spin-spin relaxation rates. Magnetic NPs act as contrast agents which are added into the system before scanning. NPs can enhance or decrease the contrast in the tissues to be imaged which can be termed as positive and negative contrast agents, respectively. Recently, these magnetic NPs are used as potential theranostic agents because of their dual functions of imaging and delivering the drug to required tissues. In a study, L-Dopa drug used against Parkinson's disease was conjugated on the surface of manganese oxide NPs which releases the drug upon release of Mn^{2+} ions. It was a novel method to obtain high resolution MRI image with combined therapeutic effect [136]

2 Materials & Methods:

2.1 Materials:

In this project, sodium alginate (Protanal® LFR 5/60, M.W: 32kDa, F_G = 0.68 which is total fraction of G blocks) used was provided by FMC Biopolymers Norway. Calcium chloride, purchased from Sigma Aldrich® was used as calcium ions source to cross link G blocks of the alginate. Fluorescein sodium salt was also purchased from Sigma Aldrich®. Milli-Q® water with 18.2 MΩ·cm resistivity at 25 °C was used in preparing solutions.

2.2 Characterization Techniques:

Characterization techniques employed in this project are Ultraviolet visible spectroscopy (U.V.Vis), spectrofluorometery, Dynamic light scattering (DLS), capillary viscometery (ubbelohde viscometer tube) & Scanning Transmission Electron Microscope (STEM).

2.2.1 UV-Vis Spectroscopy:

UV Visible Spectroscopy is a technique which measures the amount of light absorbed/ scattered by the sample. It is an important tool for characterizing nanomaterials. Sample under characterization is placed between the light source and detector,and intensity of visible region of light is measured before (incident beam) and after (transmitted beam) passing the sample. UV extinction spectrum measurements are wavelength dependent[137]. Beer's law measures the absorption spectra as:

$$\boldsymbol{A = -log\left(\frac{I}{Io}\right) = ecl}$$

Where *A* is absorption, *I* and *Io* are incident (*Io*) and transmitted beam intensities (*I*), and c is the concentration of the scatters in solution & *e* is the molar extinction coefficient. According to Beer lambert's equation, absorbance is directly proportional to the concentration & evidently darker solutions have higher absorbance values[138].

In this project, UV-24011PC developed by Shimadzu© installed at Ugelstad laboratory was used for measurements. Standard disposable cuvette was used for measurements. Baseline with MiliQ® water was performed before measuring the samples. U.V spectroscopy setup is shown here in Fig. 29

Figure 29: U.V Visible Spectroscopy

2.2.2 Fluorescence Spectroscopy:

Fluorescence is a light emitting process which occurs when incident beam of light matches the frequency of electronic oscillation in a substance or nanomaterial. Electrons are excited from ground state to vibrational levels of energy. Jablosnki diagram Fig:30 conveniently describes the excited structure and energy transitions during the fluorescence phenomenon. Excited electrons relax which leads to photon release and loss of energy in the form of heat. The emitted photon will always be at higher wavelength compared to excited photon, this energy reduction is called Stokes shift. Phosphorescence and delayed fluorescence are other fluorescent processes which lie in different excitation and emission spectra of energy[139, 140].FRET(Fluorescence Resonance

Energy Transfer) occurs when two fluorophores are placed in close proximity (1- 10nm) due to energy absorption by one from the other[139]. This leads to quenching (decrease in fluorescence) and enhancement (increase in fluorescence) of the two fluorophores causing shifts in the excitation/emission spectra. These overlaps are observed when emission spectrum of donor fluorophores overlaps with the absorption spectrum of acceptor fluorophore. Peak overlaps are higher at longer wavelengths which are commonly linked with the dipole dipole interactions between two fluorophores or exposure to the aqueous medium which is under characterization[141]

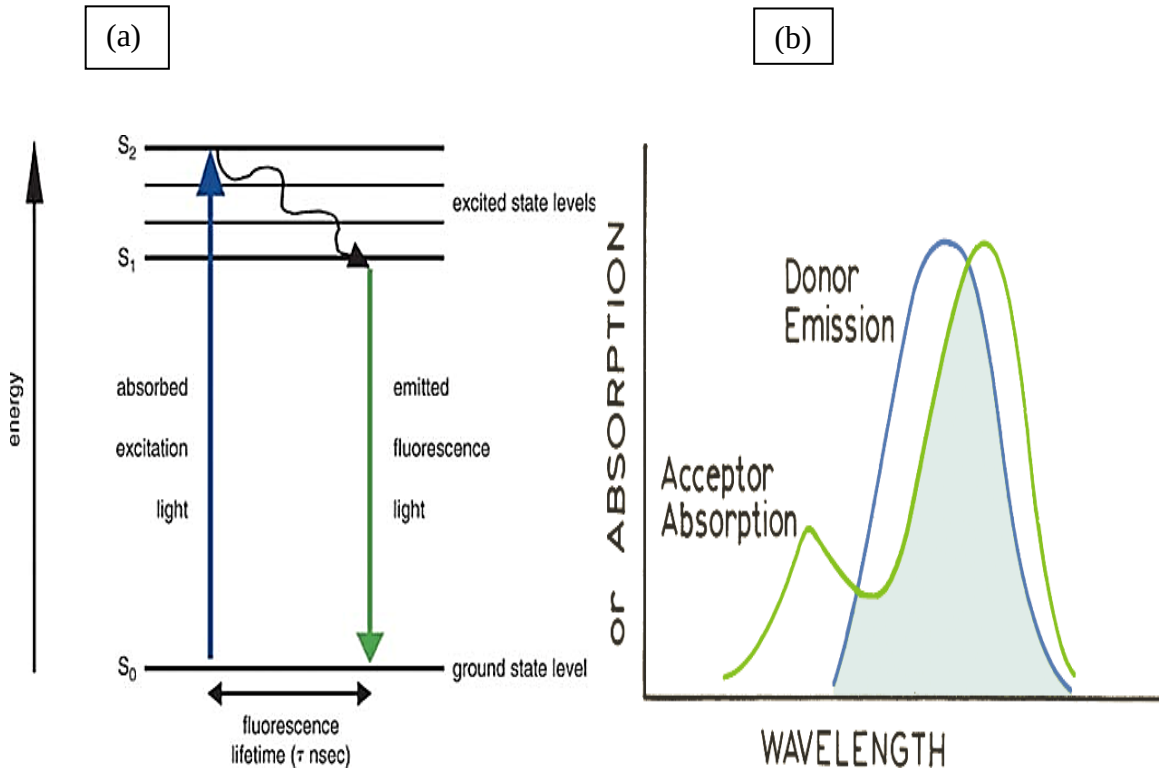

Figure 30: (a) Jablonski Diagram, (b) shows peak overlap in FRET [139, 141].

In this project, Fluorolog® spectrofluorometer was used for investigating gelation. Fig. 31 shows the instrumental setup. Alginate & $CaCl_2$ were investigated at different excitation/emission wavelengths. Gelation studies were performed at 280 nm excitation (slit width 5mm) and emission (slit width 3mm) peaks from 545-575 nm were considered. Further on, loading and release studies

are performed. Fluorescein dye was excited at 460nm (excitation slit width 3mm) (emission slit width 3mm) and emission measured in the range from 590nm to 520 nm.

\

Figure 31: Fluorolog® Spectrofluorometer instrument with cuvette for sampling.

2.2.3 Ubbelohde Capillary Viscometer:

Viscosity of liquids characterizes their intrinsic friction and flow properties. If any liquid is put between two surfaces, plane parallel to each other, force will be required to it to displace it from the upper surface. It is because, the liquid particles are bound to the surface by adhesive forces. In the measuring capillary viscometer, a laminar flow drop of a liquid is created. In ideal conditions, fluid flows in coaxial layers directed towards the pressure drop. A parabolic liquid flow occurs through the viscometer. On applying air pressure, the drop displaces through the capillary from a certain point to the other and measurement (time) recorded in automated stop watch. Viscosity of pure solvent will be taken as reference point. Poiseuille's law applies on capillary viscometers which is given by the following equation:

$$\frac{\boldsymbol{V}}{\boldsymbol{t}} = \frac{\boldsymbol{\pi R^4 \Delta \rho}}{\boldsymbol{8\, L \eta}}$$

There are different types of capillary viscometers in variety of shapes. Ubbelohde and Ostwald are common viscosity measuring instruments. In this work, Ubbelohde viscometer was equipped with an automated stop watch. Measurements of flow time are calculated manually or through automated stop watch. Automated stopwatch is more advantageous than manual timing as automated system can reduce subjective observational errors or reaction time of the observer can be different from actual reading. In certain conditions, it is difficult and hectic to take readings of highly viscous liquids that take long times to flow through the tube. Hence it is better to use automated timing device as they produce electrical signals at the start and end of the measurement giving higher accuracy[142].

In ubbelohde capillary viscometer (Fig 32), 0.1ml of alginate was added in 2.9 ml solution of $CaCl_2$ solution present in the tube. The tubes were stirred gently to mix the solutions. Temperature was set to 20^{o}C and 6 readings were taken for each experiment using automated stop watch. Their average value was used for studying viscosity of gelling alginate.

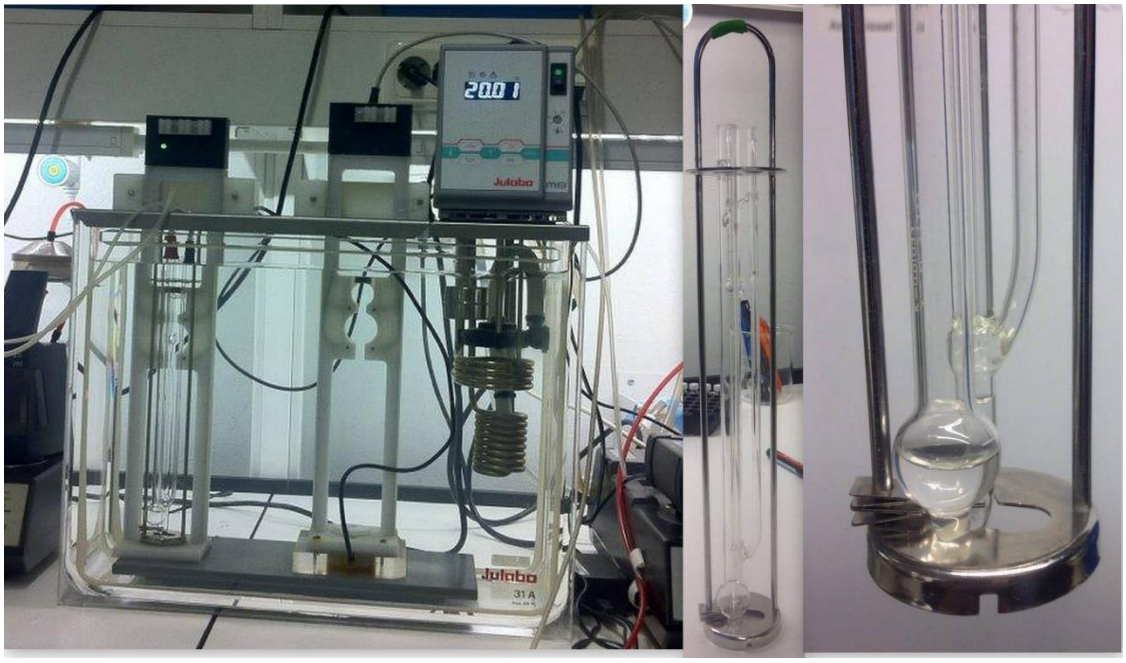

Figure 32 : Ubbelohde Viscometer Setup. On the right Alginate and $CaCl_2$ can be seen in viscometer bulb.

2.2.4 Dynamic Light Scattering (DLS):

DLS is used to characterize NP solutions. It is an important instrument which gives information about size distributions of particles in solution. DLS is based on Brownian motion. [143]. This random motion is driven by kinetic energy of particles which changes the intensity of scattered light with time. Bigger particles moving relatively slower than the smaller ones will scatter more light[144].

The principle of DLS measurement is based on measurement of diffusion coefficient of NPs. Stokes Einstein equation estimates hydrodynamic diameter which is diameter of hypothetical nonporous sphere which diffuses when the NP is being characterized. Stokes Einstein equation is:

$$\boldsymbol{D = \frac{Tk_B}{6\pi\eta R_h}}$$

Where D estimates the diffusion, k_B is Boltzmann constant, T is absolute temperature. R_h is hydrodynamic radius of the sphere and η is viscosity of solution[145].

In this project intensity of scattered light is measured by Malvern Nanosizer© which gave information about the size distribution of NPs in solution. It can measure up to nanometer scale to microns. DLS has great significance in size measurements in colloidal chemistry and also complements the size distributions measured by TEM (Transmission Electron Microscope).

2.2.5 Zeta Potential:

Zeta Potential is the property of charged particles in suspensions which can be used to characterize emulsions and solutions containing small particles. When a charged particle is mixed in solution, ions of different charge surrounds the particle forming a cloud/layer which is called electrical double layer. The layer which forms around the charged particle has two parts, inner stern layer & outer diffuse region. Inner stern layer has ions strongly bound to the surface whereas in diffuse region they are loosely bound. In diffuse layer, there are ions forming a stable boundary. When a

particle is in movement (Brownian motion), ions in the boundary move and the potential at this boundary is termed as Zeta Potential. The distance from the particle surface in the electrical solutions decreases the electrical charge of the system. Fig: 30 shows the schematic representation of Zeta Potential. The potential stability of the colloidal solution can be determined by the measurement of Zeta Potential[146]. Smoluchowski equation describes the working principle of the Zeta Potential:

$$\boldsymbol{vE = 4\pi\epsilon_0 \ \varepsilon_r \frac{\xi}{6\pi\eta} (1 + kr)}$$

vE is the velocity of particles in electrical field and *r* describes the radius of the particle. *k* is Debye-Huckel parameter $\varepsilon_0 and\ \varepsilon_r$ are relative dielectric constants which describes electrical permissiveness of the particles in the vacuum, η is the viscosity of the colloid system[147].

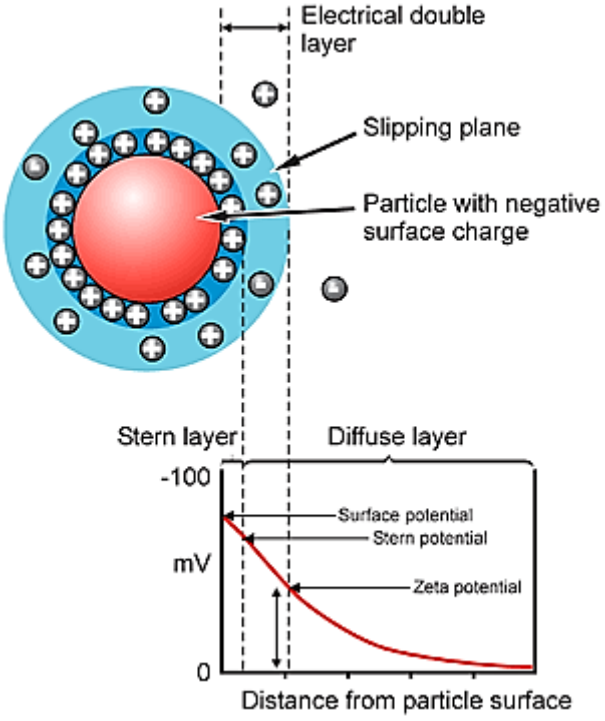

Figure 33: Scheme of Zeta Potential measurement[144].

In this project, Zeta Potential of Fe@Au, Fe@Au@PEG, Fe@AuPL NPs are measured using Zeta sizer form Malvern Instruments©. Zeta sizer is also used for measuring size distributions of NPs. Zeta Cuvettes (a) and size cuvettes (b) used are shown in the Fig 34:

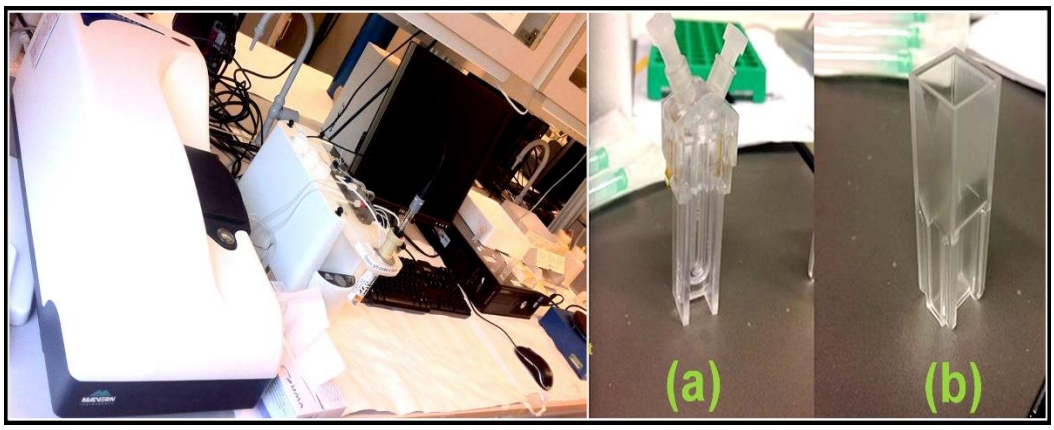

Figure 34: Malvern Zeta sizer instrument with Zeta (a) and Size (b) cuvettes.

2.2.6 Refractometer:

Refractometer (RI) measures *n* of a solution. It is measure of light refracted, scattered or passed through solution under concentration. RI described by the following equation;

$$\boldsymbol{n = \frac{c}{v}}$$

Where *c* is the speed of light in vacuum and *v* is phase velocity. Water refractive index is 1.333 which means light travels 1.333 times quicker in vacuum compared to that of water. Here RI's alginate and $CaCl_2$ solutions were measured using ARAGO refractometer. It has built in sample loading well[148]. Image of the instrument is shown here Fig: 34.

Figure 35: Refractometer.

2.2.7 Scanning Transmission Electron Microscope, S(T)EM:

S(T)EM is a robust technique used for ultra-magnification of nanomaterials. In S(T)EM, beam of electrons are emitted by electron gun focused by optical lenses before they pass through the sample. Objective lens is the main lens which focuses electrons onto the sample and important for quality of capturing images[137]. Scan coils installed within the instrument helps in creating a high magnified image by scanning over the sample.Fig:32 shows the anatomy of S(T)EM.

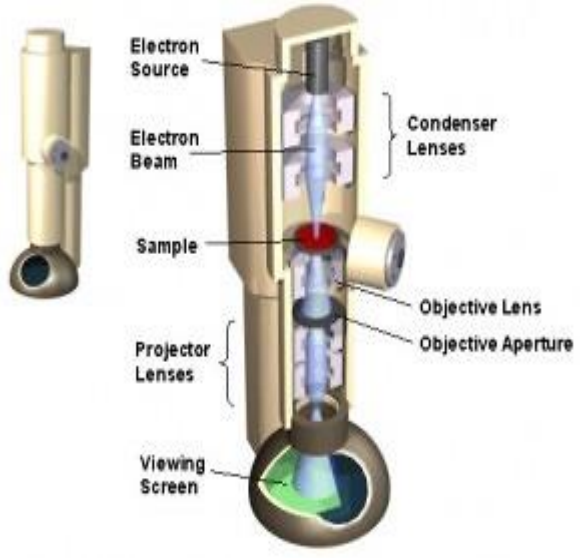

Figure 36: Schematic image of S(T)EM machine

To produce NP images, Hitachi S-5500 S(T)EM is used which is installed at NTNU NanoLab facility. Samples are set down on C-coated copper TEM grids and placed on the standard sample holder before placing it in the instrument. Flashing and measuring conditions were fulfilled before performing microscopy.

2.3 Methods:

2.3.1 Alginate Gelation Setup:

With an aim to optimize the concentrations of both alginate and $CaCl_2$ solutions that cause gelling, different aqueous solutions of sodium alginate and calcium chloride with varying concentrations were made. The detailed weights and volumes used for making the different solutions can be found in the Appendix 1.

A total sample volume of 3 ml was kept constant for all the experiments performed using UV- Vis Spectrophotometry and viscometry (0.1 ml aqueous solution of sodium alginate and 2.9 ml aqueous solution of calcium chloride). Before reaching these optimized volumes for both the solutions, different experiments were performed as outlined in Appendix 1.

In all employed techniques to study gelation, alginate solution were added to the $CaCl_2$ solution as shown in Fig 35: Ca^{2+} ions are ideal in this method because of their nontoxicity, cheap availability and they have mild ionic strength in order to produce gel [30]. Following are some of the experiments which are performed based on moles of $CaCl_2$ and alginate (Table 1).

Table 1: $CaCl_2$ – alginate molar ratio

$CaCl_2$ Conc. (mg/ml)	**Moles of $CaCl_2$**	**Alginate Conc. (mg/ml)**	**Moles of alginate**	**Mole ratio ($CaCl_2$ to Alginate)**
7.35	0.00014502	0.25	$7.812x10^{-1}$	1.86×10^{5}
7.35	0.00014502	0.50	1.562×10^{-9}	9.28×10^{4}
7.35	0.00014502	0.75	$2.344x\ 10^{-9}$	$6.19x\ 10^{-4}$
7.35	0.00014502	1.00	3.125×10^{-9}	4.64×10^{4}
14.7	0.000290039	1.00	3.125×10^{-9}	9.28×10^{4}
29.4	0.000580079	0.25	7.812×10^{-1}	7.43×10^{5}
29.4	0.000580079	1.00	3.125×10^{-9}	1.86×10^{5}
100	0.001973058	1.26×10^{-3}	$3.95x\ 10^{-12}$	5.00×10^{8}
200	0.003946115	2.53×10^{-1}	7.893×10^{-10}	5.00×10^{6}
300	0.005919173	3.79×10^{-3}	1.184×10^{-11}	5.00×10^{8}
0.7	$1.382\ x10^{-5}$	8.84×10^{-1}	2.78×10^{-9}	5.00×10^{3}
0.7	$1.382\ x10^{-5}$	8.84	2.78×10^{8}	5.00×10^{2}
1	1.973×10^{-5}	2.30	$7.175x\ 10^{-9}$	2.75×10^{3}
1000	0.019730576	1.26 x 10-3	3.947×10^{-12}	5.00×10^{9}

After series of experiments, three concentrations of both alginate and $CaCl_2$ were chosen for further studies which are given in Table 2:

Table 2 : Optimized concentrations for alginate gelation.

Solutions	**Alginate concentration (mg/ml)**	**$CaCl_2$ concentration (mg/ml)**	**Mole ratio ($CaCl_2$ to alginate)**
A1-C1	8.84×10^{-1}	0.7	5.00×10^{3}
A2-C2	2.50×10^{-1}	200.0	5.00×10^{6}
A3-C3	1.26×10^{-3}	1.00×10^{3}	5.00×10^{9}

It is to be noted here that in all experiments alginate solution was added into $CaCl_2$ solution to cross link the alginate network. Fig 46 shows the scheme of reaction.

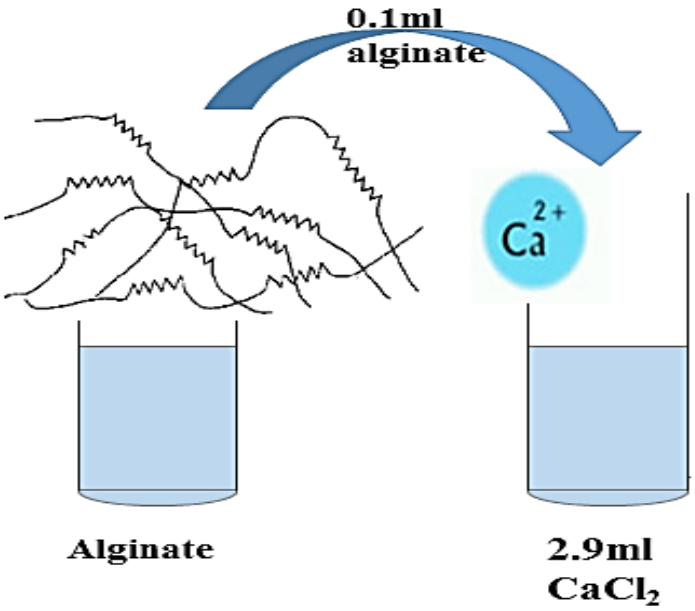

Figure 35: 0.1ml of alginate was reacted to 2.9ml volume of $CaCl_2$ under normal room conditions.

2.3.2 NPs synthesis:

2.3.2.1 Synthesis of Iron Gold NPs:

Fe@Au synthesis procedure was adapted from S. Bandyopadhyay et al.[149]. 10 ml of 10mM solution of sodium citrate was added to 5mg of already synthesized iron (Fe) NPs available with Ugelstad Laboratory. Then this mixture was sonicated for 2 hours at 80^{o}C to form citrated adsorbed Fe NPs.

Thereafter, 10 ml of 1.5 mM solution of chloroauric acid ($HAuCl_4$) was added to the brown solution of Fe NPs. The reaction temperature was maintained at 75^{o}C. After 9 minutes, the brownish color of the solution turned into purplish red. At the end of the reaction (20 minutes), the solution was cooled to room temperature and purified using centrifugation at 14500 rpm for 20 minutes. The Fe@Au NPs solution were re-dispersed in 10 ml of MQ. Concentration of Fe@Au NPs were found out by simple weighing methods. Synthesis scheme of Fe@Au NPs is given by the Fig: 36.

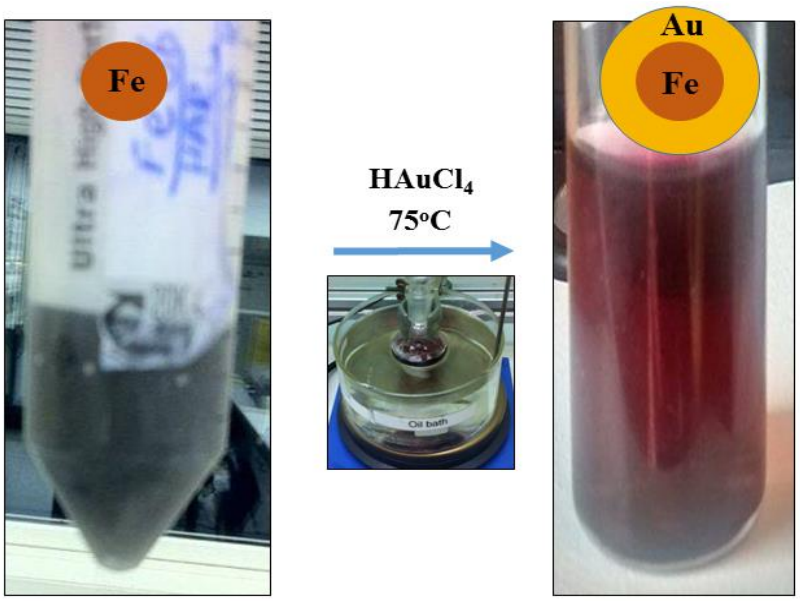

Figure 36: Fe@Au NPs synthesis setup

2.3.2.2 Functionalization with Polyethylene glycol (PEG):

In order to obtain PEG coated Fe@Au NPs, 2 mg of PEG-SH were dissolved in 5 ml of Fe@Au NPs of 1 mg/ml concentration. The reaction mixture was stirred for 1 hour at room temperature at 500rpm. Thereafter, this mixture was centrifuged at 10000 rpm for 20 minutes Fe@Au@PEG were obtained. These were re-dispersed in 5 ml of MQ water. PEG binds to the gold surface via SH bonding, it is a thiol group and has greater affinity for gold [150].

2.3.2.3 Functionalization with Polylysine (PL):

PL solution of 0.1mg/ml concentration were made. 5 ml of 1mg/ml Fe@Au NPs were centrifuged at 14500 rpm for 20 minutes and then supernatant was discarded. Then 2.5 ml of PL solution was mixed in these Eppendorf tubes containing Fe@Au NPs with 2.5 ml of MQ water. Then this mixture was poured into a vial and the solution stirred for 2 hours. After 2 hours, this mixture was centrifuged again at the same frequency of rotation. Now PL functionalized Fe@Au_PL NPs were obtained and re-dispersed into MQ water of same volume (5ml). Scheme of NP functionalization is shown in fig 37. Experimental setup was at neutral pH.

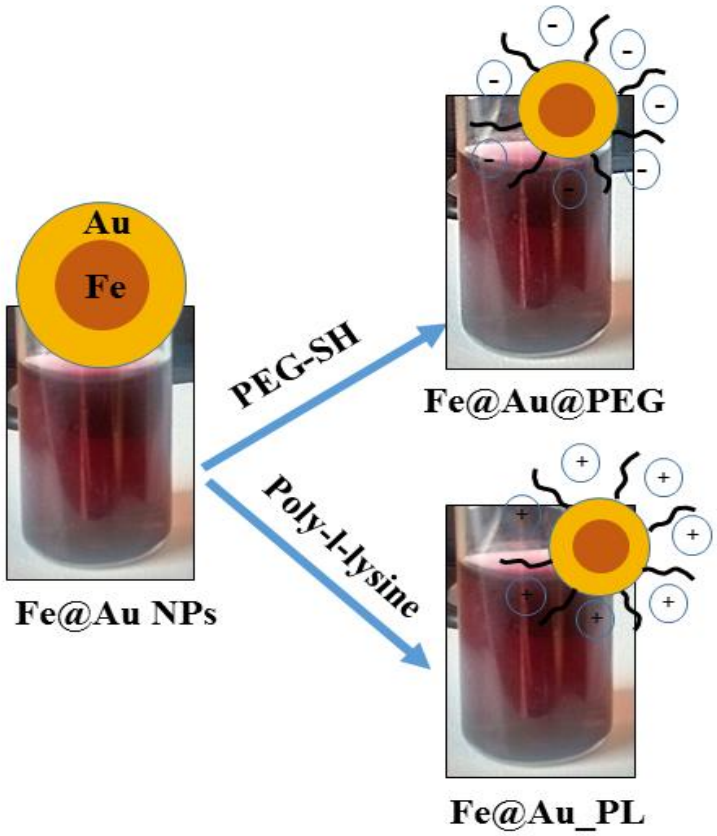

Figure 37: Functionalization of Fe@Au NPs into Fe@Au@PEG, Fe@Au_PL

2.3.3 Incorporation of NPs with alginate:

Three types of NPs were used to bind alginate i.e. Fe@Au, Fe@Au@PEG coated & Fe@Au_PL coated NPs. 1.5 ml of NPs taken from each particle type having NP concentration of 1 mg/ml and centrifuged at 14500 rpm for 20 minutes in minicentrifuge using Eppendorf tubes. NPs were obtained after discarding the supernatant. Then 0.5 ml of alginate was added to the NPs and then shaking was done for 2 hours. This procedure has been done for other each NP type and alginate concentration. After shaking, 0.1ml of this solution (which now contain alginate incorporated with the NPs) is used to react with 2.9ml of respective $CaCl_2$. 2mg/ml concentration of each NP types has also been made and then alginates are incorporated by similar procedure. Schematic diagram (Fig.38) shows the procedure.

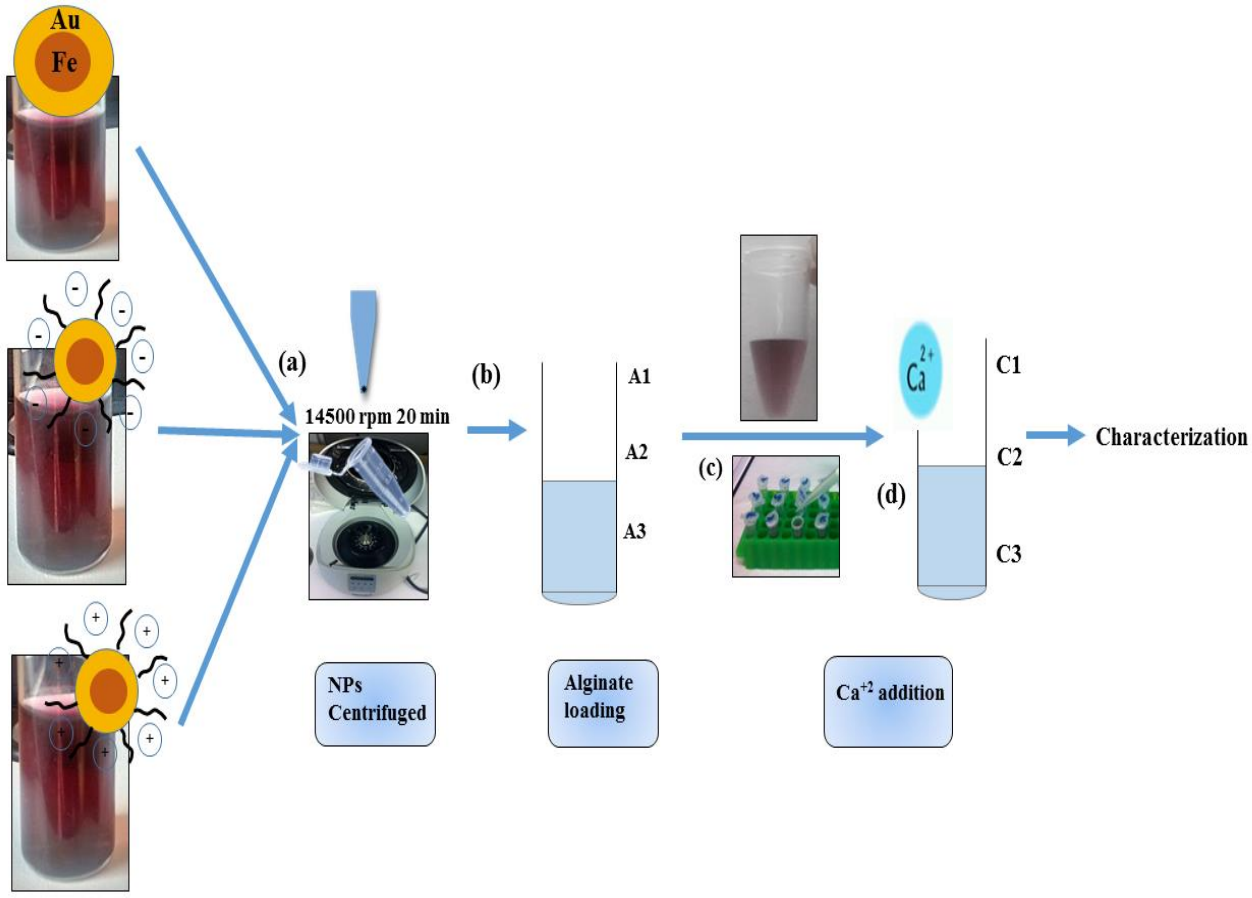

Figure 37: Scheme of NP incorporation with the alginates.

2.3.4 Loading:

2.3.4.1 Fluorescein sodium salt:

Fluorescein is used as fluorescent tracer in studying pathology of Blood Brain Barrier and spinal cord in lab animals[151],[152] .Its molecular weight is 376.27 and occurs in powder form. It is soluble in water with a solubility limit to 1 mg/ml. Its excitation fluorescent wavelength is 460nm and emission wavelength is around 515 nm. Its chemical formula is as follows:

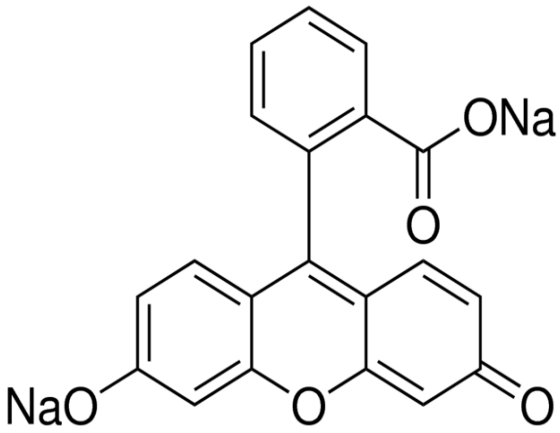

Figure 38: Chemical Formula of Fluorescein sodium salt[152].

2.3.4.2 Fluorescein dye optimization:

Fluorescein sodium salt was used in order to check it's loading and binding with NPs. For calibration, different concentrations of dye were used.0.8mg/ml solution of dye was finally chosen to perform further experiments. Dialysis tube experiment was done to check the permeability and diffusion of dye at intervals of time. 3 ml volume of dye was filled in the tube and immersed in the beaker containing de-ionized water. Time study has been done in order to see the release of investigate molecules into the water. UV. Vis spectroscopy was done to check the fluorescence intensity of the dye in the tube after lapse of every 2 hours. After every 2 hours water in the beaker was replaced with de-ionized water. It was done to ensure that greater amount of dye must release into water without attaining equilibrium. With lapse of time, water in beaker started turned to yellowish green. Three methods are employed in order to investigate the loading of fluorescein dye. Their detailed scheme is described below (Fig 40, 41, 42). All the methods of loading mentioned were investigated using Spectrofluorometer.

2.3.4.3 Fluorescein Dye Loading:

2.3.4.3.1 Method 1- Dye@NPs@Alginate:

1mg/ml and 2mg/ml concentrations of Fe@Au NPs were made. 1. 5 ml volume was taken from each concentration type and centrifuged to get the particles at the bottom of Eppendorf tube (a). 0.5 ml of fluorescein dye (0.8mg/ml) was added to the NPs and shaking was done for 2 hours (b). This procedure was repeated in order to get 1 ml total volume of dyed NPs in the tube for dialysis experiment(c). After 2 hours of shaking, dyed 1mg/ml and 2mg/ml NPs were transferred in separate tubes and immersed in the beaker containing water for dialysis. This experiment was done in order to obtain NPs with bound dye in the tube and free dye must diffuse out into the water. After 10 hours of dialysis dyed NPs were obtained which were introduced with 3 concentrations of alginate solutions (d). 0.5 ml of alginate mixed with dyed NPs making a total of 6 solutions of varying concentrations (e). They were shaken for 2 hours. 0.1ml of this mixed solution containing dyed NPs and alginate were reacted with 2.9ml of $CaCl_2$ in order to gel the alginate (f).Schematic is process flow diagram is given below (Fig 38)

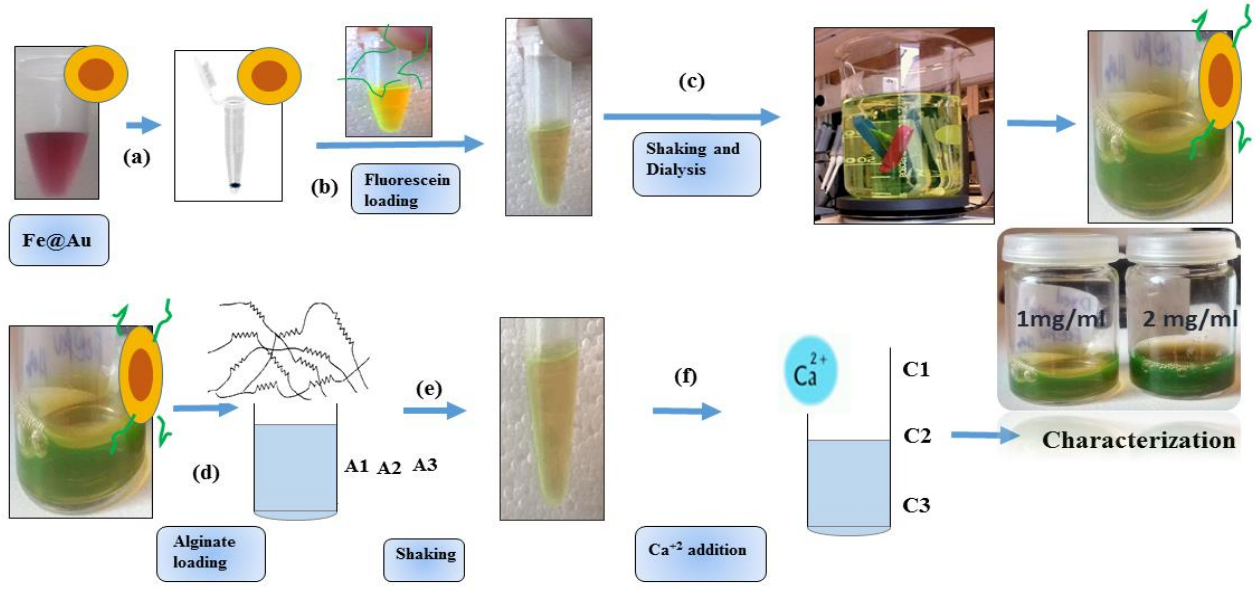

Figure 39: Scheme of dye loading Method 1 in steps (a),(b), (c). (d), (e), (f).

2.3.4.3.2 Method 2 – NPs@Alginate@Dye:

Fe@Au NP solutions were centrifuged in Eppendorf tubes to get NPs and allowed to mix with 0.5ml of alginate solutions. 6 solutions were made. They were shaken for 2 hours. And then 0.5ml of fluorescein dye (0.8mg/ml) has been added to the all the 6 tubes. Again they were shaken for two hours. Then they were filled dialysis tubes to remove the unbound dye. After 10 hours of dialysis, the solutions from tubes were transferred in vials. 0.1ml of this solution containing alginated NPs containing bound dye were mixed with 2.9ml of $CaCl_2$ to cause gelation of alginate.

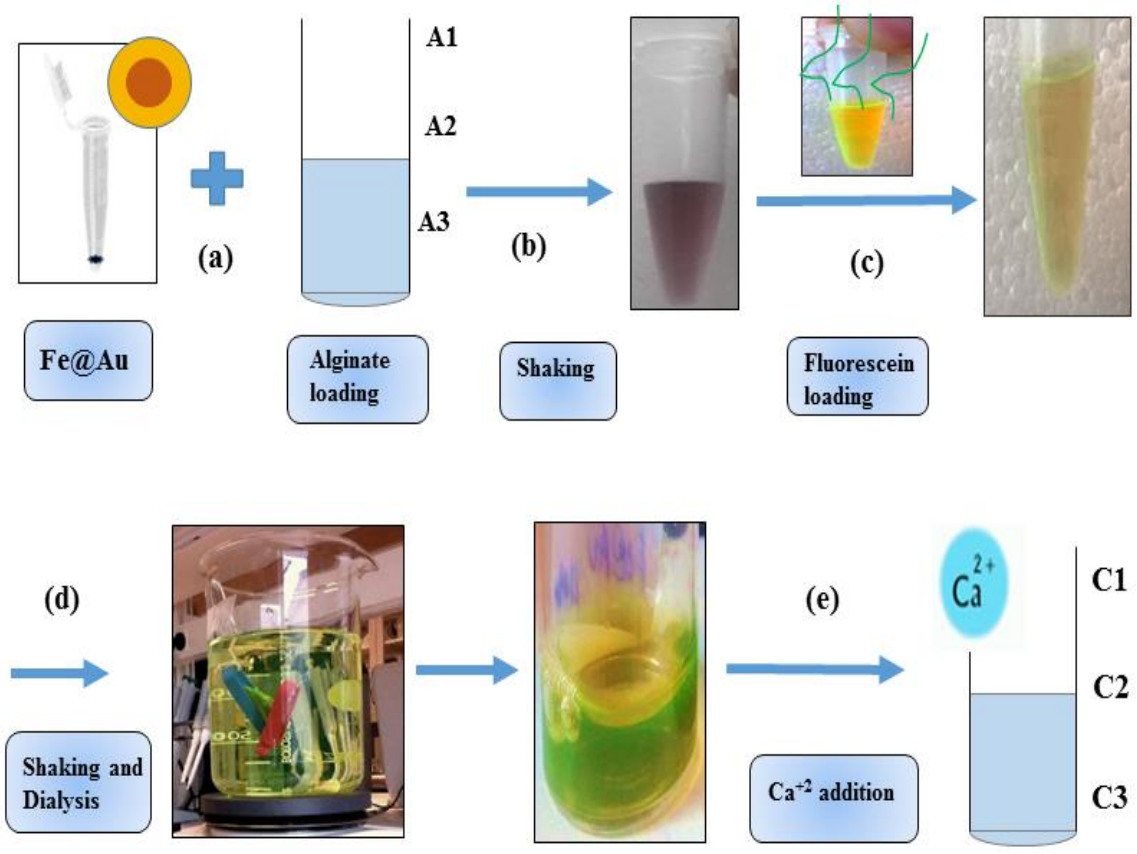

Figure 40: Schematic of dye loading method 2.

2.3.4.3.3 Method 3- Alginate@Dye@NPs :

0.5 ml of each alginate solution was mixed with 0.5 ml of fluorescein dye and they are shaken for 2 hours. After shaking, these 6 solutions were transferred in dialysis tubes for dialysis study. After 10 hours of dialysis, the free dye unbound to alginate diffused out from the tube into the beaker. NPs were centrifuged and alginate containing dye were allowed to mix with NPs. This system was shaken for 2 hours. 0.1ml of this solution containing dyed alginate containing NPs were reacted with 2.9ml of $CaCl_2$ to cause the G blocks of alginate to gel.

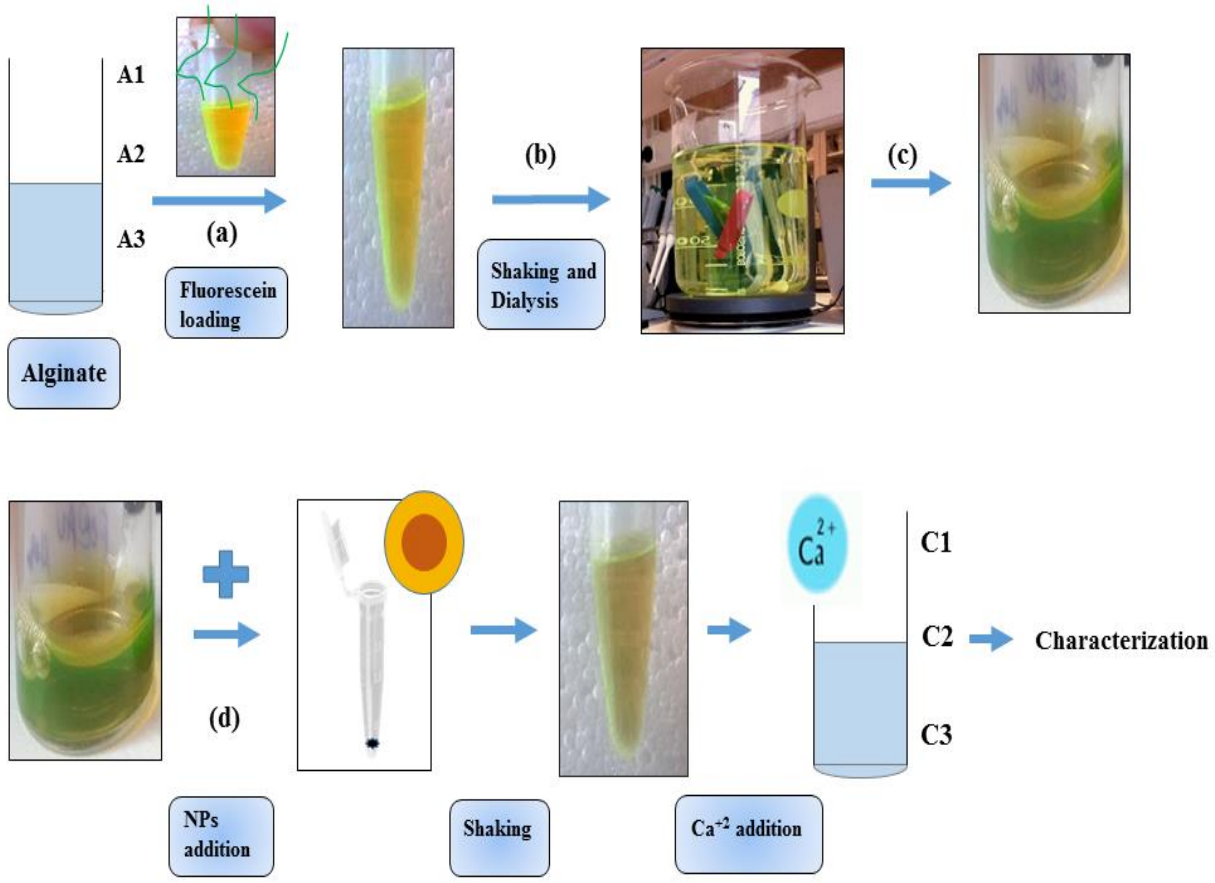

Figure 41: Dye loading Method 3.

2.4 Release:

Dyed@NPs@Alginate (Method 1) system was used to release the dye from the system. 1mg/ml and 2mg/ml dyed Fe@Au NPs were used with three samples of calcium-alginate, in total 6 solutions were investigated for release.

0.1ml of Dyed@NPs@alginate were reacted with 2.9 ml $CaCl_2$ to cause gelation of alginate. Dyed NPs were proposed to be embedded in their network. Simple diffusion method was adapted to diffuse the dye based on concentration gradient. 3ml of water was added to each (3ml) solution and stirring was done at 90 rpm. in room conditions. Characterization was done after time intervals using spectrofluorometer. Release setup can be shown in Fig 42:

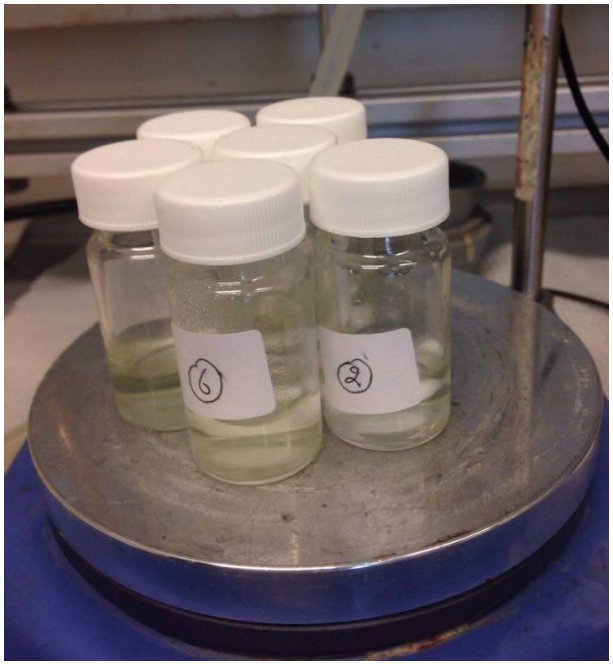

Figure 42 : Diffusion Release setup

3 Results & Discussion:

The aim of this project was to optimize and investigate alginate/NP hybrid systems for drug delivery applications. Here, gelation phenomenon of alginate at lower concentrations is studied and its interaction with Fe@Au NPs. Thereafter, loading and release of fluorescein dye from these alginate/NP systems have also been investigated. In the subsequent sections, first, alginate-Ca2+ systems have been investigated to understand the gelling phenomenon at low concentrations. Following their optimization, different NPs are characterized and incorporated into the gel networks. After successful incorporation, to further understand the behavior of such systems, three specific alginate-Ca2+ systems are studied. Interaction of fluorescein with these systems are then outlined in the next section. Finally, different combinations of NP-alginate-dye are synthesized and studied for gelation and loading of the dye. In the last section, using one of these optimized methods, diffusion-based release of the dye is described.

3.1 Alginate Gelation:

In order to understand the phenomenon of gelation, several concentrations of alginate and $CaCl_2$ solutions with varying volumes have been mixed. Characterization of $CaCl_2$ and alginate was performed before and after mixing the solutions to notice observable changes.

Initially, UV-vis spectroscopy was employed to characterize the alginate-$CaCl_2$ systems. In the measurement range (200nm to 1100nm), no absorbance peak was observed for the samples (Fig 41). The UV-Vis results from these solutions are summarized in Appendix 1. Refractive indices of alginate $CaCl_2$ mixtures were also measured using refractometer, but no significant change was observed. Refractive index of these solutions were nearly the same value as of water i.e.1.331. (Appendix 2).Thus, it was inferred that neither UV-vis spectroscopy nor refractometer could be used to detect the subtle changes in these systems owing to the low concentration range where the experiments were performed in comparison to other studies[16] [153] [154].

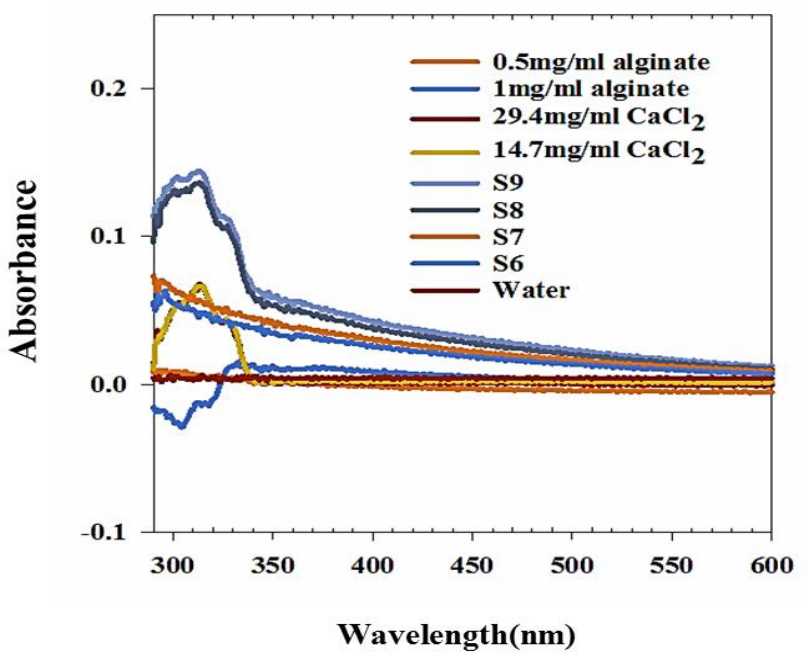

Figure 43: Individual solutions of alginate & CaCl2 with their mixtures showing no absorbance by UV-Vis spectroscopy.

Thereafter, fluorescence spectroscopy was used to study gelation of these systems. Characterization has been performed by varying excitation wavelength, slit width, and relative volumes of $CaCl_2$ and alginate solutions. Temperature was kept constant at 25^oC for all the measurements. Different excitation wavelength with varying slit width results are shown in (Fig 44). On exciting the solutions at 480 nm, fixing excitation slit width at 5mm and emission slit width at 3mm low intensity of counts were measured by spectrofluorometer. (Fig 41-a) Similar trend was observed at 495nm excitation (excitation slit width 5mm- emission slit width 3mm).Very low intensity count number and disturbed signal between water and $CaCl_2$ was obtained (Fig 41-b). On exciting the solution at 400nm with excitation slit width fixed at 5mm and emission slit width fixed at 5mm, intensity count increased significantly but it was observed that water and solution signals were indistinguishable (Fig 41-c). The excitation wavelength was then fixed at 280nm with excitation and emission wavelength 5mm slit width-3mm slit width respectively. It was observed that on this excitation emission signal was maximum and peak was consistent with all the initial experiments performed. At 280 nm excitation, other slit width were also tried. But slit 5-3 slit width for excitation and emission respectively was selected for further experiments. Since these curves obtained did not show any shifts with changes in dilution.

Characterization on the basis of relative volumes of alginate and $CaCl_2$ was also done in order to observe any change in the emission signal. Alginate solutions were diluted and reacted with the respective $CaCl_2$ and it was observed that there is successive emission drop on diluting the alginate. Since the emission signal did not saturate the detector under experimental conditions and there was no change in line shape of the emission spectra upon successive dilution, exciting these solutions at 280nm was found to be ideal for our solutions. (Fig 42.)

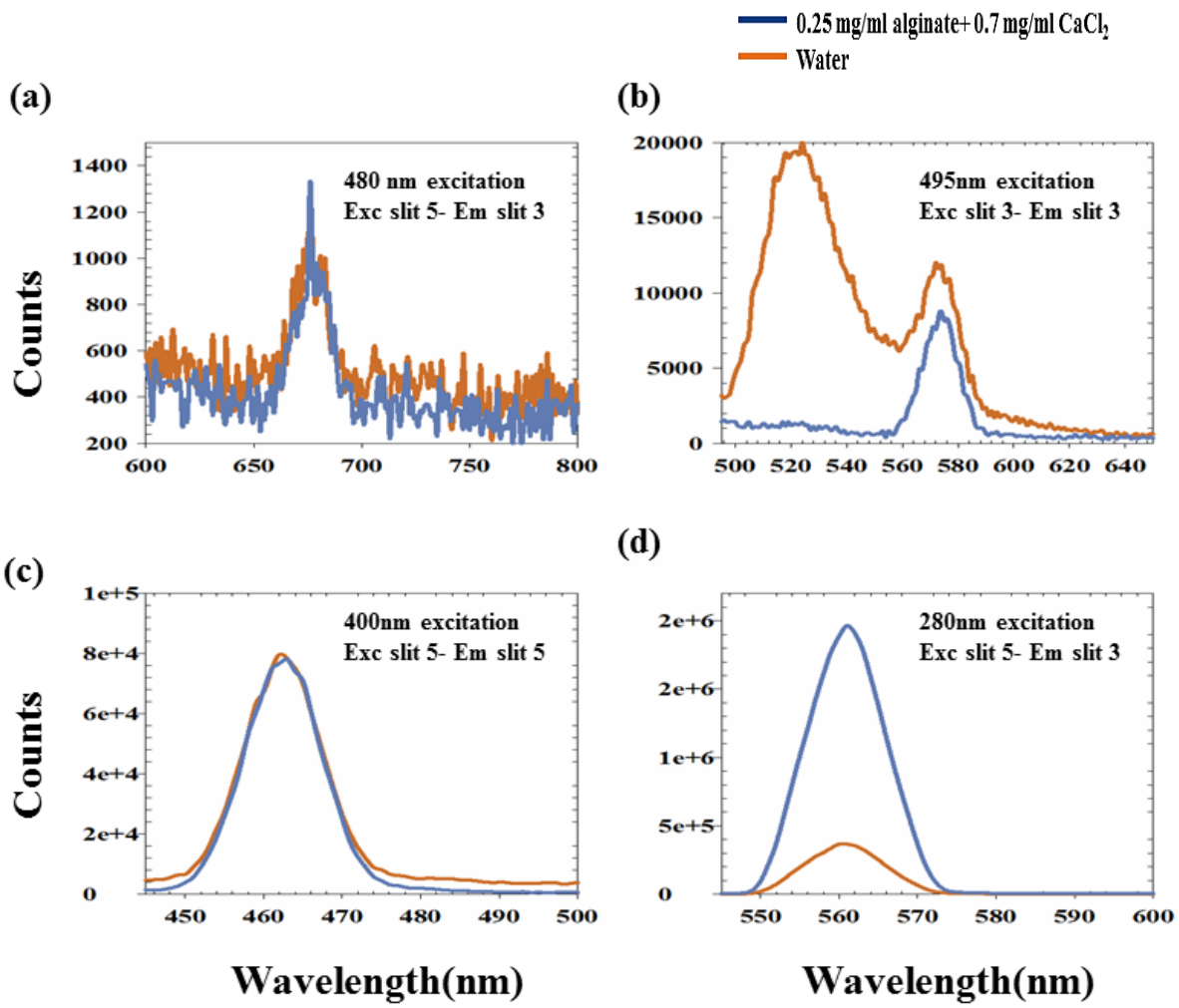

Figure 44: Excitation at 280 nm (d) yield consistent peak while at other excitations wavelengths distorted emission spectra were obtained for 480nm, 400 emitted high intensity but solution signal was not comparable with water. Lower counts were obtained for & 495 nm excited solution. Slit width were fixed to 5mm for excitation and 3mm for emission which better suited 280nm excitation signal.

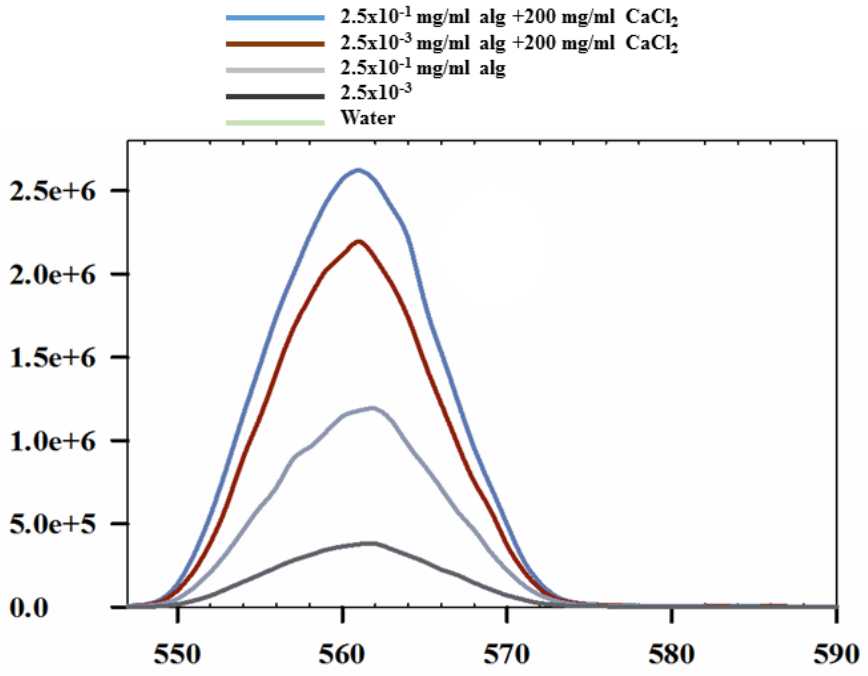

Figure 45: Alginate-$CaCl_2$ emission peaks lie on the same wavelength even after diluting alginate keeping the calcium concentration constant. By diluting the alginate, peak drop can be observed.

On exciting the samples at 280 nm, consistent emission spectra were obtained for both $CaCl_2$ & alginate in the emission range 545nm-575 nm (Fig: 46). Fluorescence spectroscopy has shown consistent peaks of Alginate $CaCl_2$ mixtures using the same solutions measured in UV-Vis as previously shown in Fig 41. Gelation studies were then continued by using spectrofluorometer. In order to get optimized concentrations and understand alginate gelation, several samples with varying concentration of $CaCl_2$ and alginate were characterized.

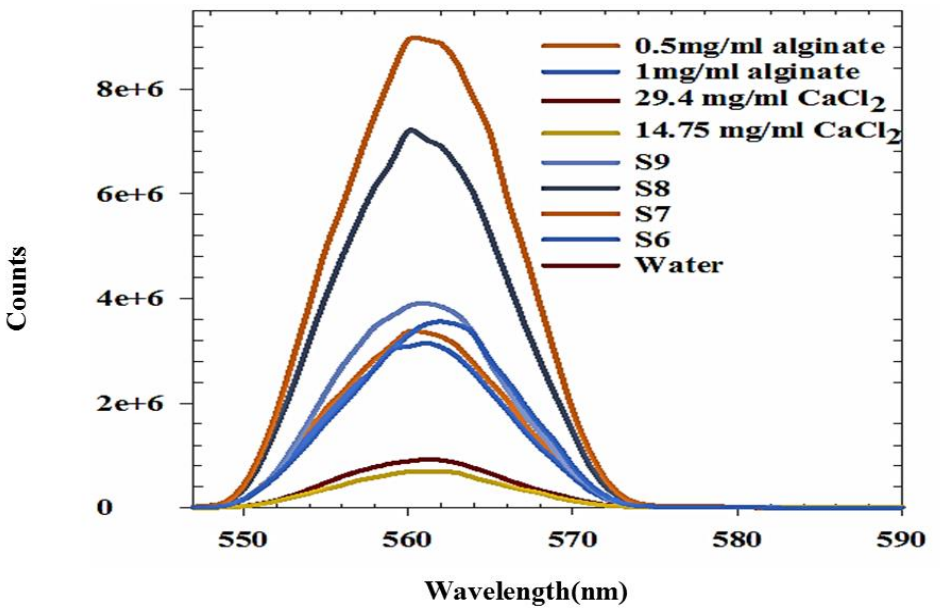

Figure 46: Spectrofluorometer spectra, showing the emission spectra from 545-575 nm range with solutions of $CaCl_2$ and alginate.

It was found that upon mixing alginate with $CaCl_2$, there is gradual rise in emission peaks (545nm – 575 nm) with increasing $CaCl_2$ concentration. Sample volumes were then fixed as 0.1 ml of alginate solution to react with 2.9 ml of $CaCl_2$ solution. 3 ml of MQ water was measured. Further studies were performed by keeping the alginate concentration fixed and varying the $CaCl_2$ concentration.

Firstly, 0.25 mg/ml alginate was reacted with each of three different concentrations of $CaCl_2$. 0.7 mg/ml, 14.7 mg/ml and 29.4mg/ml. Results showed the increase in emission peak of gelling solution with increase in calcium concentration. Fig: 47 shows the result. In graph (a), it can be seen that upon addition of 0.7 mg/ml $CaCl_2$ emission of mixture solution rises to an intensity count of $2.1x10^4$ at 560 nm peak. When concentration of $CaCl_2$ increased to 14.7 mg/ml, the peak emission count rose to $3.6x10^4$. On reacting 29.4 mg/ml $CaCl_2$ with 0.25mg/ml alginate, count number went up to $5.3x10^4$ which was intensity count at 560 nm peak. This consistent rise in the emission peak upon increasing $CaCl_2$ by keeping alginate constant confirms that calcium is responsible for this notable change in emission spectrum.

Similarly, alginate concentration was increased to 0.75 mg/ml with the same $CaCl_2$ solutions 0.7, 14.7 & 29.4 mg/ml. and similar trend been observed. On adding 0.75 mg/ml alginate to 0.7 mg/ml $CaCl_2$ emission peak count was recorded as 4.2 X 10^4 which further increased to 5.2 X 10^4 on addition of 14.7 mg/ml $CaCl_2$.When 29.4mg/ml was reacted with alginate, emission peak count of this mixture solution was recorded as 5.9 X 10^4. This further confirmed that calcium ions are responsible for inducing structural changes in the monomers of alginate, especially G blocks.

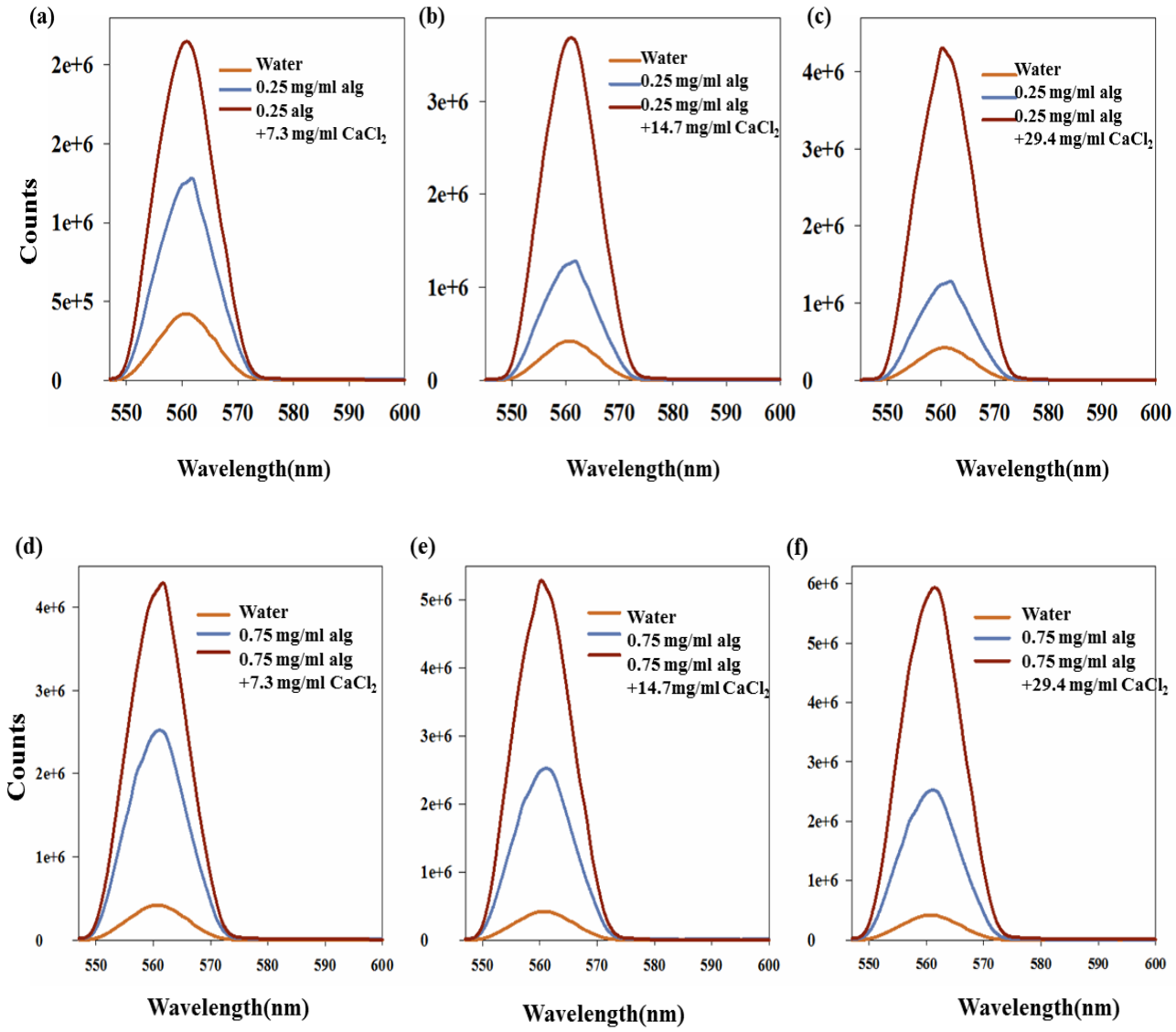

Figure 47: 0.25mg/ml alginate: Increase in the emission peak can be observed from left to right (a,b,c) with increase in $CaCl_2$ concentrations. 0.75 mg/ml alginate: Increasing calcium concentration from left to right (d), (e), (f), and increase in emission was observed.

Lesser calcium ions in the alginate system will yield lesser dimerization of G- blocks. As it is reported in previous studies that egg box has four G units which chelates with a single calcium ion [17, 155]. M blocks can act as terminator of dimerization of G units due to their flatter structure which is unable to nest divalent cations [156].So upon increasing the concentration of calcium ions in alginate, we are increasing the possibility that more G units will be dimerized to form complex 3D network.

Different $CaCl_2$ concentrations (0.7, 14.7 &29.4 mg/ml) were fixed and plotted against 0.25 mg/ml alginate and 0.75 mg/ml alginate. Increasing trend in emission was observed which are represented in Fig 48.

These preliminary studies showed that observable signals in the emission range vary consistently as a function of Ca^{2+} and alginate concentrations. From here on, spectrofluorometry was used as the characterization technique for understanding alginate-Ca^{2+} systems.

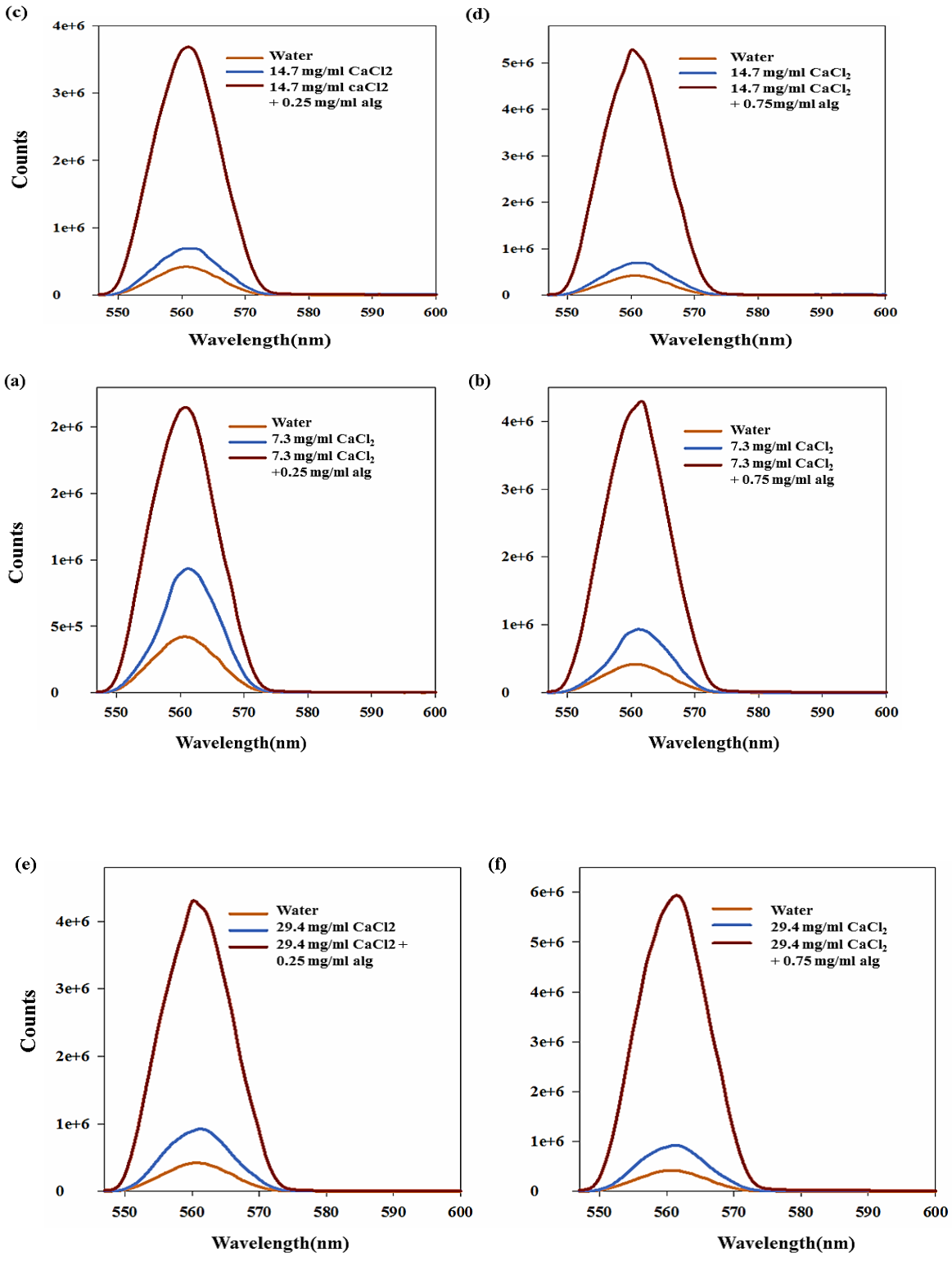

Figure 48 : $CaCl_2$ concentrations were fixed with varying alginate concentrations (a), (b), (c), (d), (e) & (f). Evident rise in the emission spectrum of alginate-$CaCl_2$ mixture (Emission 545-575nm).Peak value 560nm.

3.1.1 Gelation Phases:

Preliminary results confirmed that increasing calcium ions in the system bind to available G blocks to form aggregates of polymer network. More solutions of alginate and $CaCl_2$ were made in order to identify different phases by which alginate forms gel. $CaCl_2$ concentrations were increased during this part of study.

In order to identify the subtle changes happening in the system, area under the emission curve (545nm-575nm) was calculated for each of the systems described above. Sigma Plot Macros function was used to measure area under the curves. Calculated areas of different solutions were than plotted against respective solutions to see any observable change. No meaningful trend was observed by plotting the area under the curves as shown in Fig. 49 (a). To better understand how these systems behave, the individual samples were replaced with mole ratios (ratio of moles of Ca^{2+} to alginate).It is to be noted that from here onwards, the mole ratio is always plotted on log scale. With an increase in the mole ratio, an initial decrease in the area is obtained followed by a local minimum and thereafter the area increases. The area under the curve indicates the number of gelled units as well as micro-aggregate formation. At this point, it was not possible to ascertain in which range gelling is dominant and if the nature of the curve is a monotonic decrease with random fluctuations or one that has a local minimum. Hence, it was decided to definitely conclude the results using the same samples with viscometry – a technique that is more efficient in understanding gelling systems at low concentrations. The results are reported in subsequent sections.

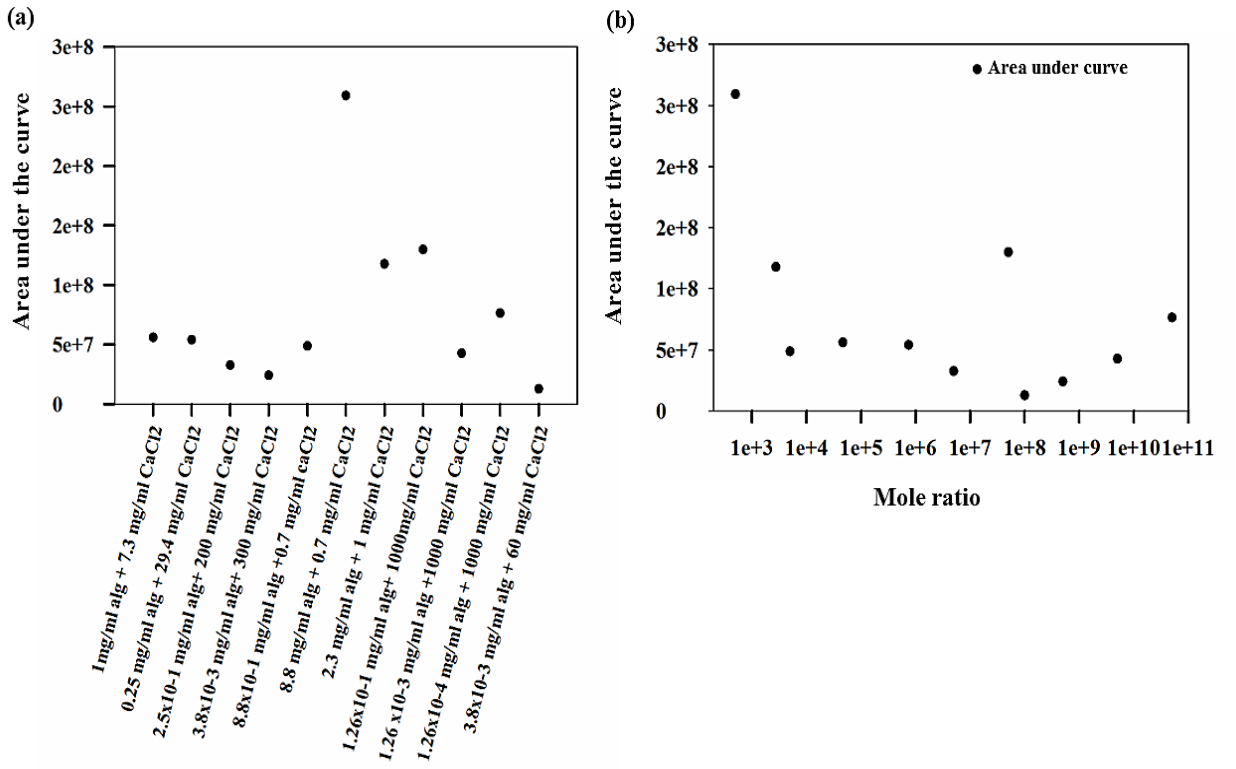

Figure 49: Left (a) graph showing an invalid representation of area. Whereas on right (b) log.Mole raio against area provides a meaningful representation of increase in area with respective molar ratio

3.1.2 Viscometry:

Viscometer measures flow time of different solutions and helps in calculating the intrinsic viscosity. In Ubbelohde capillary viscometer, **tW** was calculated as the flow time of water (3ml). Alginate and $CaCl_2$ mixture were added and the time flows of respective $CaCl_2$ and alginate before and after mixing them were measured using automated stopwatch **'t'** is the flow time measured which is of mixture containing both $CaCl_2$ and alginate whereas flow time of $CaCl_2$ and alginate were termed as **tC** and **tA** respectively. The results from Ubbelohde viscometer showed a similar trend with rise in time of the solutions with increasing $CaCl_2$ concentration which can be evident from the results shown in Fig 50 that increasing $CaCl_2$ in the system is responsible for increase in flow time of respective $CaCl_2$ **(tC)** and subsequent increased flow time of mixture solution **(t)**.Automated stop watch attached to viscometer measures time in seconds. Standard deviation

was also calculated for each value and plotted as error bars on respective scattered points shown in graphs. It can be seen that tC and t values showing an increasing trend which gives the indication that calcium is dominant factor in increased flow rate of alginate mixture. tA values of alginate lie between 94-107 seconds which represents that not much change is happening when you increase the alginate concentration. Red dot denotes micro aggregates gel phase, yellow represents intermediate phase of gelation and green dot denotes complete gelation phase. From now onwards these dots will denote gelation phases

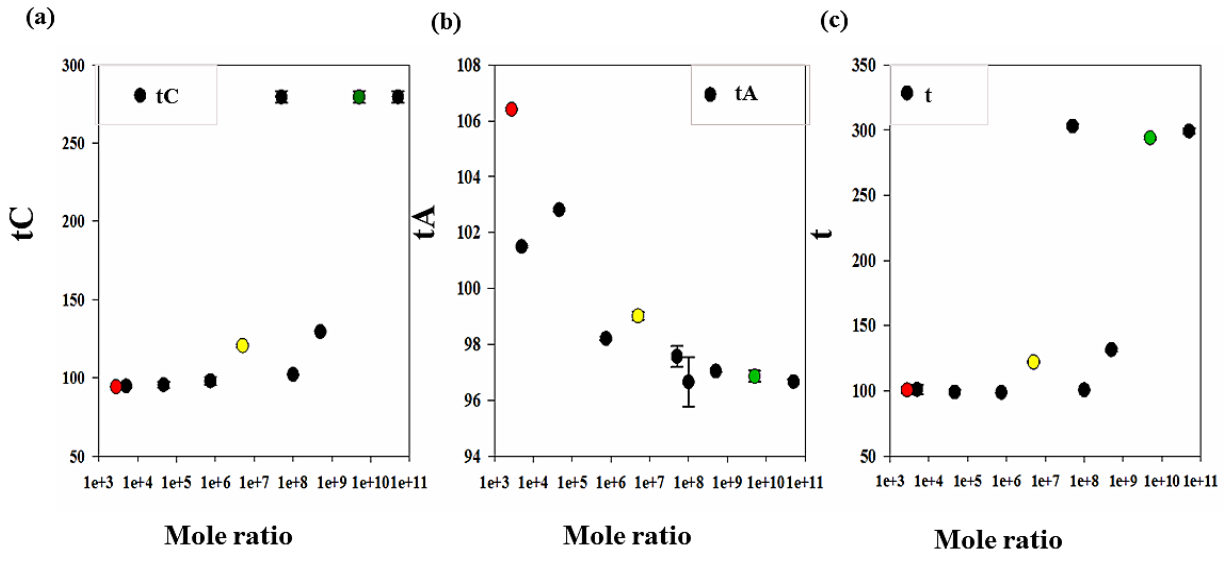

Figure 50: Viscometer Time Flow: (a), (b) showing time flow of CaCl2 and alginate respectively plotted with error bars against respective molar ratio. (c) Represents the mixture solution which shows similar trend with tC, which describes increased aggregation in polymer network by increasing calcium ions.

Further working data set was normalized, **t** values were divided with the respective **tA** and **tC** values in order to understand more about the system (Appendix 2). It is to be noted here **t** values corresponds to the mixture of $CaCl_2$ and alginate with volumes of 2.9ml and 0.1ml respectively. To measure **tC** 2.9ml of $CaCl_2$ were added with 0.1 ml of water and measured. Similarly, 0.1ml of alginate with 2.9ml water corresponds to measure of **tA**. Whereas **tW** is time flow of 3ml water. By dividing t values with respective constituents, nature of solution can be estimated. Equation (a) shows that by dividing **t** with **tW,** cancels the effect of water which is pure solvent in all the solutions. Therefore, it is possible to compare **t/tW** with **t.** Both **t** and **t/ tW** were plotted and

similar trend was observed (Fig 50). Similarly, **t/tC** and **t/tA** describes the nature of solution when we divide t with respective **tC** and **tA** as shown in equation (b) and (c). $\boldsymbol{\eta_{mw}}$ describes the relative viscosity of mixture w.r.t to water. It corresponds to t/tW measurements. Whereas $\boldsymbol{\eta_{ma}}$ describes the relative viscosity of mixture w.r.t. alginate which gives the same meaning as t/tA. Relative viscosity of mixture w.r.t. $CaCl_2$ is denoted by $\boldsymbol{\eta_{mc}}$ which corresponds to t/tC measurements performed. Equations derived from the viscosity data sets are briefed below:

Equation (a): describes relative viscosity of mixture w.r.t. water.

$$\boldsymbol{\eta_{mw}} = \frac{\boldsymbol{t}}{\boldsymbol{tW}} = \frac{\textbf{Flow time of 2.9ml CaCl2 + 0.1 ml alginate}}{\textbf{Flow time of 2.9ml water + 0.1ml water}}$$

Equation (b) describes relative viscosity of mixture w.r.t. alginate

$$\boldsymbol{\eta_{ma}} = \frac{\textbf{t}}{\textbf{tA}} = \frac{\textbf{Flow time of 2.9ml CaCl2 + 0.1 ml alginate}}{\textbf{Flow time of 2.9ml water + 0.1ml alginate}}$$

Equation (c) describes relative viscosity of mixture w.r.t. $CaCl_2$

$$\boldsymbol{\eta_{mc}} = \frac{\textbf{t}}{\textbf{tC}} = \frac{\textbf{Flow time of 2.9ml CaCl2 + 0.1ml alginate}}{\textbf{Flow time of 2.9ml CaCl2 + 0.1ml water}}$$

Afterwards, different approaches were adapted to further analyze the data**, tC** and **tA** were divided with each other, which gave the same meaning as of **t** and **t/tW**. Equation (d) explains that **tC/tA** is the measure of mixture solution cancelling the effect of water from the system.

Equation (d) describes relative viscosity of $CaCl_2$ w.r.t. to alginate

$$\eta_{ca} = \frac{\mathbf{tC}}{\mathbf{tA}} = \frac{\mathbf{0.1ml\ water + 2.9ml\ CaCl2}}{\mathbf{0.1ml\ alginate + 2.9ml\ water}}$$

Equation (e):

$$\frac{\left|\left(\frac{\mathbf{t}}{\mathbf{tW}}\right) - \left(\frac{\mathbf{t}}{\mathbf{tA}}\right)\right|}{\frac{\mathbf{t}}{\mathbf{tC}}}$$

.

$$\frac{|\boldsymbol{\eta}_{\mathbf{mw}-}\boldsymbol{\eta}_{\mathbf{ma}}|}{\boldsymbol{\eta}_{\mathbf{mc}}}$$

, which refers to absolute ratios of relative viscosity

Hence it was found that **t/tW** and **tC/tA** were the same mixture systems containing calcium ions bound to G blocks of alginate. Results are compared as follows (Fig 51).

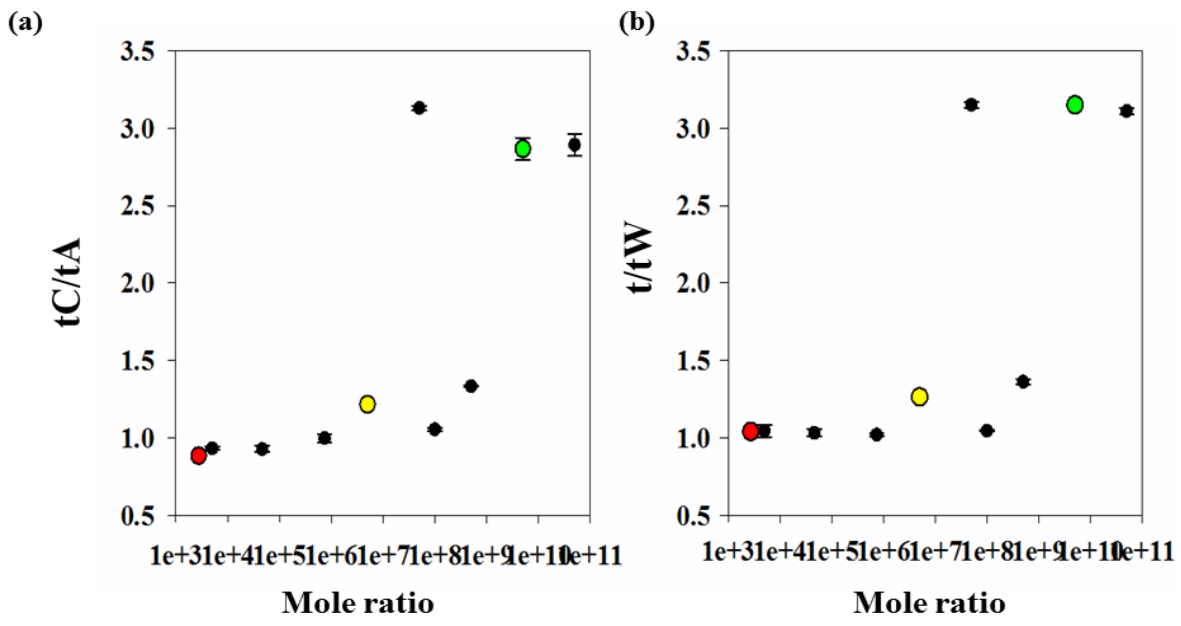

Figure 51: (a) tC/tA, (b), t/tW descibes the same systems of Alginate $CaCl_2$ mixture. From these graphs, different phases of alginate gelation can be explained. Increasing molar ratio w.r.t to calcium concentration increasing the viscosity of the system which becomes evident to say that small aggregates are starting to transform into a 3D gel network.

Both spectrofluorometer and viscometer results, show an increasing trend. Increasing Ca^{2+} in the alginate solution resulted in 4 G- units to come together to accommodate a Ca^{2+} forming egg box [157].More calcium ions yielded more aggregated units leading to formation of gel. The results obtained were divided into three phases of gelation; Micro-aggregates, intermediate and gel phase (Fig 52 (a), (b)).

Equation (e) was used to calculate the effect of gelling networks when compared to the pure alginate solutions. With an increase in the mole ratio (Ca^{2+} to alginate), there is a decrease in the relative viscosity of alginate network based on pure alginate solutions. (Fig 52 (c)The drop in this ratio is indicative of the fact that as Ca^{2+} ions increase, more G blocks dimerize, leading to decreased mobility of the alginate units. This results in reduced mobility and hence, a higher relative viscosity of the gelled networks. It means number of dimerized alginate units are increasing and it is extending into a gelling network

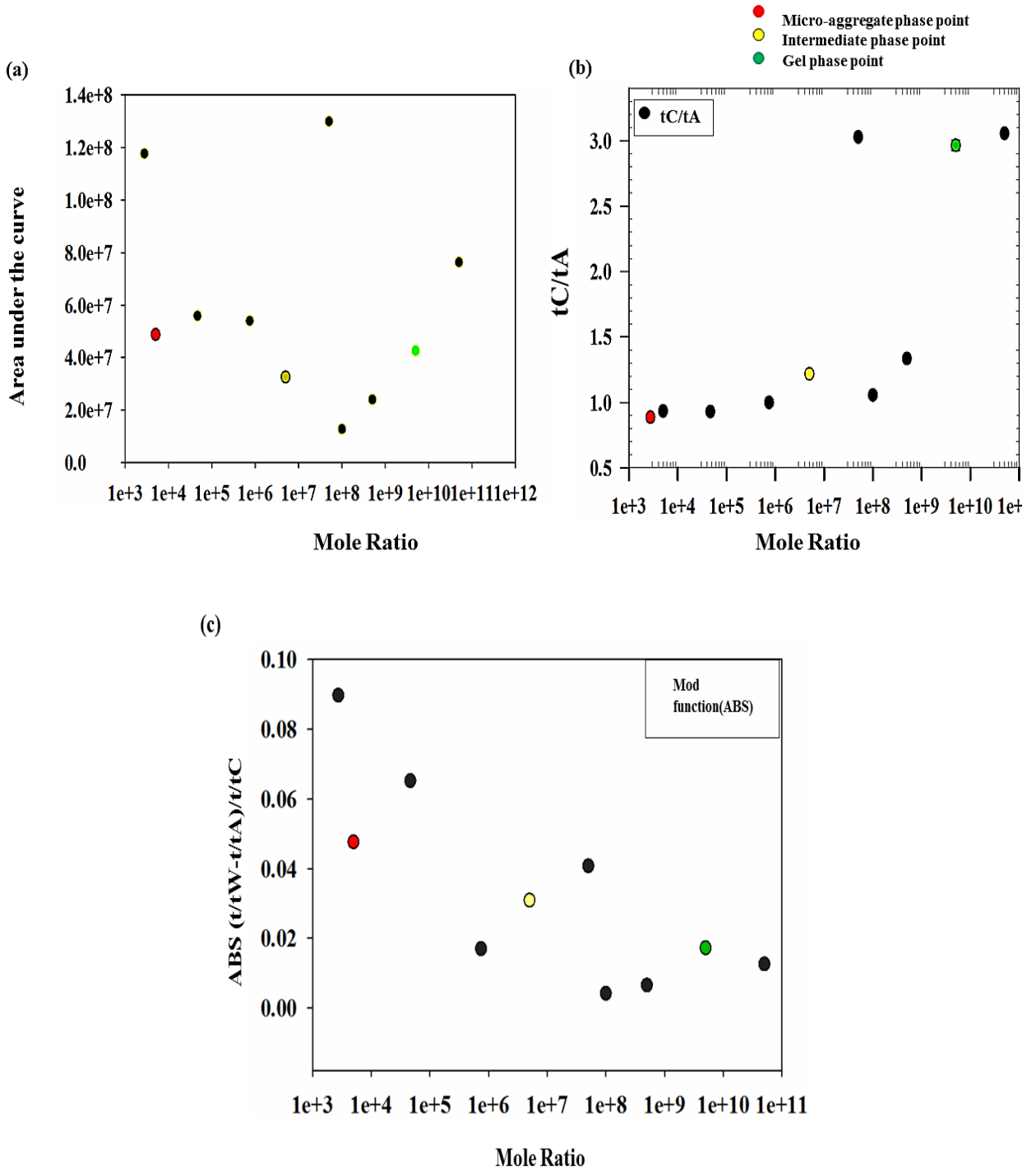

Figure 52: (a) Showing the spectrofluorometer result while on the right (b) shows the viscosity result of tC/tA with different gelation phase points highlighted.(c) shows the mod function of viscosity data showing a decreasing trend means alginate gelling units are increasing with increasing molar ratio.

Three gelling phases were identified and three $CaCl_2$-alginate mixtures from each of these phases were selected for further experiments. A schematic diagram of the process is shown in figure 53.

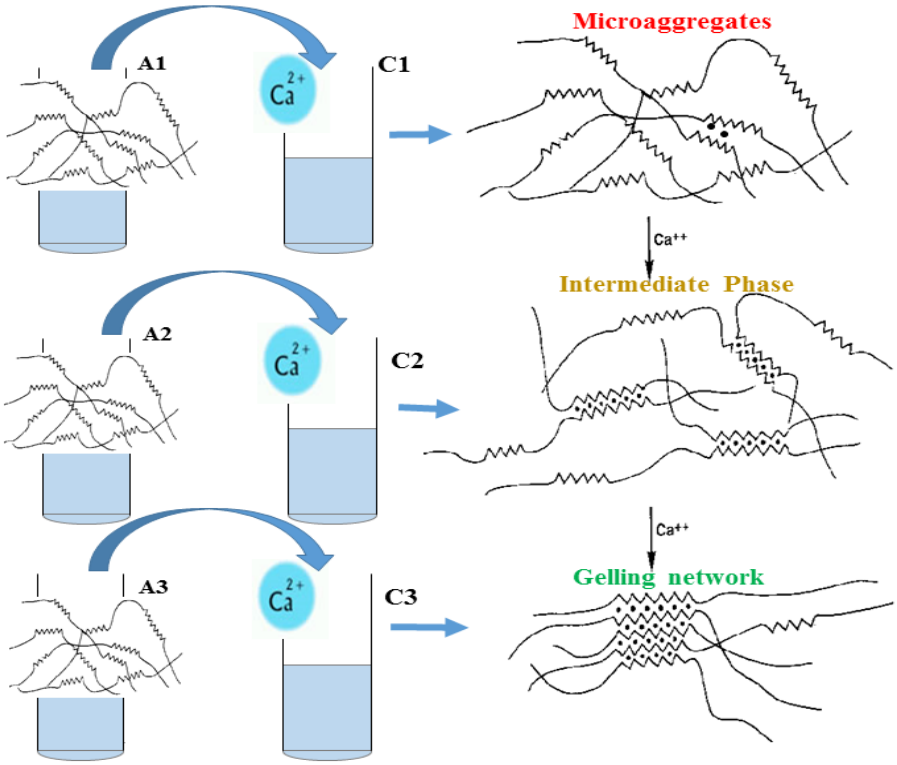

Figure 53: Schematic formation of three phases of gelling alginate.

Identification of three critical phases of alginate gelling was a significant result due to the fact that lower concentrations of alginate were used. Critical overlap concentration of alginate has not been reached and studies were conducted in dilute phase. Alginate having a high molecular weight cannot form gels until any cross linking substance (e.g. divalent cations, Ca^{++}) induces gelation[158]. Micro aggregates formation may have referred as phase of very limited gelation. Here, presence of relatively large amount of alginate with a small amount of calcium yielded small

aggregates which was not be able to form a network due to the shortage of calcium ions. Lower signal in emission spectrum and less viscosities corresponds to the limited aggregation of G units and hence unable to form any complex network[155].

In Intermediate phase, more calcium was introduced to the system, which resulted in more aggregation and more G units were able to dimerize forming a network. In this phase, moderate gelation occurred[159]. In Gel phase, most of the calcium ions were occupied by G units to form a three dimensional network. In this phase, complete gelation of alginate occurred due to the presence of large amount of calcium ions engaging with alginate[157].

Spectrofluorometric emission peaks of these gelling mixtures are shown in figure 54. Huge rise in emission spectrum was observed in gelling condition (c).

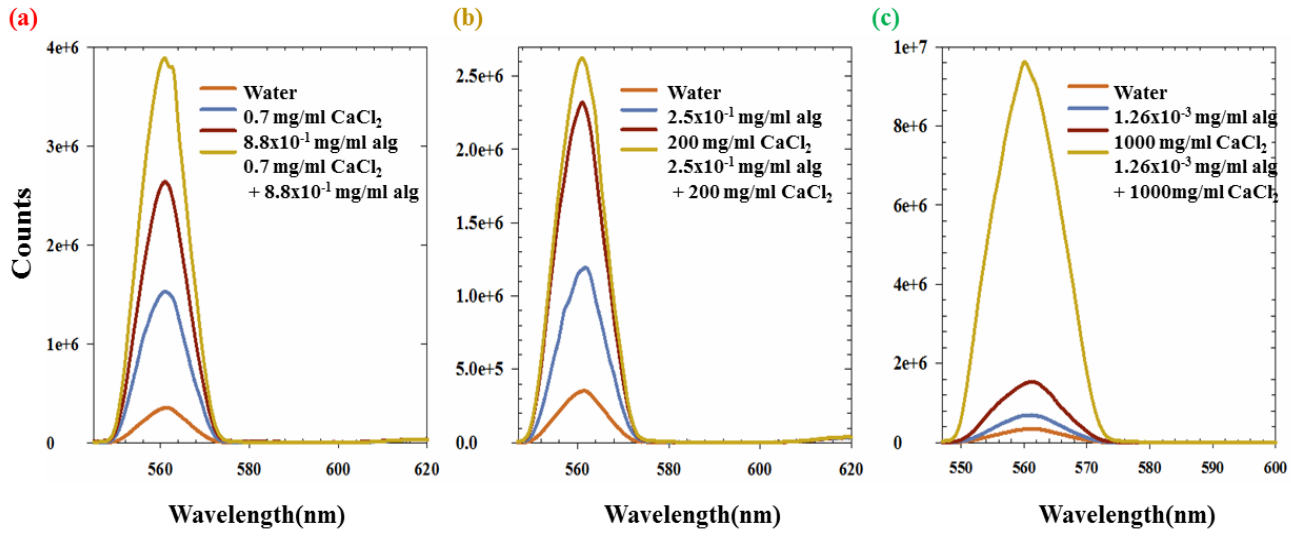

Figure 54: Emission peaks of three mixtures from three phases of gelation.(a) Micro-aggregation, (b)Intermediate gelation & (c) showing a higher emision after addition of large amount of calcium which represents gelation.

In this section, results described that system is behaving as predicted. Increasing $CaCl_2$ concentrations induces gelation in G blocks of alginate. Three phases of alginate gelation were devised. Loading of NPs and afterwards binding of fluorescein dye was performed using these mixtures containing respective concentrations of alginate and $CaCl_2$ determining different phases of alginate gelation.

3.2 Synthesis of NPs & Incorporation in Alginate:

NPs were synthesized in order to investigate loading of NPs in the alginate network. The aim was to check NPs with different coated functional groups binding with alginate. Three types of NP systems (Fe@Au Fe@Au@PEG, Fe@Au_PL) were used with 2 different concentrations to interact with 3 different alginate gel phase conditions.

3.2.1 NP characterization:

Synthesis of NPs are described here in Methods section. Fe@Au, Fe@Au@PEG and Fe@Au_PL were characterized using DLS and Zeta Potential. Functionalization of Fe@Au were observed in U.V Vis and absorbance spectra were obtained. For Fe@Au NPs absorbance peak was at 526 nm which represents the LSPR from gold surface. 526nm absorbance peak was observed for Fe@Au@PEG and 527 nm for Fe@Au_PL NPs. Average Zeta Potential for Fe@Au NP solution was -45 m.V. For Fe@Au@PEG it was recorded as -26 m.V and for Fe@Au_PL the average zeta potential was measured as 27 m.V.

Zeta Potential is important in determining the stability of colloidal solutions. Higher values of zeta potential (negative of positive) determines their stability in the solution. Colloidal systems with lower zeta potential are more prone towards flocculation and coagulations [160]. Here -45 m.V zeta potential was observed for Fe@Au NPs which confirms that their charge is stable .Stability is mainly due to the coulombic repulsive forces among negatively charged NPs due to the presence of citrate ions in the Fe@Au NP solution. Temperature was kept constant at 25^{o}C for all measurements done in U.V Vis, Zeta and DLS.

S(T)EM image of Fe@Au were also obtained and size was compared with the DLS size. DLS measures the diameter at nanometer scale. Average size of Fe@Au measured by DLS was 74nm whereas average S(T)EM size was 23nm. The difference in size is because DLS measures hydrodynamic diameter which is the diameter of NPs present in the aqueous solution. Whereas, NP solutions were first dried and then characterized in S(T)EM which measures dry diameter of the particles. High resolution image of Fe@Au NPs was captured from S(T)EM Fig 55(d).

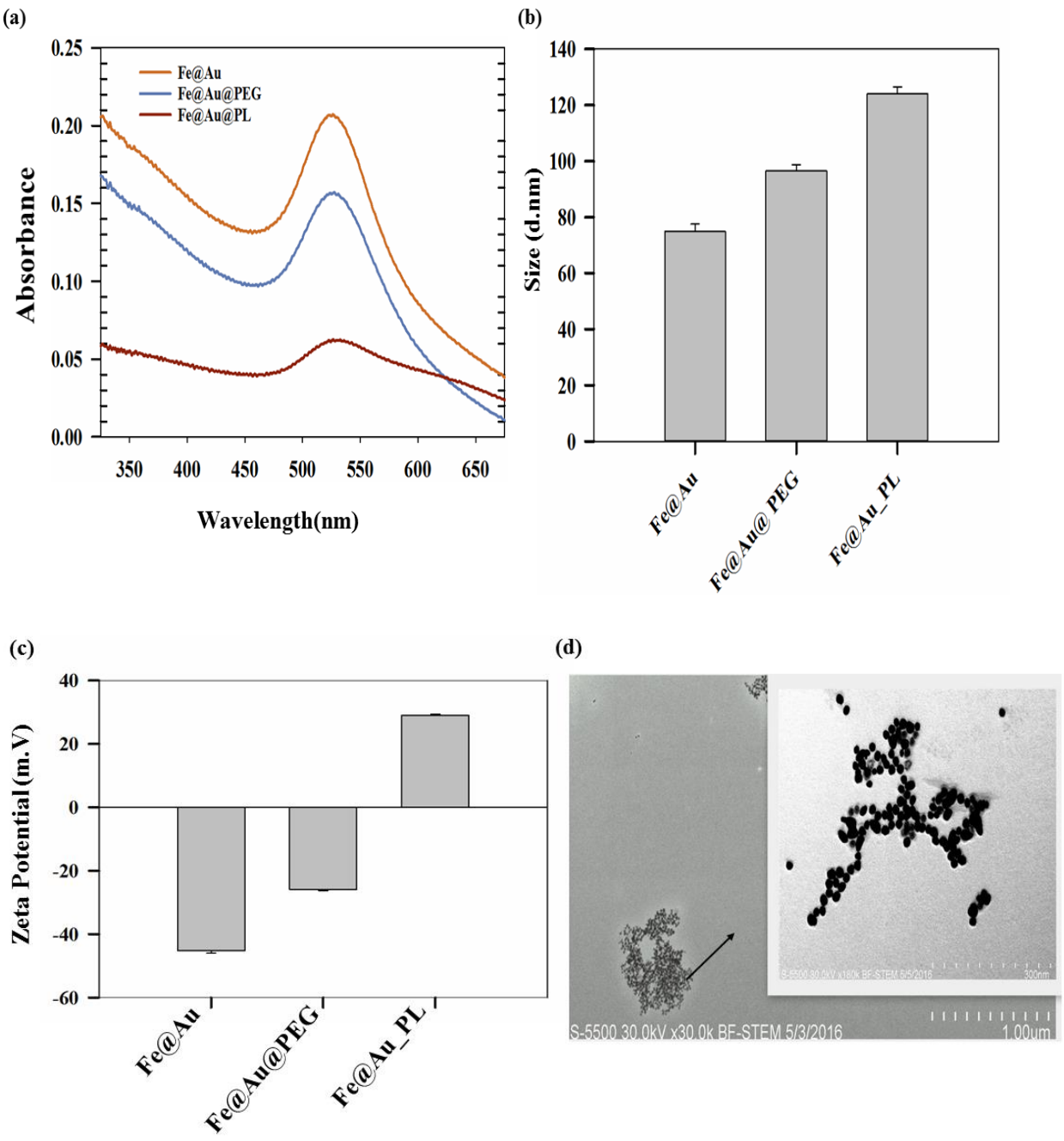

Figure 55: (a) Absorbance peaks of Fe@Au were observed at 526 nm whereas it was 526 and 527nm for Fe@Au PEG and FeAu_PL respectively. (c) showing the Zeta Potential of three NP types. (b) compares the size of Fe@Au which is around 74nm, 96nm and 124nm for Fe@Au PEG & Fe@AuPL respectively. (d) image showing the spherical Fe@Au NPs in S(T)EM.

3.2.2 NPs in Alginates:

To investigate the effect of NPs in alginate networks and to understand the changes in the system by addition of these NPs at micro aggregation, intermediate and complete gelation phases of alginate.

NPs were incorporated in the 3 alginate solutions. Schematic representation of incorporation method is shown in Fig 36. 1 mg/ml and 2mg.ml NP concentrations of each NP type (Fe@Au, Fe@Au@PEG, Fe@Au_PL) NPs were obtained after centrifugation and they are allowed to mix with 3 alginate concentrations. After alginate mixing with NPs, shaking was done for 2 hours so that NPs can bind to alginate. Thereafter this mixture was reacted with $CaCl_2$ and characterization was done using viscometer.

$\boldsymbol{\eta_{ca}}$ and $\boldsymbol{\eta_{mw}}$ values with and without NPs were calculated. A significant change was observed in NP incorporated solutions especially at higher molar ratio. In Figure 56, (a) It can be seen that solutions containing 1mg/ml Fe@Au have higher t/tW values with increasing molar ratio. At micro aggregation, this change is insignificant but as the calcium in the system increases, more G blocks of alginate forms networks leading to incorporation of NPs in the gel network. Significant change can be observed at gelation condition. It can be concluded that gelling units are holding the NPs in the system and subsequent rise in t/tW values can be observed. But it is not evident that how much incorporation has been taken place.Similar trend can be observed in 1mg/ml Fe@Au@PEG (b) and 1mg/ml Fe@Au_PL (c) containing systems. It can also be seen that regardless of NP coating, t/tW values are increasing in similar fashion. Coating of NPs (b),(c) didn't show any difference from naked Fe@Au (a) t/tW values.

NP concentrations were increased to 2mg/ml (Fig 56, (d), (e), (f)) and bind to alginate solutions and characterized before and after addition of $CaCl_2$. Similar trend was observed in t/tW values as that of 1mg/ml NP concentrations (a), (b), (c). It means that only a specific amount of NPs has incorporated in the gel systems and increased concentration of Fe@Au, Fe@Au@PEG and Fe@Au_PL have no influence in changing the viscosity in three phases of alginate gelation.

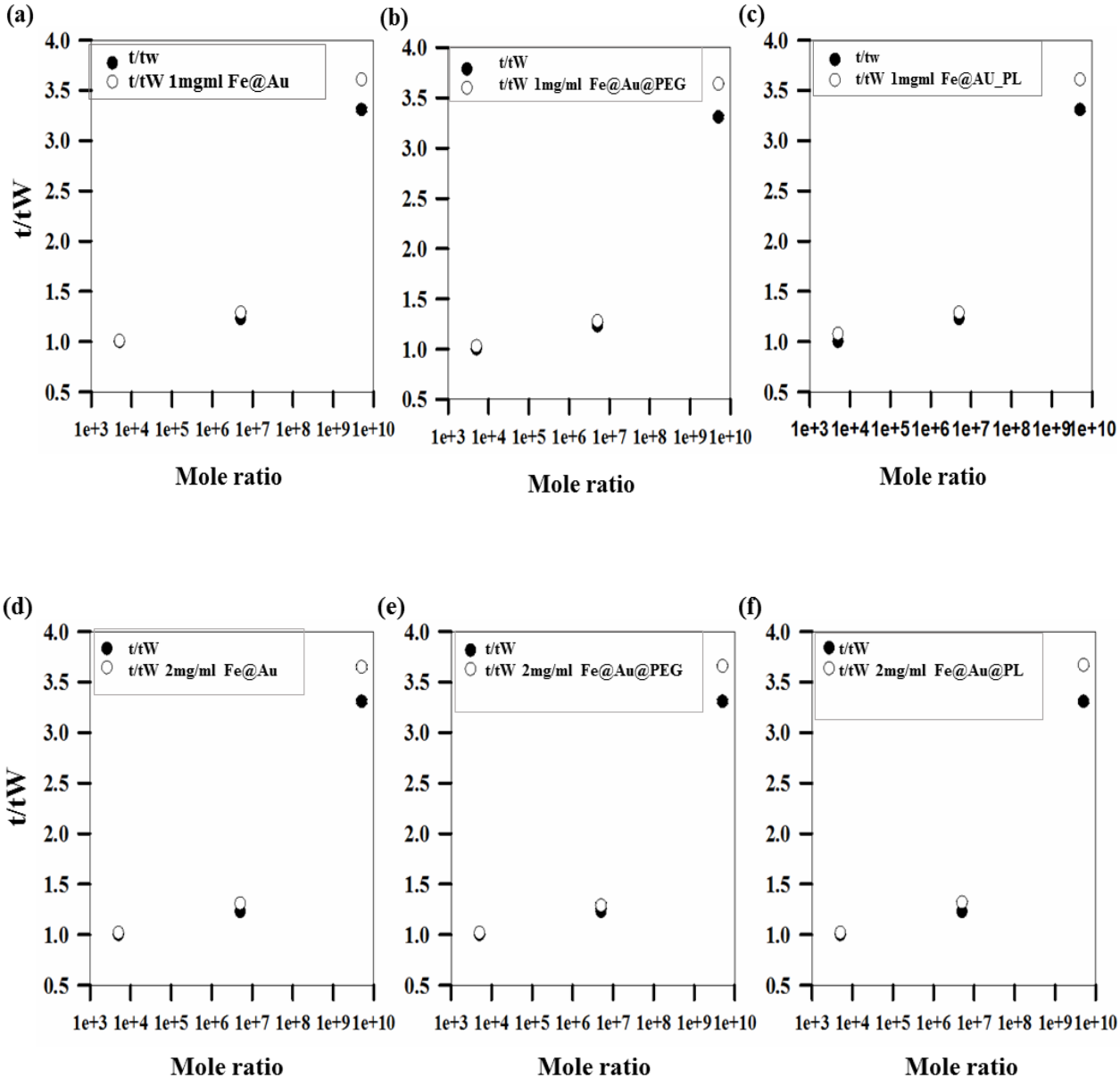

Figure 56: t/tW : (a), (b), (c) graphs represent the t/tW values for 1mg/ml FeAu, Fe@AUPEG and Fe@Au_PL respectively. Similar trend can be observed in t/tW values for 2mg/ml NPs Fe@Au(d), Fe@Au@PEG (e), Fe@Au_PL (f). Oberveable increase in NP containing solutions especially at higher molar ratio.

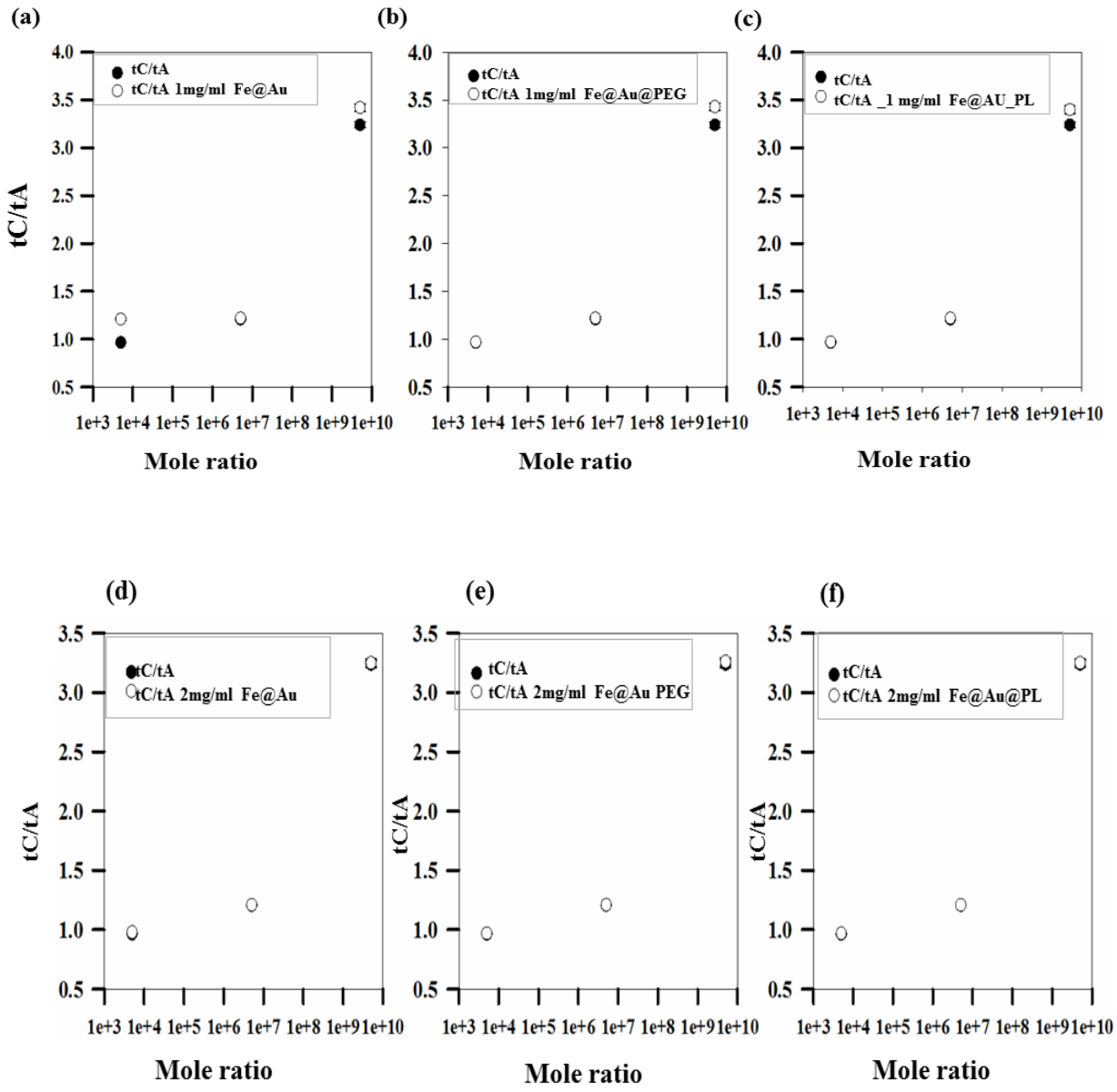

Figure 57: tC/tA for 1 mg/ml NPs are shown in graphs (a),(b),(c) Fe@Au,Fe@Au@PEG, & Fe@Au_PL, observable increase in the tC/tA values at gelling condition. For 2mg/ml NP solutions (d),(e),(f), no signoficant change can be seen which maybe because of their less cooperative binding with the alginate

In graph 57,(a), (b), (c), It can be seen that tC/tA values are increasing with NPs in the system at higher molar ratios. Trend and values lie at the same range as that of t/tW values (Fig 56, (a), (b), (c). But in 2mg/ml NP containing systems (d), (e) (f), the difference is indistinguishable to the

values that are without NPs. It may be due to the reason that NPs have not been able to bind themselves to the alginate network.

By carefully analyzing the data obtained, relative percentage change with respect to $CaCl_2$ was calculated from viscosity values for systems with or without NPs. Mole ratio was plotted on X-axis to see the observable conversion percentage of $CaCl_{2.}$ In Fig 58, (a) showing the change for Fe@Au NP systems with both concentrations compared with systems having no NPs. It can be seen that on calcium conversion percentage is higher for NP concentrations when compared to systems without NPs. Systems with no NPs have 0-1 percentage change with respect to calcium whereas with increasing NP concentrations & at higher mole ratio, 13 % change can be observed. Similar trend was followed for Fe@Au@PEG and Fe@Au_PL containing system observable from graphs (b), (c) respectively.

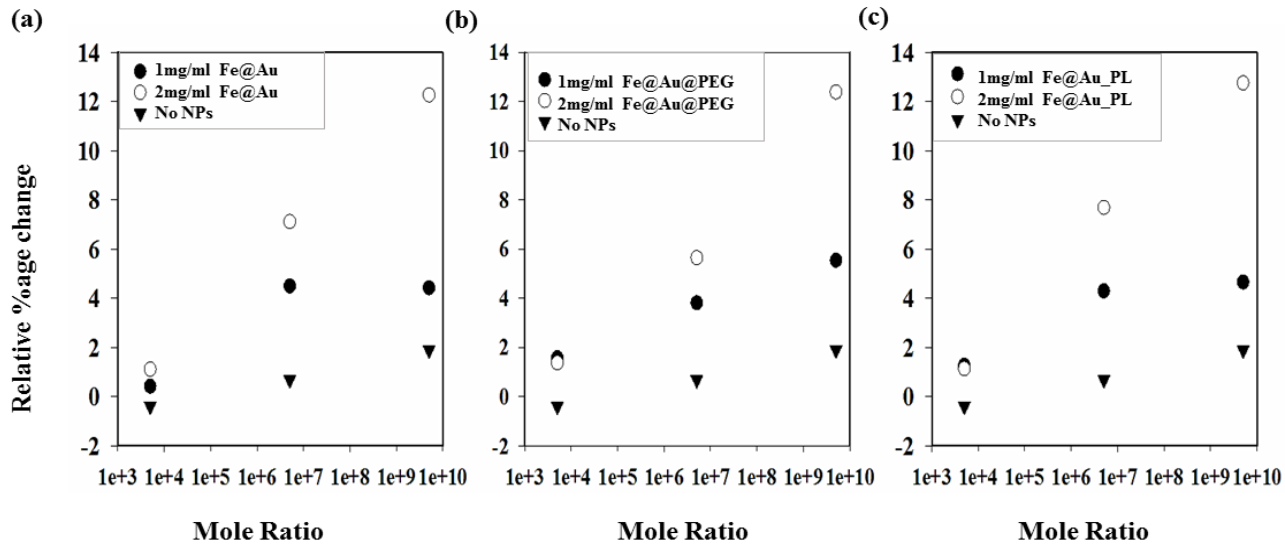

Figure 58: (a) Showing Fe@Au containing alginate system with relative percent change w.r.t. $CaCl_2$, (b) and (c) shows relative percentage change for Fe@Au@PEG, Fe@Au_PL respectively. At higher molar ratio with increasing NP concentrations percentage change monotonically increases.

The results from t/tW and tC/tA values showing no significant change with regards to Fe@Au NP coating with PEG and PL. Hence it can be concluded that incorporation of NPs in the alginate is independent of the nature of coating on NPs. It means that the interaction of alginate with NPs is

nonspecific. Only a small change can be observed at gelling condition in t/tW Figures. Hence in order to understand Alginate/NP interaction in depth more studies were required. Fluorescein dye was used in order to investigate loading phenomenon of these NP/alginate systems.

3.3 Fluorescein dye Calibration & Optimization:

3.3.1 Calibration

Fluorescein sodium salt was used as dye for loading studies. Fluorescein dye was excited at 460 nm with different slit widths Calibration was done by using different concentrations and emission was observed at different slit widths. The calibration curves are shown in Fig 59:

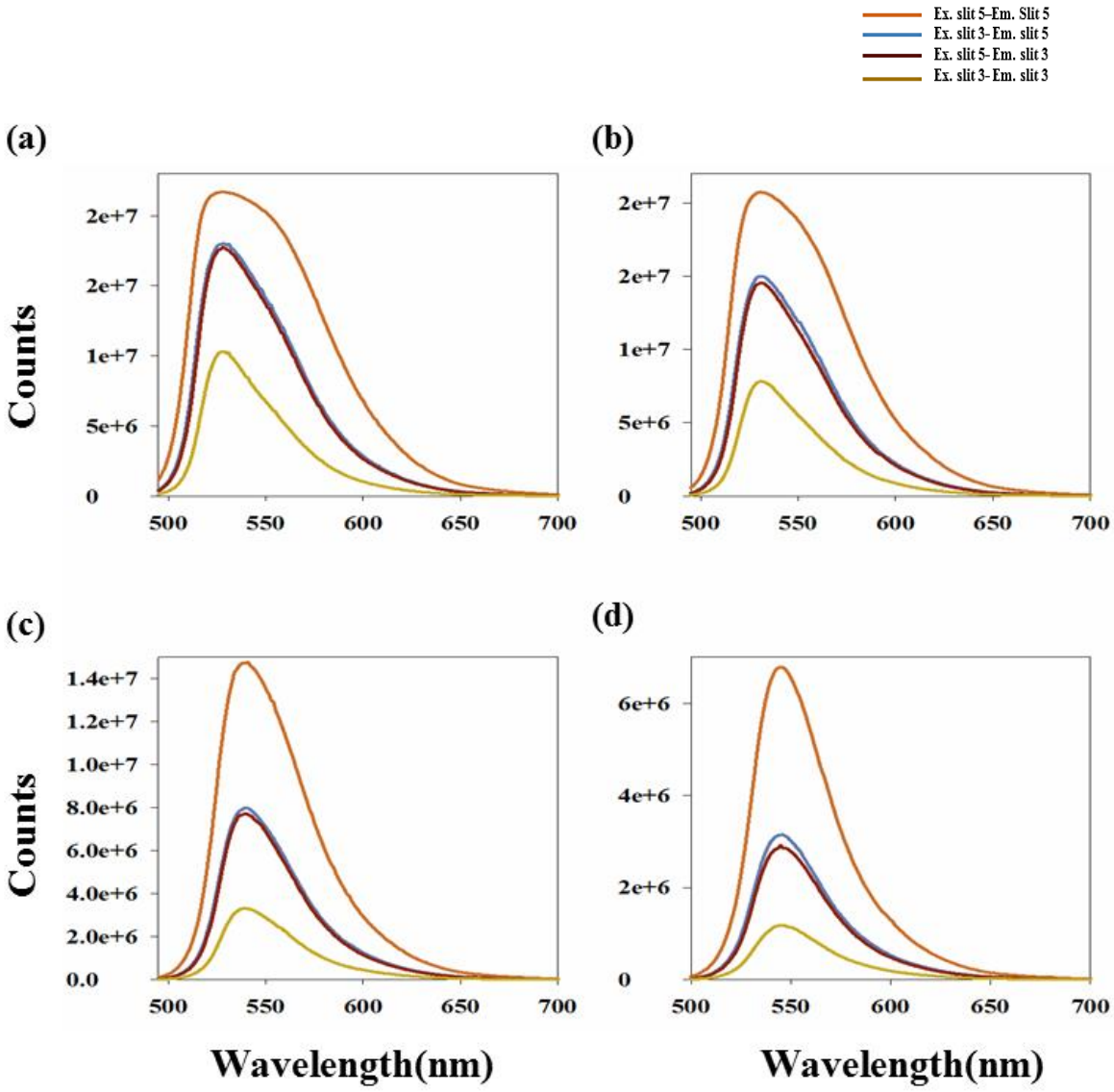

Figure 59: Fluorescein calibration curves with different slit widths. (a) , (b), (c) and (d) showing emission counts of dye for 0.1, 0.2, 0.4 and 0.8 mg/ml respectively.

Emission peaks obtained were in the range from 525nm t0 650nm.Using 0.1mg/ml fluorescein dye the nature of the peaks obtained was broadened by exciting the sample at 460nm at different slit widths as shown in Fig (a. In figure (b), having 0.2mg/ml dye similar broadening of the peak was observed. This peak broadening may refers that it is under the effect of water content present in the mixture, or due to the saturation of signal by detector and hence distorted shaped peaks were obtained.(c) with 0.4 mg/ml gave better emission signal. 0.8mg/ml produced a nice at different slit widths (d).

The concentration 0.8 mg/ml at (excitation 3mm- emission 3mm) slit width were chosen for further loading studies. Other concentrations with different slid widths were neglected. The reason for choosing the bigger concentration is that it would be right for alginate/NP hybrids loading studies. This concentration would be driving force for absorption and will be possible to obtain a subtle fluorescence peak in spectrofluorometer. It was also important to note that during the release studies it is important that dye emit a detectable signal of measurable counts on subsequent release in diluted environment.

3.3.2 Removal of dye:

To ascertain that dye move out of the dialysis tube with experimental time frame 0.8 mg/ml fluorescein dye was used. Optimization of dye was performed using dialysis at room temperature. A dialysis tube containing dye was immersed in beaker containing de-ionized water. Removal of dye from the tube was examined. Time study was performed to observe the absorbance peaks using UV-Vis spectroscopy at intervals (Fig 60,a). It was observed that absorbance peaks were kept on decreasing with time even after increasing the sample volume. This showed the dye is removing at consistent rate from the dialysis tube outward in the water. After 7 hours, 91 % of dye was removed from the dialysis tube. Percentage removal of dye was calculated as shown in Fig 60,b)

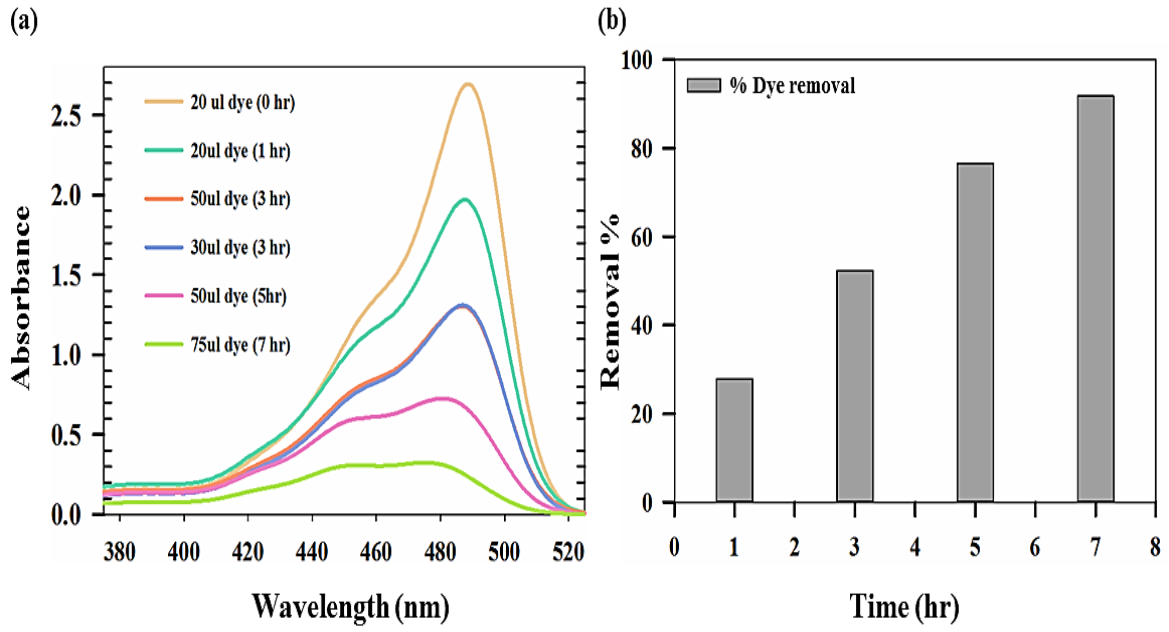

Figure 60: (a) Showing the UV-Vis spectra of decreasing dye peak on subsequent removal of dye with time. (b) Showing the percentage removal. 91 % in 7 hours.

These results were important for loading studies and dialysis was used as crucial step in removing the extra dye and leaving the other dye behind bound to the substance of interest. Similar dialysis studies have shown the efficiency of this method for removal the free dye [161] [162]. Here 10 hours of dialysis were performed in loading studies.

3.3.2.1 Dye Interaction with NPs:

Fluorescein dye was mixed with 1mg/ml and 2mg/ml Fe@Au NPs. In order to bind dye with the NPs water in beaker for dialysis were replaced with fresh one after 2 hours of dialysis in order to remove the possibility of equilibrium in and out of the dialysis tube. The mixture was dialyzed for 10 hours. Changes in emission peaks observed in spectrofluorometer shown in In Fig 61.Sample volume was fixed as 0.1ml mixed with 2.9 ml water for measurements. From the graphs (a), (b) it can be seen that only dye has emission peak at 525nm with emission count of 18632. Fe@Au NP

solution has no emission and a flat line was obtained along the x –axis. When Fe@Au NP solution was mixed with dye emission signal increased to $2.1x10^4$ counts. The extended signal was obtained with mixing both dye and Fe@Au because Au surface exhibits LSPR in the same range (526nm). Then after measuring dyed Fe@Au NPs (after dialysis) the peak shifted towards left of the X-axis. Peak shifted to 506 nm from 525 with decrease in counts recorded as $11.2x10^4$. This peak shift is due to the fluorescence quenching of Fe@Au NPs in presence of dye[163]. Gold surface is good quencher of fluorescence when it is close in proximity to a dye or fluorescent molecule. Resonance Energy transfer (RET) takes place when two fluorophores comes together[164].

Earlier rise when Fe@Au were mixed with dye, extended spectrum was obtained which was due to enhancement of fluorescence by Fe@Au NPs [165]. It was due to the reason that there is no binding between gold and dye molecule and gold surface is exhibiting its LSPR at 525 nm wavelength.

After dialysis, it was concluded that dye has bind to the Fe@Au NPs via weak bonding. As Fe@Au surface have negatively charged citrate ions having 2 lone pairs of electrons. Fluorescein dye and gold shared their electronic cloud and exhibited a weak interaction between them.

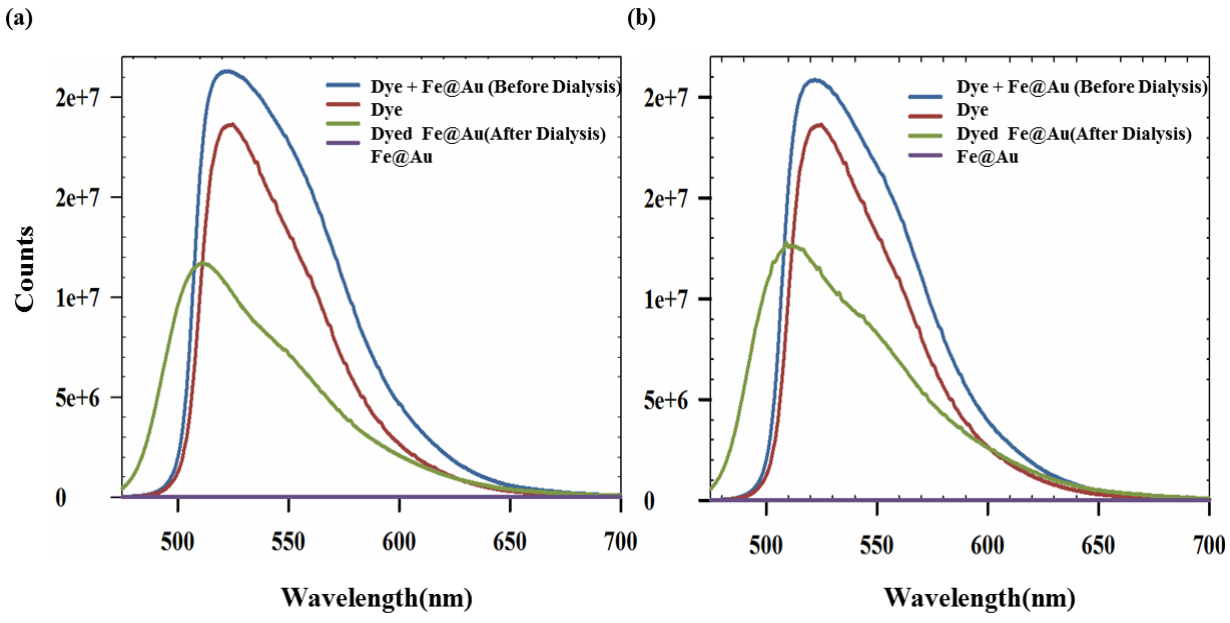

Figure 61: (a) Showing the graphs of 1mg/ml Fe@Au NPs interacting with dye (b) with 2mg/ml Fe@Au NPs intearcting with dye showing the similar trend.

3.3.2.2 Dye Interaction with $CaCl_2$:

Dye interaction with $CaCl_2$ was characterized in order to see any observable change in emission spectra of dye on addition of 3 $CaCl_2$ concentrations that was used for gelation studies. 2 concentrations of Fe@Au were used to bind with the dye 1mg/ml & 2mg/ml. Characterization was done in spectrofluorometer before and after dialysis. Thereafter dyed Fe@Au NPs (after dialysis) were reacted with 3 concentrations of $CaCl_2$ which are 0.7, 200 and 1000 mg/ml. Results are shown in Fig. 62.

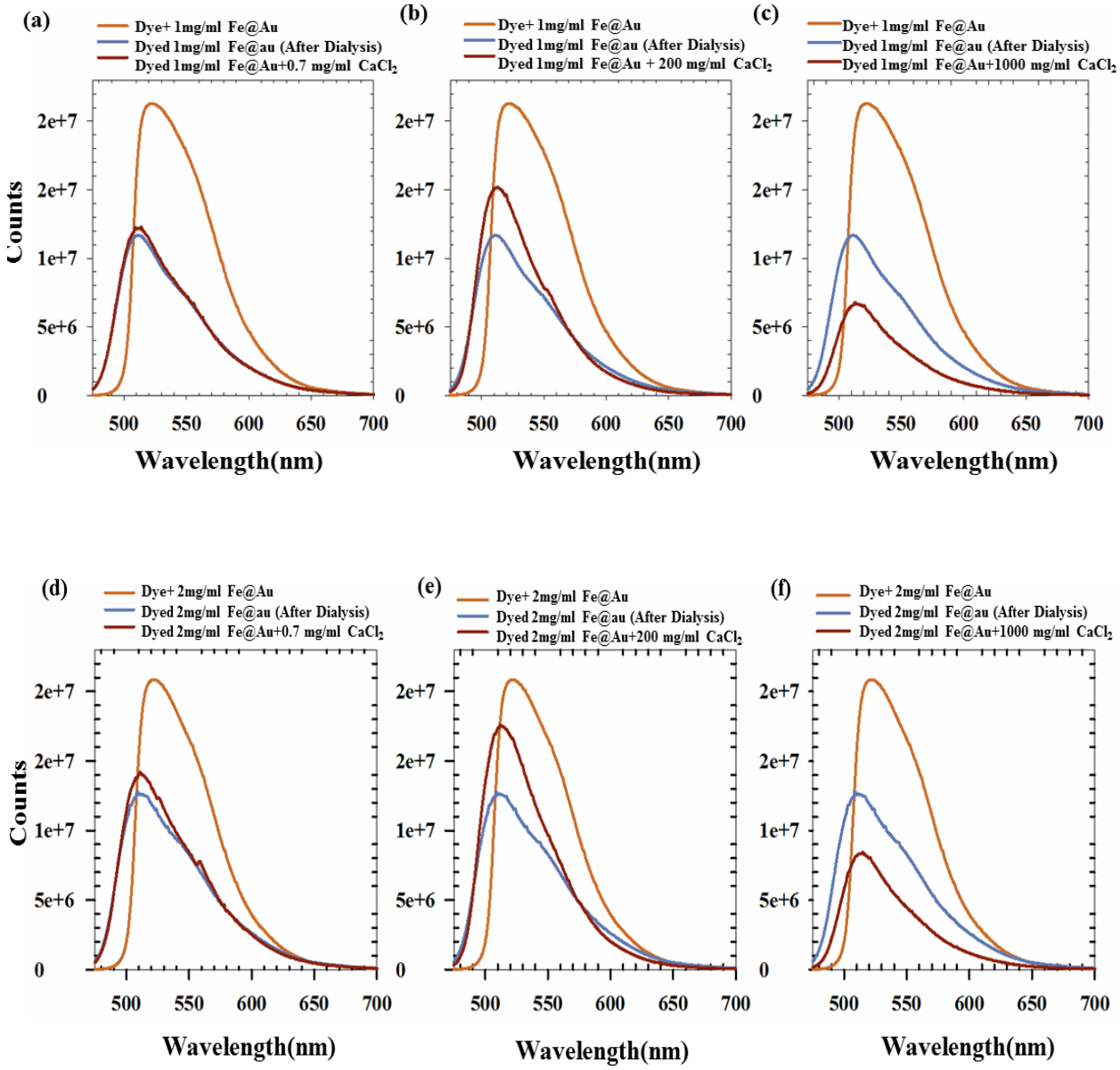

Figure 62 : Interaction of dye with different calcium concentrations. (a), (b), (c) showing 1mg/ml dyed Fe@Au NPs inteacting with calcium and (d) (e) (f) 2mg/ml dyed NP interaction. At higher concentration of CaCl2 the emission spectrum drops which might be due to masking of dye fluorescence by high concentration of calcium.

It can be observed from the figure that there is increase in emission when lower concentrations of $CaCl_2$ react with dyed NPs for both 1 mg/ml (a) (b) and 2mg/ml (d), (e) graphs. But when calcium concentration rises (which is the same concentration at which alginate gelation observed), the

emission signal drops well below the dyed NPs curve (c), (f). This drop in peak might be due to exposure of fluorescein dye is hindered by high calcium salt concentration. This gave early understanding of how the system will behave upon addition of alginate and cause gelation by $CaCl_2$ ions.

3.4 Loading of Fluorescein dye:

In order to evaluate the loading efficiency of the alginate/NP system, loading experiments were performed. Here three methods were used in order to investigate binding of dye.

3.4.1 Method 1 Dye@Fe@Au@Alginate:

Dyed Fe@Au 1mg/ml and 2mg/ml were mixed with alginate. Shaking was done. Detailed method is described in Materials and method section. 0.1 ml of these dyed NPs containing alginate were added to $CaCl_2$ to induce gelation in alginate. Results of loading of dyed NP in alginate network is shown in Fig: 63.. Red label color in the figures denotes micro-aggregation, yellow and green represents intermediate and gelation phase respectively. In the figure 61, dyed 1mg/ml Fe@Au system has been shown which was reacted with alginate and then $CaCl_2$ was added to cross link G units of alginate. (a) (b) (c) describing the system at 280 nm excitation which is excitation wavelength at which alginate emission spectrum can be obserced. (d) (e) (f) showing the same system with 460 nm excitation wavelength which is actually representing the dye emission behavior.

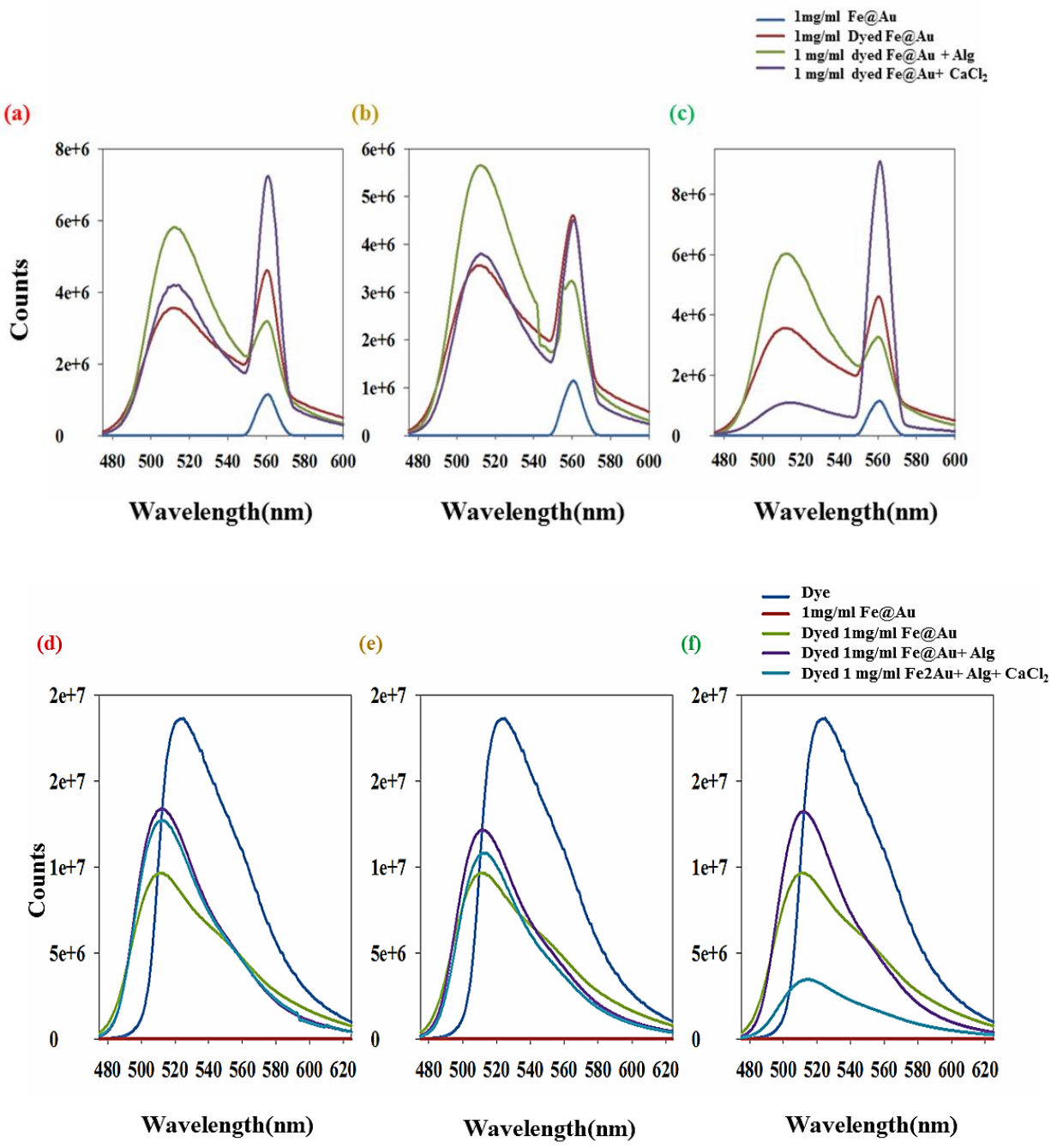

Figure 63: Method 1 : Dyed 1mg/ml Fe@Au incorporation in alginate network in different phases (a),(b) (c) represents micro aggregation ,intermediate gelation and complete gelation phase respectively. Similar solutions excited at 460nm (d) (e) (f) which reveals the behavior of dye in different phases of gelation.

It is interesting to note in (a) (b) (c) graphs that there is dye emission signal in similar range to that of dye emission excited at 460 nm. It was observed before that dye emitted signal only when it

was excited at 460 nm. But in this system dye is emitting signal at 280 nm excitation which was fixed for observation of gelling phenomenon. This might be due to the reason that emitting signal of fluorescein dye is according to the system and can be independent of excitation wavelength (Kasha's rule)[141]. Generally at 280 nm excitation single gelation peak was obtained which gives the behavior of gelling alginate. But here (a) (b) (c) there are 2 peaks 480nm emission range which is due to the reason that dye is also expressing itself here which is bound to the gelled system. So two peaks were obtained at 280nm excitation and only one peak was obtained at 460 nm excitation which was dye emission peak in the gelling system. During release studies, these three peaks were compared and release percentages were calculated these systems.

From graphs (a), (b) (c) it can be observed that solution mixture containing dyed NPs and alginate on moving from micro aggregation to gelled system is changing. At gelled state (Fig 61:c) it can be observed that peak of gelled mixture gets lowered at dye emission wavelength range(475-540nm). But when it gets to the gelling state emission wavelength(545-575nm) the same peak rises up to the same number of counts where gelling happens. This means that at dye emission wavelength the mixture solution signal gets lowered because dye has not been able to express itself due to its incorporation in the alginate gel network. Meanwhile, gelling condition has also been satisfied due to sudden peak rise from 545-575nm at gelling wavelength. The results concluded from these graphs that upon changing the systems from micro aggregation to gelation state, increase in incorporation efficiency of dye inside the alginate gel network can be estimated.

Area under the curves were calculated from dye emission graphs (d) (e) (f) which gave the amount of dye loaded on Fe@Au NPs. The loaded dye at Fe@Au NPs was 61.57 % . Similarly, area under the curves was calculated for three gelling conditions in order to calculate incorporation percentage of dye w. r. t. decrease in the dye peak counts with increase in number of gelled units in the system. Incorporation percentage can be stated as the amount of dye loaded with Fe@Au NP incorporated in the gelled units of alginate. Calculations can be found in (Appendix). 70 % of the drug was incorporated in the gel phase system which is due to reason that number of gelled units is greater in this phase compared to others and gel network is able to bind the dyed NP. At intermediate phase of gelation, only 12 % dye incorporated in the gelled units which is logical number in terms of limited amount of gelling units which can bind dye loaded NP. Only 3.3 % loading efficiency

of dye was calculated at micro aggregation phase system. Figure 64 shows the incorporation percentage of dye at three phases of alginate gelation.

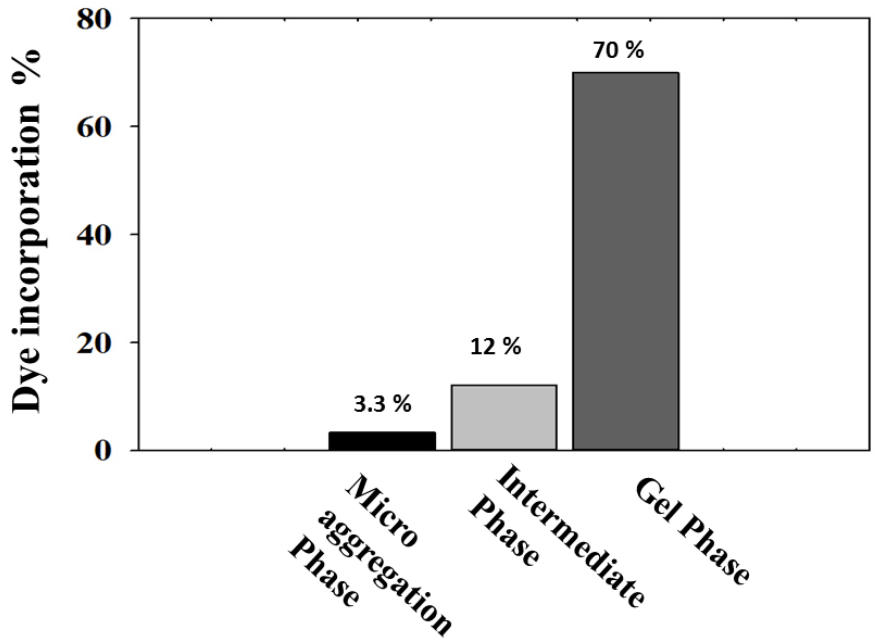

Figure 64: Dye incorporation percentage in dyed 1mg/ml Fe@Au NP/alginate system incorporated in three states of alginate gel network. 3.3 % , 12% and 70 % dye was incorporated in microaggregates,intermediate phase and at gelling phase.

Similar trend can be observed for 2mg/ml dyed Fe@Au NP/alginate system (Fig 65) in which masking of dye fluorescence was observed at higher levels of gelled units in the system. Incorporation percentage was increased in micro aggregates and intermediate systems compared to 1mg/ml Fe@Au dyed NP/alginate system (Fig 63). Incorporation percentage was calculated as 63.23 %. 21 % incorporation of dye was recorded at intermediate phase. 14. 2 % incorporation was obtained for micro aggregates Increase in incorporation percentage of de in microaggregates in intermediate gelling units might be because of increased dyed NP concentration has surrounded the gelled unit/units when a few amount of dye going into the gelled units interfering with the dye

emission signal. Fig 66 showing the bars representing the incorporation percentage of 2mg/ml dyed Fe@Au/alginate system.

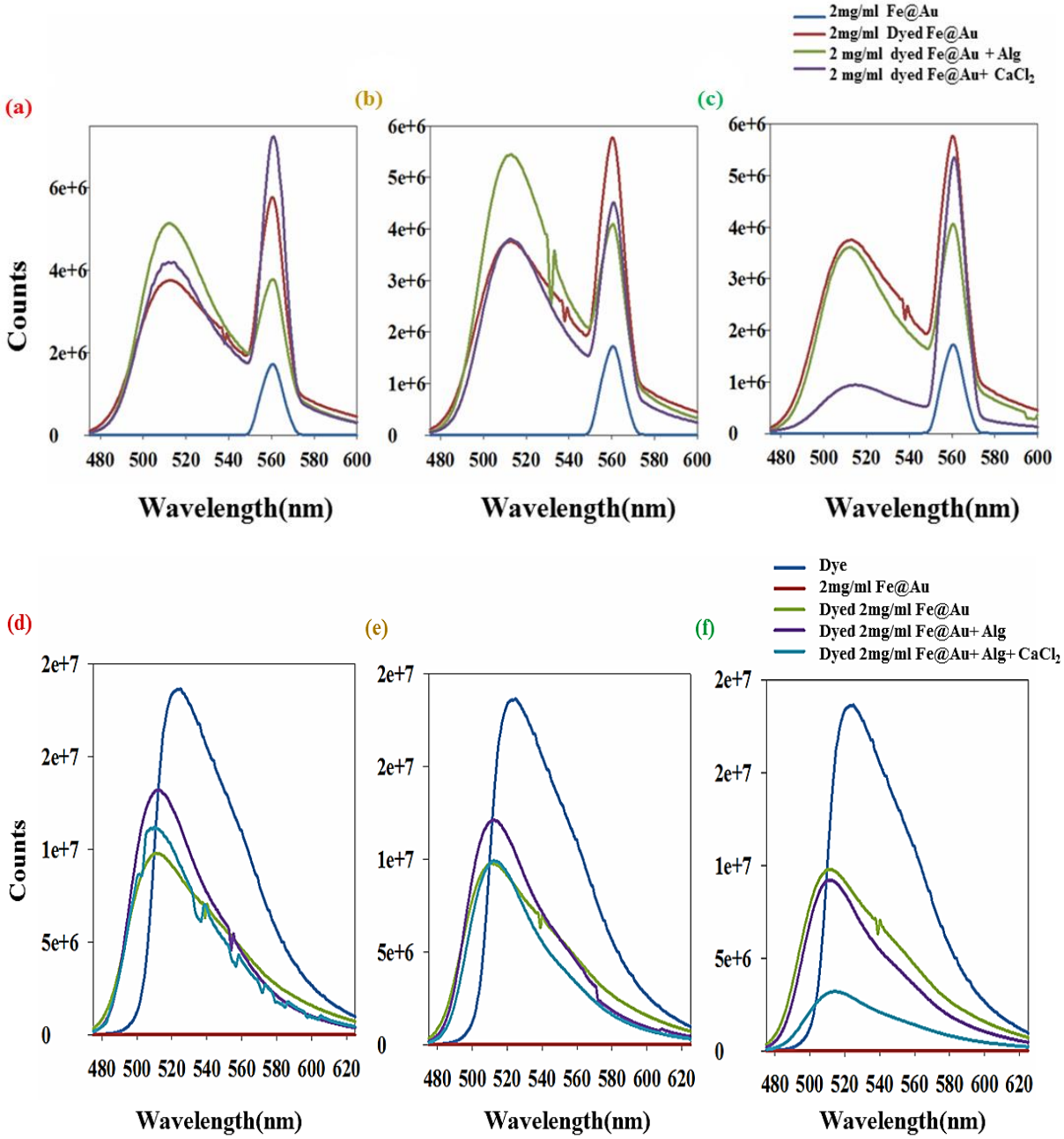

Figure 65 : 2mg/ml dyed NP system. (a) (b) (c) showing loading at microaggregation,intermediate phase and gelling phase respectively from left to right. These are peaks obtained at 280 nm excitation.Which was used for previous gelling studies.(d) (e), (f) represents 460 nm excited peaks showing dye emission signal in different phases of gelation.

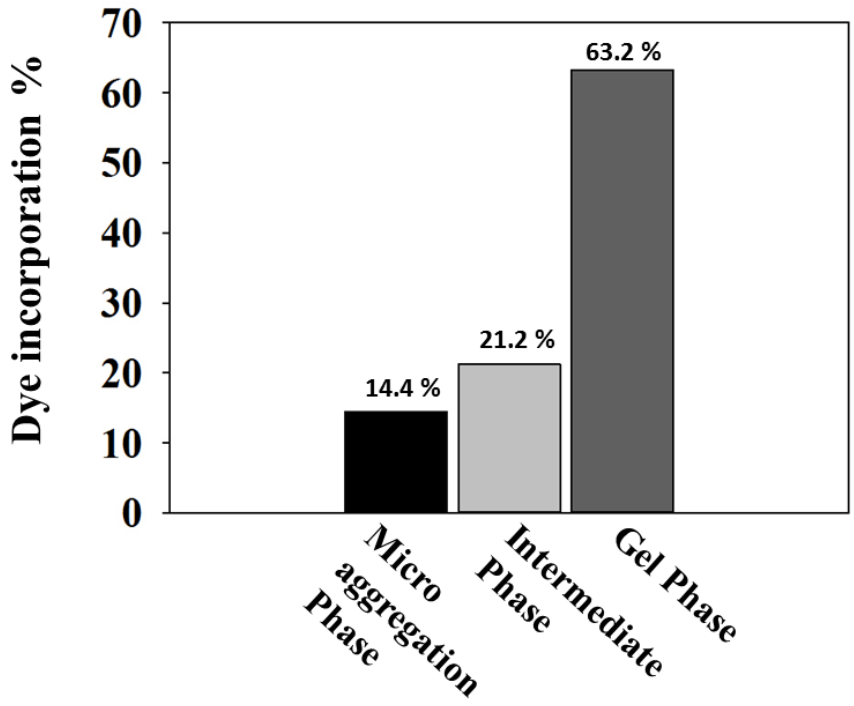

Figure 66 : Dyed 2mg/ml NP/Alginate system. Bars are showing incorporation percentage of dye at 3 phases of alginate gelation.

Table 3 : Representation of loading and incorporation percentage of Method 1

Gelation Phase	**Dye Loading (%)**		**Dye Incorporation %**	
	1mg/ml Fe@Au	2mg/ml Fe@Au	1mg/ml Fe@Au	2mg/ml Fe@Au
Micro-aggregation	61.57	61.57	3.32	14.42
Intermediate	61.57	61.57	12.05	21.21
Gelation	61.57	61.57	70.01	63.23

This method showed good results in terms of binding of dye with Fe@Au and loading studies further complemented its encapsulation efficacies in NP/alginate system. Similar studies have been previously performed where dyes were bound to NPs to investigate loading and release from similar NP based systems[166] [167]. Schematic representation of this method is shown in Fig 67

explaining encapsulating phenomenon of dyed NP/alginate system. Percentage of dye loading on Fe@Au NPs is also given in Table 3.

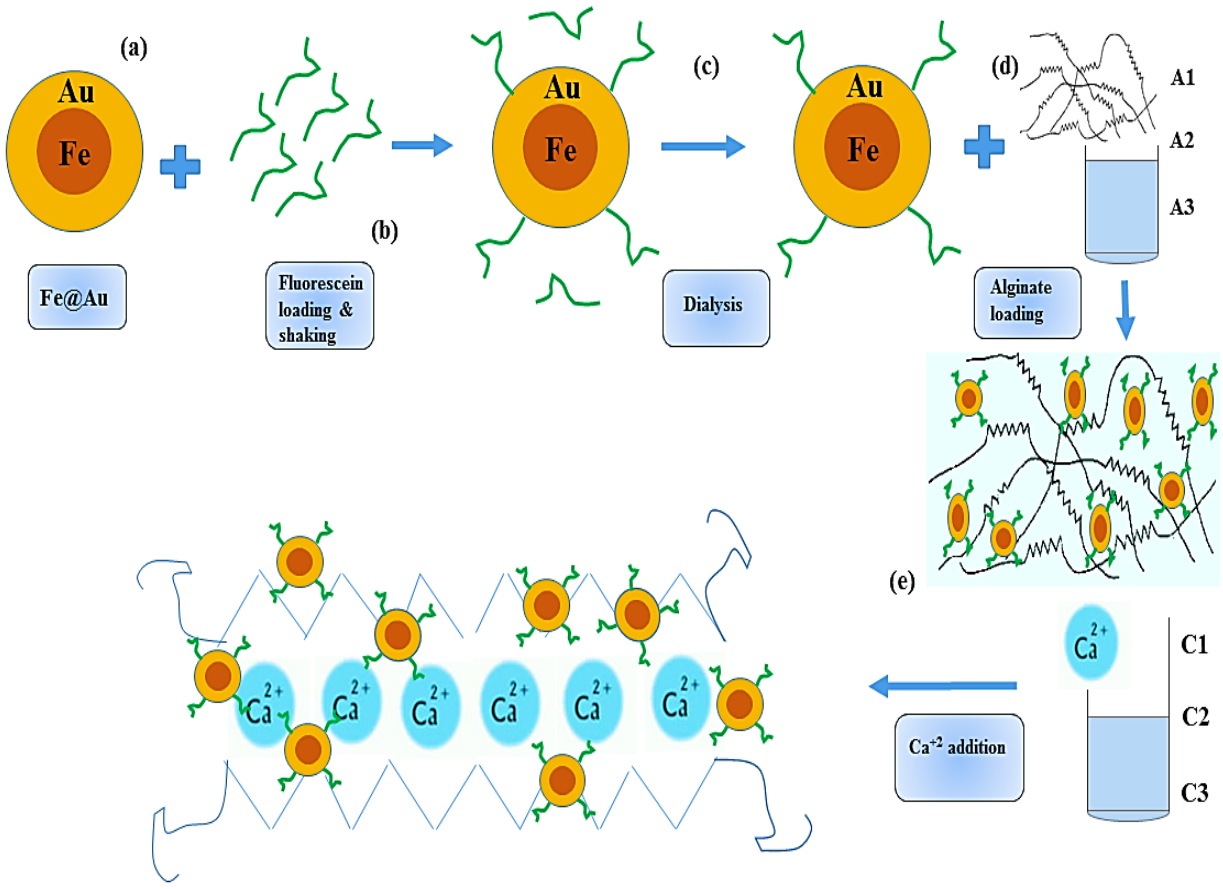

Figure 67: Schematic representation of Method 1 where Fe@Au NPs were dyed and then incorporated into alginate and then by introducing calcium, gelation occurred encapsulating Dyed Fe@Au inside the network. Scheme representing higher gelation state.

3.4.2 Method 2 NP@Alg@Dye:

In this method, Fe@Au NPs were incorporated in alginate first and then dye was added to NP/alginate system and loading was characterized. Loading percentage and incorporation

efficiency was calculated from area under the curves. In graph 68, results are shown. (a) (b) (c) showing 1mg/ml NP/alginate binding with dye in micro-aggregation, intermediate phase and gelation phase respectively. (d) (e) (f) showing the dye emission peaks excited at 460nm at different phases of alginate gelation. Before addition of the dye to Alginate & Fe@Au solution they emit no signal at 460 excitation which can be shown in (d) (e) (f) .Loading of dye on each of gelation system is summarized in table below in Table 3. Variations in the loading of dye on each of the NP/alginate systems. Which could be due to the reason that dye has not bind well to both alginate/NP hybrid together and at phase of higher gelation phase a good loading percentage was calculated. It can be observed in (a) (b) (c) graphs that gelation emission peaks are consistent at gelation wavelength (545-575nm) and after introducing calcium in the system to mixture containing dyed NP/alginate similar pattern of increase in curve was observed as observed in earlier studies of gelation without dye and NP in the system. It further confirms the gelation by inducing calcium in the system. But binding of dye has been less as compared to Method 1 where dyed Fe@Au has shown higher affinity towards fluorescein dye and 61. 5 % drug was loaded on Fe@Au surface.

Table 4 : Loading & incorporation percentage of fluorescein dye for Method 2.

Gelation Phase	**Dye Loading (%)**		**Dye Incorporation %**	
	1mg/ml Fe@Au	2mg/ml Fe@Au	1mg/ml Fe@Au	2mg/ml Fe@Au
Micro-aggregation	4.89	6.07	14.04	8.07
Intermediate	30.55	11.71	13.78	32.69
Gelation	41.91	51.21	72.63	73.66

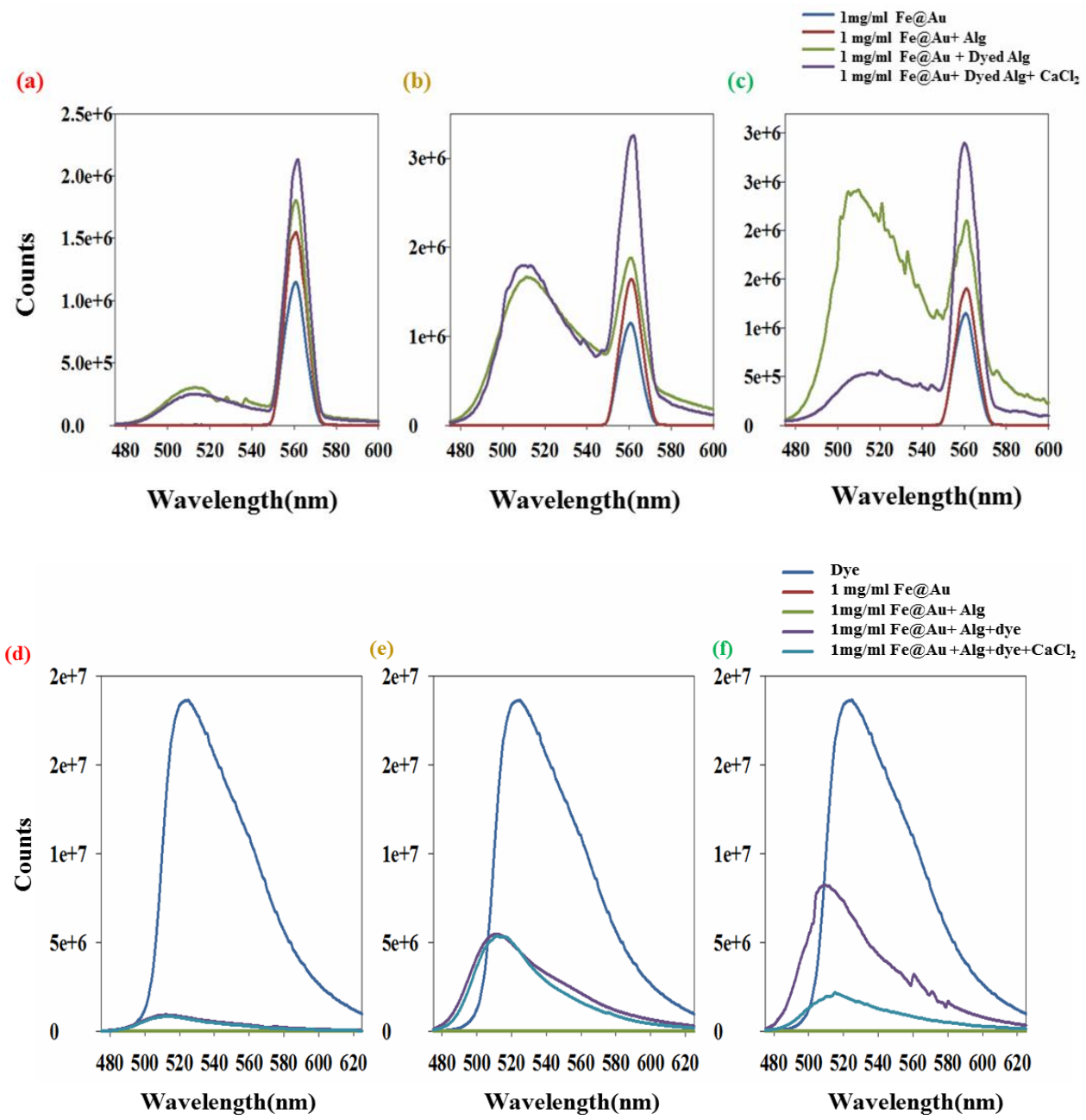

Figure 68 : Method 2: 1mg/ml Fe@Au system. Dyed together with alginate and then induced gelation by calcium ions. (a) (b) (c) showing results at 280 excitation and (d) (e) (f) showing the system excited at 460 nm.

In Fig 68 (d) (e) (f), emission peak for mixture solution lowered down when calcium ions were introduce the gel the network. Trend is similar in micro aggregation phase and gelled phase. Dye signal repression can also be observed which corresponds to gelation networks overshadowing the fluorescence of the dye with increase in number of gelling units on moving from micro aggregation to gelation. Intermediate system has shown less incorporating results compared to micro - aggregation and gel phase which might be due to less binding of less number of NPs carrying dye reaching and incorporating into the gel network. Dye incorporation percentage for Method 2, 1mg/ml Fe@Au/Alginate system has been shown in Fig 69. 14% of drug was incorporated in micro-aggregated gel network. 13.7 % incorporation was calculated for intermediate system and 72.6 % dye incorporation was observed in gelling phase which is due to the increased gelling units forming a network leading to increased incorporation of dyed system.

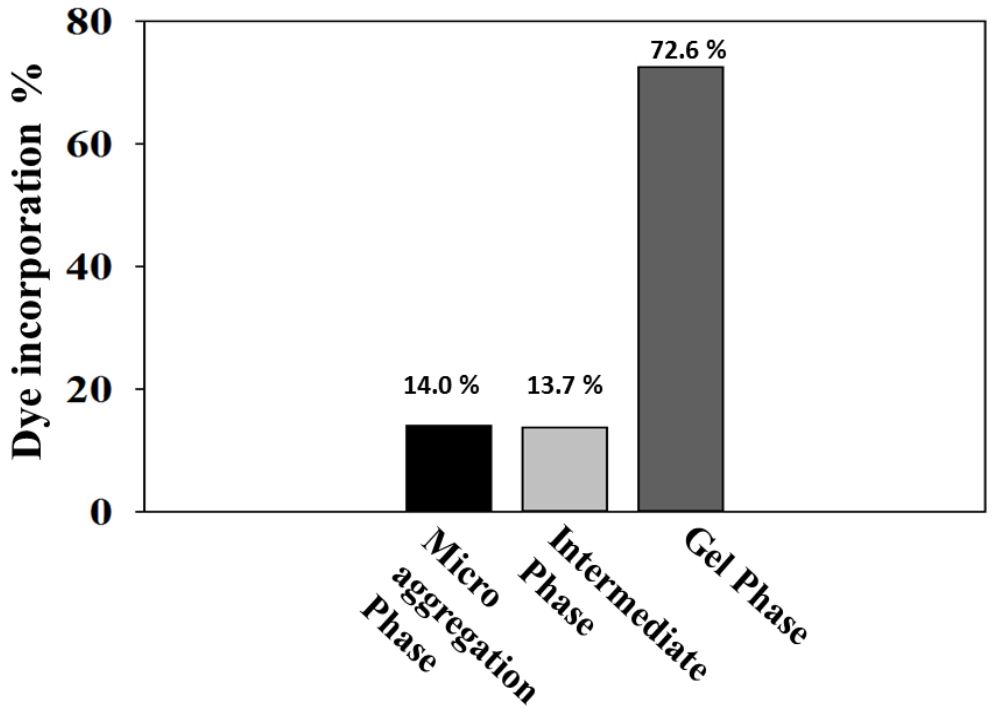

Figure 69: Method 2:1mg/ml Fe@Au NP/ alginate dyed and gelled at three different phases. Incorporation percentage of the dye is described her. 14, 13.7 & 72.6 % of incorporation was calculated for microaggregation phase, intermediate and gelling phase respectively.

Similar trend can be observed for dyed 2mg/ml NP/alginate systems where fluorescence of dye repressed on increasing the number of gelled G blocks of alginate by increasing calcium concentration. (Fig 70 (a) (b) (c) which were excited at 280 nm yielding consistent peaks at gelling wavelength. In case of (d) (e) (f) which were excited at 460nm showing less binding of dye with alginate/NP system especially at micro aggregated phase but overshadowing of fluorescence is higher at intermediate and gelation phases, which is evident that gelled units can hold the dyed system into its network.

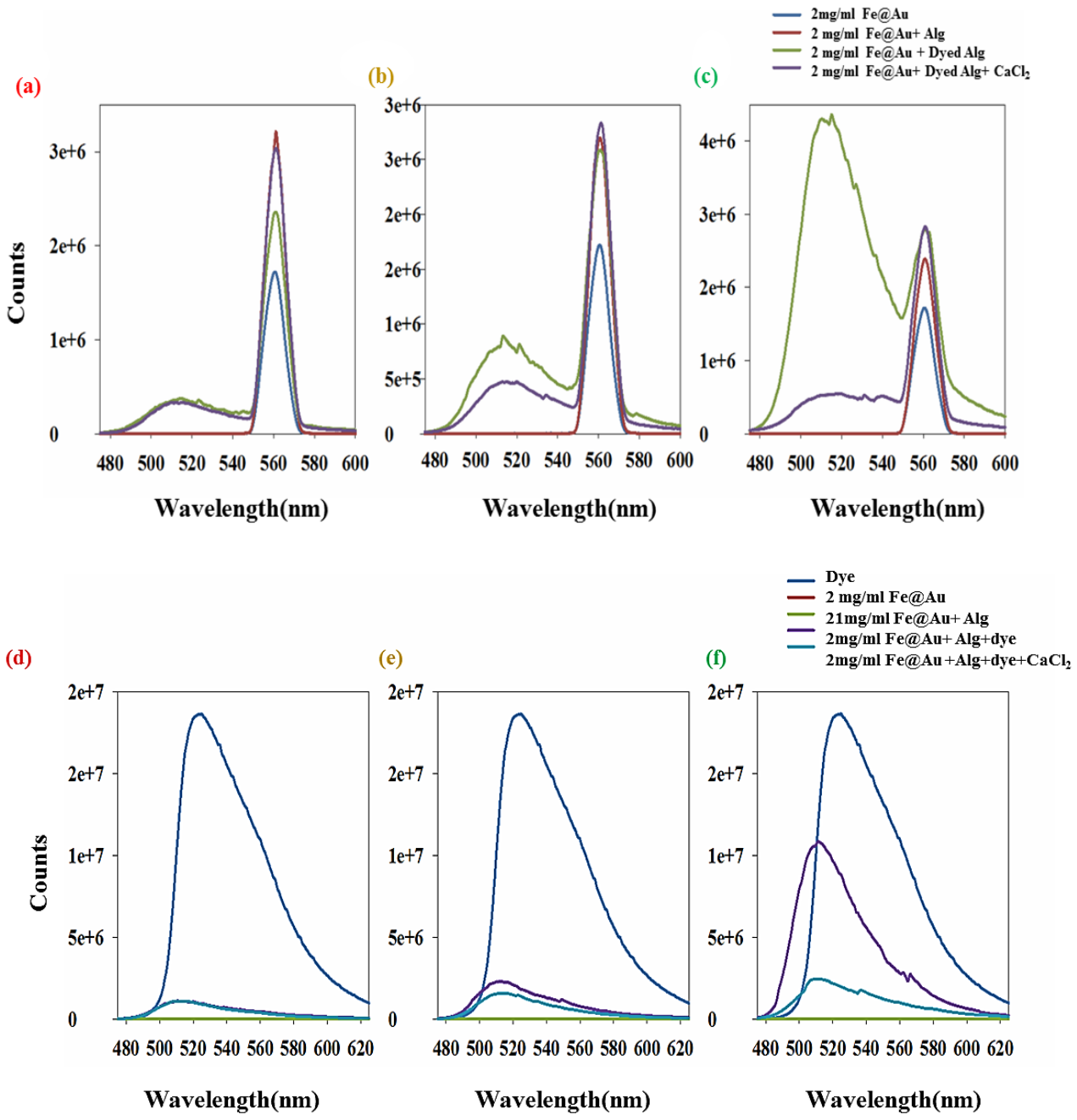

Figure 70 : 2mg/ml Fe@Au with dyed alginate and addition of $CaCl_2$ in the system. (a) (b) (c) are excited at gelling excitation which was 280 nm and (d) (e) (f) represents 460 nm excited peaks which gives information of dye behavior in the alginate network going from micro aggregation to gelling conditions (from left to right)

Dye incorporation percentage was calculated. Only 8 % of dye was incorporated in small aggregates of alginate gelled units whereas 33 % of dye was incorporated in intermediate phase of gelation. Which could be due to increase in number of NPs containing dye have increased the possibility of dye to move into the gelled units which previously was not the case in this phase when 1mg/ml dyed system was used (13 %). 73.6 % percent dye was incorporated in the gelation phase where number of gelled G blocks are large in number and more dyed NP were vulnerable to go into the gel network. Fig 71 showing the dye incorporation percentage in three gelling conditions.

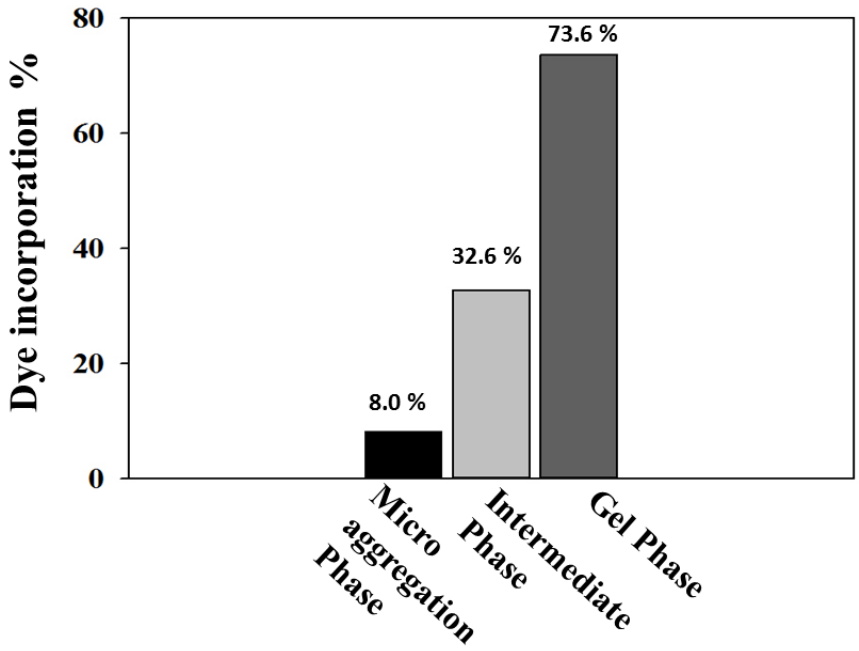

Figure 71 : Method 2: 2mg/ml dyed NP/alginate system. 8, 33, & 73.6 % of drug was incorporated in micro-aggregation, intermediate phase and gelation phase respectively

3.4.3 Method 3 Alg@Dye@NP:

In this method alginate were mixed with dye in order to check dye binding with alginate and then after dialysis Fe@Au NPs were added. Loading percentage of dye on this alginate were calculated

using area under the curves. Same alginate concentrations were used for both system and then mixed with NP for incorporation studies in alginate network. Loading and incorporation percentage of this method is summarized in Table 5.

Table 5: Loading & incorporation percentage of dye in Method 3.

Gelation Phase	**Dye Loading (%)**		**Dye Incorporation %**	
	1mg/ml Fe@Au	2mg/ml Fe@Au	1mg/ml Fe@Au	2mg/ml Fe@Au
Micro-aggregation	3.34	3.34	0	0
Intermediate	13.33	13.33	23.09	0.24
Gelation	10.61	10.61	61.17	63.66

In figure 72, (a) (b) (c) it can be observed that there are very consistent emission curves before and after addition of $CaCl_2$ at gelling excitation wavelength which confirms the system's gelation features. In same graphs emission spectrum of dye can be observed which give the same behavior of dye on 460 excitation of dye in the same system (d) (e) (f). At increasing gelation, exposure of dye emission reduces which can be observed from (e) and (f) graphs. This decrease in exposure in non-recognizable at micro aggregation phase (d), which is due to the fact that very few gelled units are present in this phase to capture and mask the fluorescence of dyed system. Incorporation percentage of the system was calculated by trends in area under the curve.

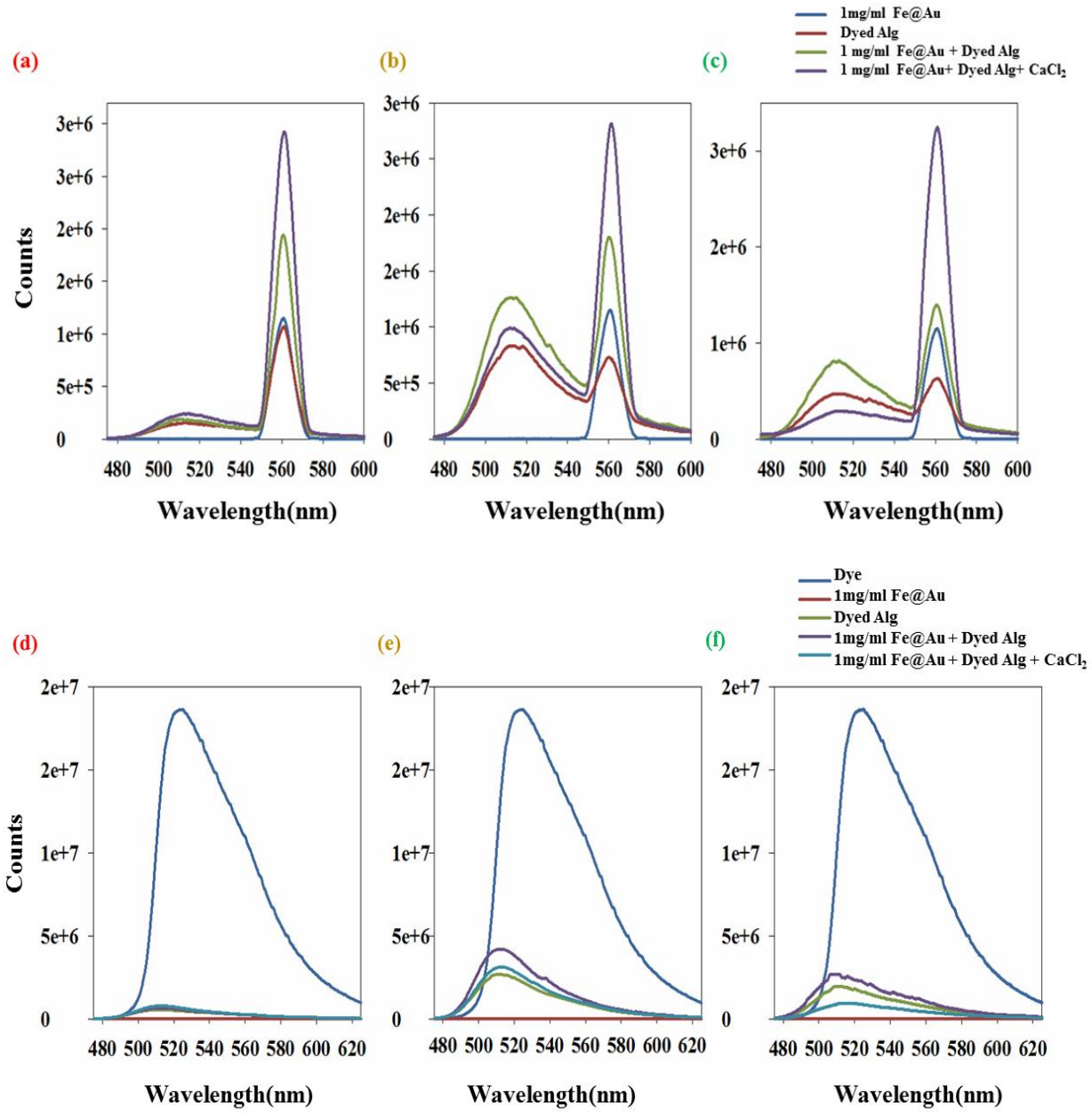

Figure 72 : Method 3: Dyed alginates were loaded with 1 mg/ml Fe@Au NPs and then system was gelled using $CaCl_2$.(a) (b) (c) represents 280 nm excited peaks and (d) (e) (f) showing 280 nm excited peaks going from microaggregation to gelled networks(left to right).

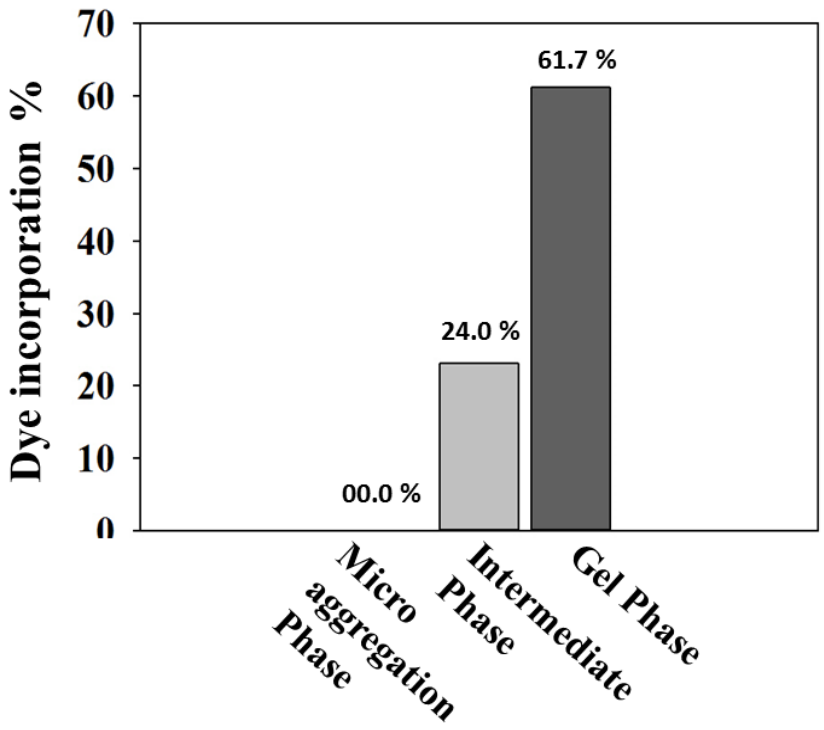

Figure 73: Method 3 : 1mg/ml Np system with dye loaded to alginate and then NP incorporation was done before cross linking the system with CaCl2. No incorporation was observed at micro aggregated state. 23 % of dye incorporation was calculated at for intermediate phase while 61 % dye incorporated in gelled units of alginate.

In another setup (Fig 74). Which exploited the same experimental procedure but by increasing NP concentration to bind with the dyed alginate. It can be noticed that at gelation excitation (280nm) the curves are giving the same trend before and after mixing of $CaCl_2$ .But at 460 nm excitation it can be seen that dye incorporation is zero in case of micro aggregated units. But increasing gelled units loading and and encapsulation become more significant especially when the whole system gels. Incorporation percentage was calculated (Fig 75). So in order to provide more efficiency to this system higher gelation states may be required to encapsulate the dye for release studies.

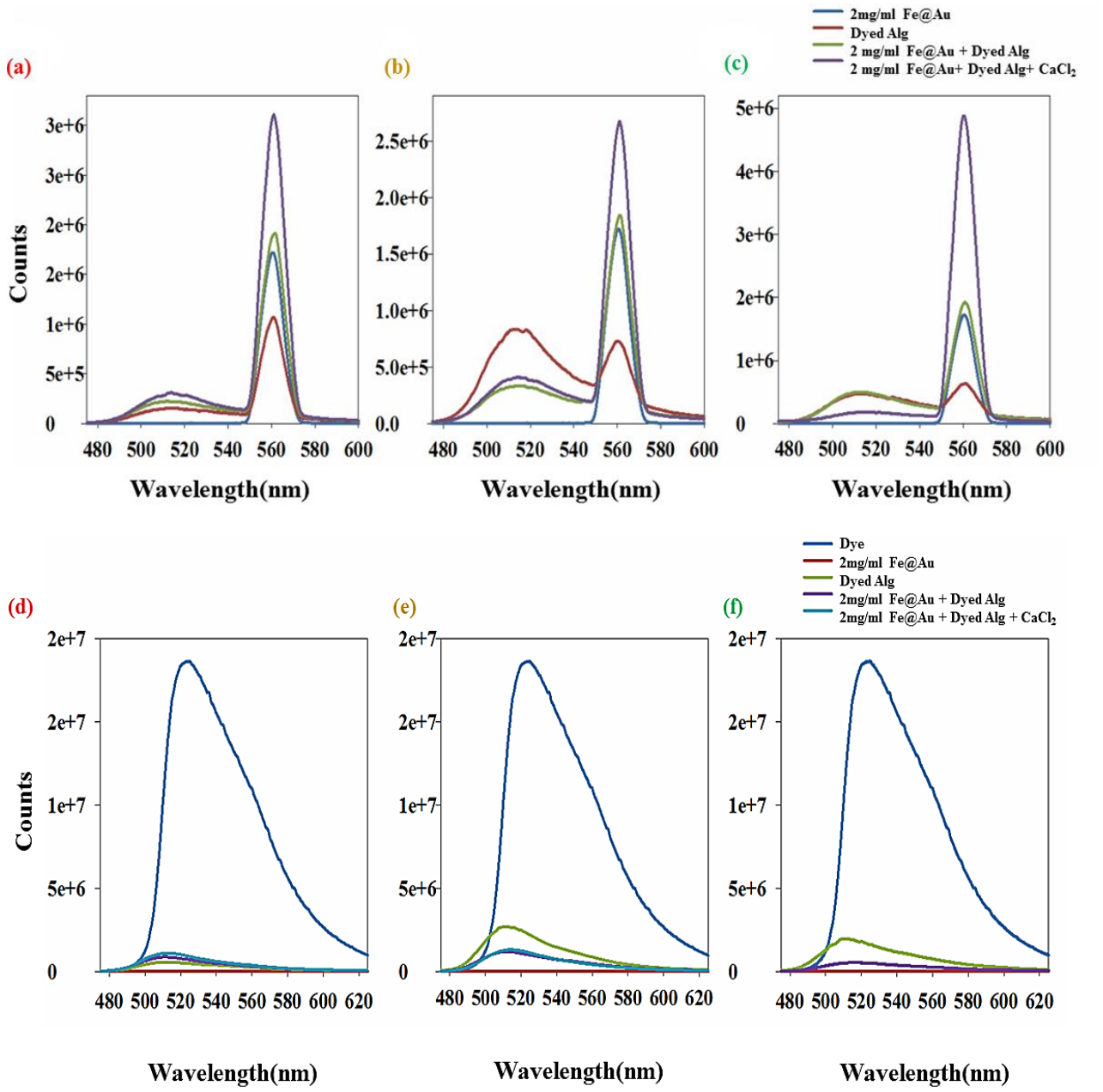

Figure 74 : Method 3. 2mg/ml Fe@Au system. Dyed alginate mixed with Fe@Au to investigate loading phenomenon. (a) (b) (c) were at excited at 280 nm and (d) (e) (f) showing the results of solutions excited at 460 nm. It can be seen that very limited percentage of loading is observable from this system especially at (d) micro aggregation.

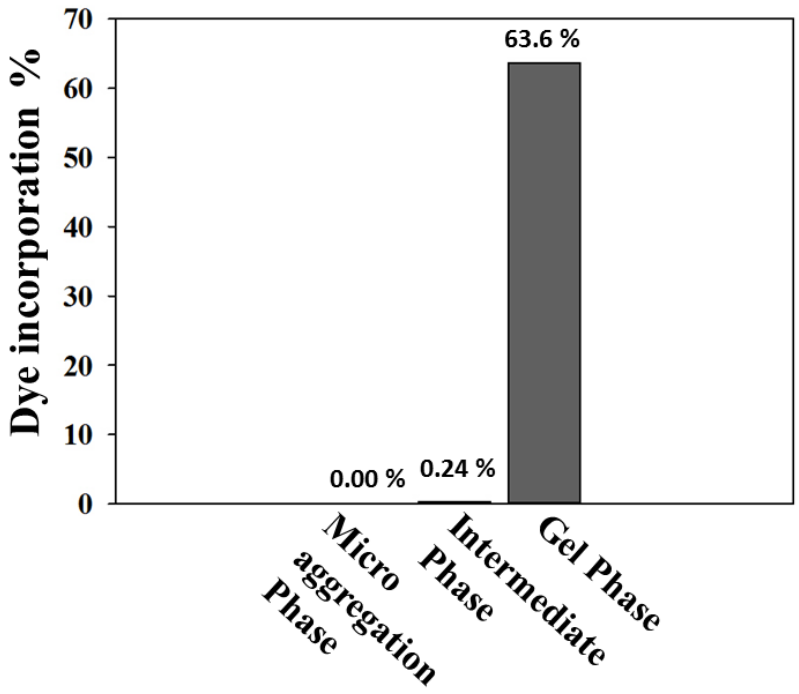

Figure 75 : Method 3 Dye incorporation for 2mg/ml NP/dyed Alginate system, 63 % dye incorporated especially at gelation phase

First method of loading (Dye@NP@Alg) proved to be better one in loading and incorporation efficacies. Due to their higher percentage of recognizable loading (61.57 %). It is also Method 1 is better system in terms of incorporation dye/drug inside the alginate gel network. Incorporation efficiencies were observed for three all the three phases of gelation which is very promising in terms of designing the release system. Release studies were performed by adapting this method.

Table 6: Comparison of three methods of loading & incorporation in Gelling Phase

Loading Method	**Dye Loading (%)**		**Dye Incorporation %**	
	1mg/ml Fe@Au system	2mg/ml Fe@Au system	1mg/ml Fe@Au	2mg/ml Fe@Au
Method 1	61.57	61.75	70.01	63.23
Method 2	41.91	51.21	72.63	73.66
Method 3	10.61	10.61	61.17	63.66

3.5 Release:

Release studies were performed at room temperature. Six different solutions were made using Method 1 as mentioned above. Emission spectra were recorded over time by exciting the solution at 280nm and 460 nm. The first wavelength has been used all throughout this study to understand gelling, while the second wavelength corresponds to the excitation wavelength of the dye. The release percentage was calculated based on the areas obtained under the emission spectra of the dye (excitation 460nm) over 475nm – 650nm range.

1 mg/ml Dyed Fe@Au/alginate system showed good release behavior at gelling condition as depicted in Fig 76 (a). Consistent release was observed in this system with 27 % release in 20 hours. The release kinetics can be compared with gelling condition of 2mg/ml dyed NP/alginate system which showed fluctuating release behavior (b).

Other solutions also showed discontinuous release behavior with time at micro aggregation and intermediate states. (Appendix 5).This might be due to less incorporation of dye into the hybrid system or measurement techniques employed in the studyThis behavior might also be due to the static nature of system and lack of external stimulus that might be required for the release of dye from gelled networks.

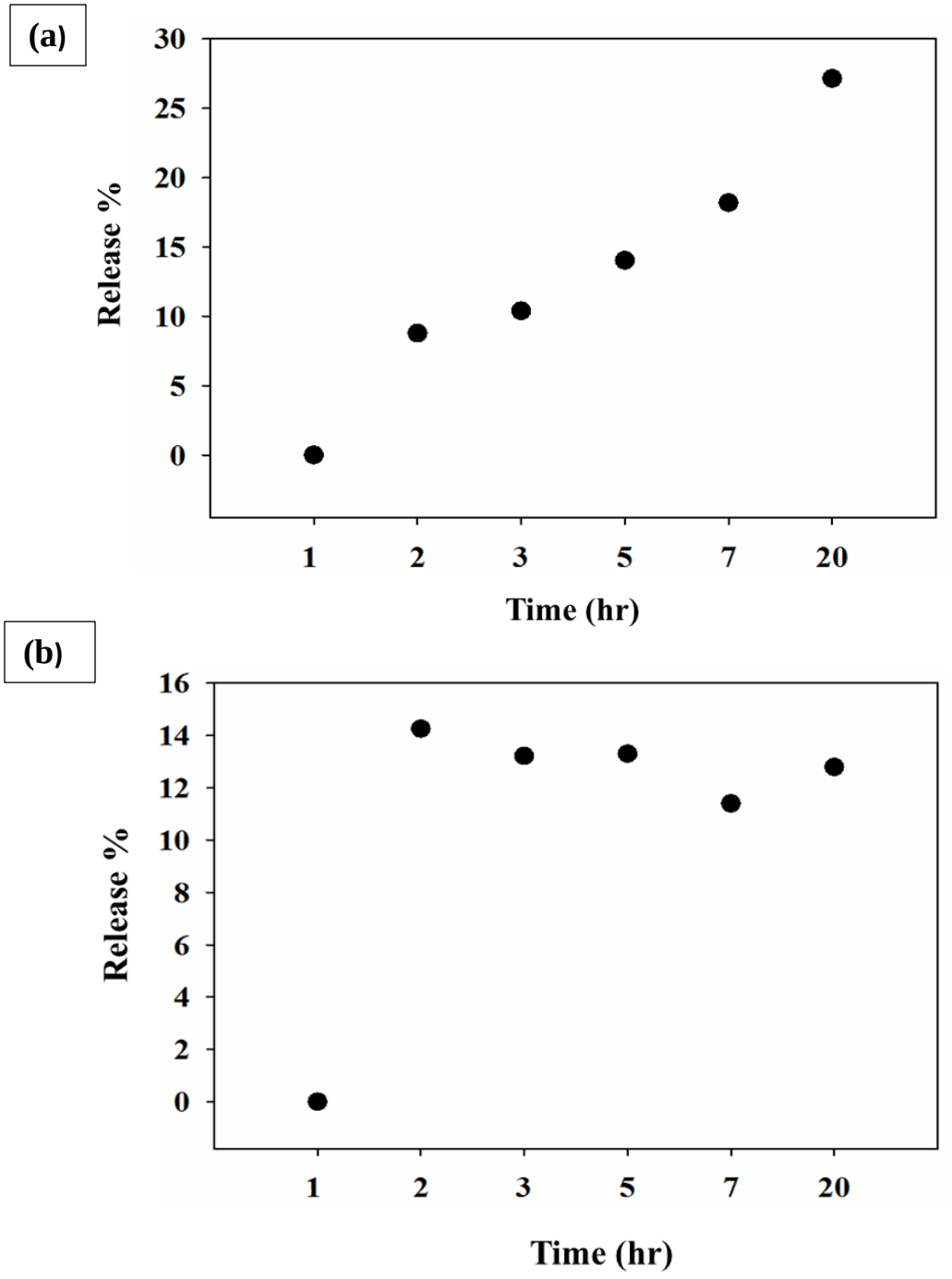

Figure 76 : (a) Shos the release behavior of 1mg/ml Dyed Fe@Au Alginate gelled system. Consistent release pcan be observed with 27 % release percentage after 20 hours. , whereas (b) shos the 2mg/ml dyed Fe@Au/alginate gelled system with discontinous release behavior.

4 Conclusion:

In this project, gelation of alginate was investigated at several lower concentrations in dilute phase with an aim to develop Alginate/NP hybrid drug delivery system. It was noted that alginate gelation goes through phases of aggregation before forming a complex gel network. G units of alginate due to their nest like structure holds divalent cations (Ca^{2+}) which leads to the three dimensional gel network. Alginate gelation is dependent on number availability of G- units in the polymer structure and also concentration of divalent cations ($Ca^{2+)}$ to bind with G units to induce gelation. Here, $CaCl_2$ was used as ionic source to cross link alginate G blocks. Very low concentrations of alginate was used. Gelation was characterized starting with UV-Vis spectroscopy and then fluorescence spectroscopy was employed. Data from the spectrofluorometry were analyzed to understand how the alginate systems behave. Experiments were then performed using Ubbelohde viscometer to complement the spectroscopic results. It was found that upon increasing. $CaCl_2$, fraction of gelled networks increased in the system. The monotonic increase in the trends was obtained for both the data sets derived from spectrofluorometer and viscometer.

Preliminary results helped to identify three different phases of alginate gelling architectures. Firstly, micro aggregate phase ,in which very limited amount of G units gelled due to lower concentrations. Secondly, intermediate corresponded to the mild state of gelation where moderate gelation occurred with increase in $CaCl_2$ concentration. Finally, gelling phase was observed with the largest number of G units being bound to Ca^{2+} ions. Calcium chloride was observed to be the dominant factor in gelation.

Further, loading and interaction of alginate with three types of NPs depending on their coating. Fe@Au, Fe@Au@PEG & Fe@Au_PL were synthesized and characterized by UV-Vis, DLS and, zeta potential measurements. Behavior of NPs binding was investigated at different phases of alginate gelation. Significant change/rise in viscosity was observed in systems containing NPs especially at gelling condition. The nature of the coating of the NPs did not affect the gelling conditions, however, the concentration of the NPs affected the incorporation of the NPs in the

networks. Therefore, Fe@Au NPs were further used in the study to understand loading and release of the model dye.

Fluorescein dye was used as model dye to check loading and release from these NP/alginate systems and also to ascertain the different gelling architectures hypothesized form the preliminary experiments. Fluorescein dye was calibrated and its binding was studied with alginate, NPs and $CaCl_2$.

Three methods of loading of dye was used. In Method 1, Dye was loaded to Fe@Au NPs dialyzed and then alginate was added to the mixture. This system was gelled with $CaCl_2$ and characterized. Loading of dye on Fe@Au NPs was calculated as 61 % . In Method 2, Fe@Au NPs were mixed with alginate and then dye was loaded to the system. In Method 3, alginate was dyed and then after dialysis Fe@Au NPs were added. These systems were characterized using spectrofluorometer. Method 1 showed high dye incorporation inside the gel networks (70%) for the gel phase. Method 2 and 3 results indicated they are behaving similar to method 1 in terms of incorporation of dye especially at gelling condition. But Method 1 results were consistent with increase in number of gelled units and both loading and incorporation were observed at three phases of alginate and two NP concentrations. Thus, Method 1 was adapted for release studies of dye.

Diffusion based release was investigated .At gelling phase of 1mg/ml dyed Fe@Au/alginate system, a consistent 27 % release was observed in 20 hours. Although the preliminary studies show a sufficient release of the model dye, enhancement can be effected by inducing external stimuli like temperature or pH change.

5 Future Work

The preliminary studies in gelation have shown that it is possible to characterize gelation in alginate based systems at low concentrations. Further study can be done with other alginates to understand the effect of molecular weight, cross-linking affinity among other parameters.

Loading and release have been investigated using a model dye. Future studies could focus on specific drugs like L-Dopa, Doxorubicin, e.t.c. used for treatment of various diseases, like cancer, Parkinson's and so on.

Release has only been monitored based on diffusion. In further studies, different external stimuli like temperature, pH, light can be used with an intent to enhance release from these systems.

6 References:

1. Painter, P.C. and M.M. Coleman, *Fundamentals of polymer science a CD/ROM and on-line material.* Abstracts of Papers of the American Chemical Society, 1999. **217**: p. U636-U636.
2. Vieira, M.G.A., et al., *Natural-based plasticizers and biopolymer films: A review.* European Polymer Journal, 2011. **47**(3): p. 254-263.
3. Stupp, S.I. and P.V. Braun, *Molecular manipulation of microstructures: Biomaterials, ceramics, and semiconductors.* Science, 1997. **277**(5330): p. 1242-1248.
4. Geresh, S., et al., *Bioadhesive grafted starch copolymers as platforms for peroral drug delivery: a study of theophylline release.* Journal of Controlled Release, 2004. **94**(2-3): p. 391-399.
5. Liu, Z.H., et al., *Polysaccharides-based nanoparticles as drug delivery systems.* Advanced Drug Delivery Reviews, 2008. **60**(15): p. 1650-1662.
6. **Q.Liu, S.**, *Bioregenerative Engineering: Principles and Applications*. 2006: John Wiley & Sons, Inc. 1104.
7. University, T.P.S., *Structure of Starches*. USA.
8. Klemm, D., et al., *Cellulose: Fascinating biopolymer and sustainable raw material.* Angewandte Chemie-International Edition, 2005. **44**(22): p. 3358-3393.
9. *Cellulose*. 2007, My Organic Chemistry.
10. Lee, D.W., et al., *Strong Adhesion and Cohesion of Chitosan in Aqueous Solutions.* Langmuir, 2013. **29**(46): p. 14222-14229.
11. Nitta, S., S. Kaketani, and H. Iwamoto, *Development of chitosan-nanofiber-based hydrogels exhibiting high mechanical strength and pH-responsive controlled release.* European Polymer Journal, 2015. **67**: p. 50-56.
12. Lai, P., et al., *Overview of the preparation of organic polymeric nanoparticles for drug delivery based on gelatine, chitosan, poly(D,L-lactide-co-glycolic acid) and polyalkylcyanoacrylate.* Colloids and Surfaces B-Biointerfaces, 2014. **118**: p. 154-163.
13. Younes, I. and M. Rinaudo, *Chitin and Chitosan Preparation from Marine Sources. Structure, Properties and Applications.* Marine Drugs, 2015. **13**(3): p. 1133-1174.
14. Lee, K.Y. and D.J. Mooney, *Alginate: Properties and biomedical applications.* Progress in Polymer Science, 2012. **37**(1): p. 106-126.
15. Tonnesen, H.H. and J. Karlsen, *Alginate in drug delivery systems.* Drug Dev Ind Pharm, 2002. **28**(6): p. 621-30.
16. Abreu, F.O.M.S., et al., *Effect of the preparation method on the drug loading of alginate-chitosan microspheres.* Express Polymer Letters, 2010. **4**(8): p. 456-464.
17. Augst, A.D., H.J. Kong, and D.J. Mooney, *Alginate hydrogels as biomaterials.* Macromol Biosci, 2006. **6**(8): p. 623-33.
18. George, M. and T.E. Abraham, *Polyionic hydrocolloids for the intestinal delivery of protein drugs: alginate and chitosan--a review.* J Control Release, 2006. **114**(1): p. 1-14.
19. Lee, K.Y., et al., *Controlling mechanical and swelling properties of alginate hydrogels independently by cross-linker type and cross-linking density.* Macromolecules, 2000. **33**(11): p. 4291-4294.
20. Grant, G.T., et al., *Biological Interactions between Polysaccharides and Divalent Cations - Egg-Box Model.* Febs Letters, 1973. **32**(1): p. 195-198.
21. Siew, C.K., P.A. Williams, and N.W.G. Young, *New insights into the mechanism of gelation of alginate and pectin: Charge annihilation and reversal mechanism.* Biomacromolecules, 2005. **6**(2): p. 963-969.

22. Crow, B.B. and K.D. Nelson, *Release of bovine serum albumin from a hydrogel-cored biodegradable polymer fiber.* Biopolymers, 2006. **81**(6): p. 419-427.
23. Roy, D., J.N. Cambre, and B.S. Sumerlin, *Future perspectives and recent advances in stimuli-responsive materials.* Progress in Polymer Science, 2010. **35**(1-2): p. 278-301.
24. Rzaev, Z.M.O., S. Dincer, and E. Piskin, *Functional copolymers of N-isopropylacrylamide for bioengineering applications.* Progress in Polymer Science, 2007. **32**(5): p. 534-595.
25. H. Cui and , P.B.M., *Thermally Triggered Gelation of Alginate for Controlled Release*. 2009.
26. Westhaus, E. and P.B. Messersmith, *Triggered release of calcium from lipid vesicles: a bioinspired strategy for rapid gelation of polysaccharide and protein hydrogels.* Biomaterials, 2001. **22**(5): p. 453-462.
27. Eiselt, P., K.Y. Lee, and D.J. Mooney, *Rigidity of two-component hydrogels prepared from alginate and poly(ethylene glycol)-diamines.* Macromolecules, 1999. **32**(17): p. 5561-5566.
28. Higham, A.K., et al., *Photo-activated ionic gelation of alginate hydrogel: real-time rheological monitoring of the two-step crosslinking mechanism.* Soft Matter, 2014. **10**(27): p. 4990-5002.
29. Biopolymers, F. *Alginates*. 2015; Available from: http://www.fmcbiopolymer.com/portals/pharm/content/docs/alginates.pdf.
30. Dennis J. McHugh. ***Chapter 2- production,properties and uses of alginates***. Production and utilization of products from commercial seaweeds [cited 2015 26/12/2015]; Available from: http://www.fao.org/docrep/x5822e/x5822e04.htm.
31. Sosnik, A., *Alginate Particles as Platform for Drug Delivery by the Oral Route: State-of-the-Art.* ISRN Pharm, 2014. **2014**: p. 926157.
32. Galant, C., et al., *Altering associations in aqueous solutions of a hydrophobically modified alginate in the presence of beta-cyclodextrin monomers.* Journal of Physical Chemistry B, 2006. **110**(1): p. 190-195.
33. Venkatesan, J., et al., *Seaweed Polysaccharide-Based Nanoparticles: Preparation and Applications for Drug Delivery.* Polymers, 2016. **8**(2).
34. Yang, S.J., et al., *Alginate-folic acid-modified chitosan nanoparticles for photodynamic detection of intestinal neoplasms.* Biomaterials, 2011. **32**(8): p. 2174-2182.
35. Bidarra, S.J., et al., *Injectable in situ crosslinkable RGD-modified alginate matrix for endothelial cells delivery.* Biomaterials, 2011. **32**(31): p. 7897-7904.
36. Yu, J.S., et al., *The use of human mesenchymal stem cells encapsulated in RGD modified alginate microspheres in the repair of myocardial infarction in the rat.* Biomaterials, 2010. **31**(27): p. 7012-7020.
37. Drury, J.L. and D.J. Mooney, *Hydrogels for tissue engineering: scaffold design variables and applications.* Biomaterials, 2003. **24**(24): p. 4337-4351.
38. Gatti, A.K., J. , *Biocompatibility and biological tests.* Integrated Biomaterials Science.
39. Kong, H.J., M.K. Smith, and D.J. Mooney, *Designing alginate hydrogels to maintain viability of immobilized cells.* Biomaterials, 2003. **24**(22): p. 4023-9.
40. Flo, T.H., et al., *Involvement of Toll-like receptor (TLR) 2 and TLR4 in cell activation by mannuronic acid polymers.* Journal of Biological Chemistry, 2002. **277**(38): p. 35489-35495.
41. Orive, G., et al., *Biocompatibility of microcapsules for cell immobilization elaborated with different type of alginates.* Biomaterials, 2002. **23**(18): p. 3825-3831.
42. Boontheekul, T., H.J. Kong, and D.J. Mooney, *Controlling alginate gel degradation utilizing partial oxidation and bimodal molecular weight distribution.* Biomaterials, 2005. **26**(15): p. 2455-2465.
43. Gombotz, W.R. and S.F. Wee, *Protein release from alginate matrices.* Advanced Drug Delivery Reviews, 2012. **64**: p. 194-205.

44. Akagi, T., et al., *Sodium alginate as an ideal submucosal injection material for endoscopic submucosal resection: preliminary experimental and clinical study.* Gastrointestinal Endoscopy, 2011. **74**(5): p. 1026-1032.
45. Kerdjoudj, H., et al., *Cellularized alginate sheets for blood vessel reconstruction.* Soft Matter, 2011. **7**(7): p. 3621-3626.
46. Park, H., et al., *Shear-reversibly Crosslinked Alginate Hydrogels for Tissue Engineering.* Macromolecular Bioscience, 2009. **9**(9): p. 895-901.
47. Fragonas, E., et al., *Articular cartilage repair in rabbits by using suspensions of allogenic chondrocytes in alginate.* Biomaterials, 2000. **21**(8): p. 795-801.
48. Boateng, J.S., et al., *Wound healing dressings and drug delivery systems: A review.* Journal of Pharmaceutical Sciences, 2008. **97**(8): p. 2892-2923.
49. Therese Andersen, P.A.-E.a.M.D., *3D Cell Culture in Alginate Hydrogels.* Microarrays 2015. **4**(2): p. 133.
50. Ghidoni, I., et al., *Alginate cell encapsulation: new advances in reproduction and cartilage regenerative medicine.* Cytotechnology, 2008. **58**(1): p. 49-56.
51. Jain, S., D.G. Hirst, and J.M. O'Sullivan, *Gold nanoparticles as novel agents for cancer therapy.* British Journal of Radiology, 2012. **85**(1010): p. 101-113.
52. Rizzo, L.Y., et al., *Recent progress in nanomedicine: therapeutic, diagnostic and theranostic applications.* Current Opinion in Biotechnology, 2013. **24**(6): p. 1159-1166.
53. Ventola, C.L., *The nanomedicine revolution: part 1: emerging concepts.* P T, 2012. **37**(9): p. 512-25.
54. Michael L. Etheridge, B., Stephen A. Campbell, PhD, Arthur G. Erdman, PhD, Christy L. Haynes, PhD, Susan M. Wolf, JD, and Jeffrey McCullough, MD, *THE BIG PICTURE ON SMALL MEDICINE: THE STATE OF NANOMEDICINE PRODUCTS APPROVED FOR USE OR IN CLINICAL TRIALS.* 2012.
55. Janz, A., et al., *Fundamental Calculations on the Surface Area Determination of Supported Gold Nanoparticles by Alkanethiol Adsorption.* Langmuir, 2010. **26**(9): p. 6783-6789.
56. Myroshnychenko, V., et al., *Plasmon Spectroscopy and Imaging of Individual Gold Nanodecahedra: A Combined Optical Microscopy, Cathodoluminescence, and Electron Energy-Loss Spectroscopy Study.* Nano Letters, 2012. **12**(8): p. 4172-4180.
57. Erickson, H.P., *Size and Shape of Protein Molecules at the Nanometer Level Determined by Sedimentation, Gel Filtration, and Electron Microscopy.* Biological Procedures Online, 2009. **11**(1): p. 32-51.
58. Thaxton, C.S., et al., *Nanoparticle-based bio-barcode assay redefines "undetectable'' PSA and biochemical recurrence after radical prostatectomy.* Proceedings of the National Academy of Sciences of the United States of America, 2009. **106**(44): p. 18437-18442.
59. Korin, N., et al., *Shear-Activated Nanotherapeutics for Drug Targeting to Obstructed Blood Vessels.* Science, 2012. **337**(6095): p. 738-742.
60. Yang, C., D. Yohan, and D.B. Chithrani, *Increase in Uptake of Peptide Modified Gold Nanoparticles (GNPs).* 2014 Ieee 14th International Conference on Nanotechnology (Ieee-Nano), 2014: p. 124-126.
61. Jia, F., et al., *Multifunctional nanoparticles for targeted delivery of immune activating and cancer therapeutic agents.* Journal of Controlled Release, 2013. **172**(3): p. 1020-1034.
62. Huang, X.H., et al., *Gold nanoparticles: interesting optical properties and recent applications in cancer diagnostic and therapy.* Nanomedicine, 2007. **2**(5): p. 681-693.
63. Vallée, F., *Nanomaterials and Nanochemistry*. 2007: Springer Berlin Heidelberg.
64. Zhang, X.Y., et al., *Fabrication and spectroscopic investigation of branched silver nanowires and nanomeshworks.* Nanoscale Res Lett, 2012. **7**(1): p. 596.

65. Nehl, C.L. and J.H. Hafner, *Shape-dependent plasmon resonances of gold nanoparticles.* Journal of Materials Chemistry, 2008. **18**(21): p. 2415-2419.
66. Dreaden, E.C., et al., *Size matters: gold nanoparticles in targeted cancer drug delivery.* Ther Deliv, 2012. **3**(4): p. 457-78.
67. Cytodiagnostics. *Gold Nanoparticle Properties*. 2016 [cited 2016 05/02/2016]; Available from: http://www.cytodiagnostics.com/store/pc/Gold-Nanoparticle-Properties-d2.htm.
68. Chen, Y.H., et al., *Methotrexate conjugated to gold nanoparticles inhibits tumor growth in a syngeneic lung tumor model.* Molecular Pharmaceutics, 2007. **4**(5): p. 713-722.
69. Pissuwan, D., T. Niidome, and M.B. Cortie, *The forthcoming applications of gold nanoparticles in drug and gene delivery systems.* Journal of Controlled Release, 2011. **149**(1): p. 65-71.
70. Horimoto, N.N., K. Imura, and H. Okamoto, *Dye fluorescence enhancement and quenching by gold nanoparticles: Direct near-field microscopic observation of shape dependence.* Chemical Physics Letters, 2008. **467**(1-3): p. 105-109.
71. Dubertret, B., M. Calame, and A.J. Libchaber, *Single-mismatch detection using gold-quenched fluorescent oligonucleotides (vol 19, pg 365, 2001).* Nature Biotechnology, 2001. **19**(7): p. 680-681.
72. Choi, Y.H., T. Kang, and L.P. Lee, *Plasmon Resonance Energy Transfer (PRET)-based Molecular Imaging of Cytochrome c in Living Cells.* Nano Letters, 2009. **9**(1): p. 85-90.
73. Pankhurst, Q.A., et al., *Applications of magnetic nanoparticles in biomedicine.* Journal of Physics D-Applied Physics, 2003. **36**(13): p. R167-R181.
74. Demas, V. and T.J. Lowery, *Magnetic resonance for in vitro medical diagnostics: superparamagnetic nanoparticle-based magnetic relaxation switches.* New Journal of Physics, 2011. **13**.
75. Krahne, R., et al., *Physical properties of elongated inorganic nanoparticles.* Physics Reports-Review Section of Physics Letters, 2011. **501**(3-5): p. 75-221.
76. Liong, M., et al., *Multifunctional inorganic nanoparticles for imaging, targeting, and drug delivery.* Acs Nano, 2008. **2**(5): p. 889-896.
77. Rao, C.N., et al., *Recent progress in the synthesis of inorganic nanoparticles.* Dalton Trans, 2012. **41**(17): p. 5089-120.
78. Chaudhuri, R.G. and S. Paria, *Core/Shell Nanoparticles: Classes, Properties, Synthesis Mechanisms, Characterization, and Applications.* Chemical Reviews, 2012. **112**(4): p. 2373-2433.
79. Cao, G., *Nanostructures & Nanomaterials: Synthesis, Properties & Applications* Imperial College Press.
80. Cushing, B.L., V.L. Kolesnichenko, and C.J. O'Connor, *Recent advances in the liquid-phase syntheses of inorganic nanoparticles.* Chemical Reviews, 2004. **104**(9): p. 3893-3946.
81. Müller, A.K.a.T.E., *Applications of Ionic Liquids in Science and Technology*. 2011.
82. Teja, A.S. and P.Y. Koh, *Synthesis, properties, and applications of magnetic iron oxide nanoparticles.* Progress in Crystal Growth and Characterization of Materials, 2009. **55**(1-2): p. 22-45.
83. Tavakoli, A., M. Sohrabi, and A. Kargari, *A review of methods for synthesis of nanostructured metals with emphasis on iron compounds.* Chemical Papers, 2007. **61**(3): p. 151-170.
84. Lee, K.T., Y.S. Jung, and S.M. Oh, *Synthesis of tin-encapsulated spherical hollow carbon for anode material in lithium secondary batteries.* Journal of the American Chemical Society, 2003. **125**(19): p. 5652-5653.
85. CENTEXBEL. *Solgel Treatment*. Solgel Technology for textile treatment [cited 14-02-2016; Available from: http://www.centexbel.be/solgel-treatment.
86. Ganguli, A.K., A. Ganguly, and S. Vaidya, *Microemulsion-based synthesis of nanocrystalline materials.* Chemical Society Reviews, 2010. **39**(2): p. 474-485.

87. Gupta, A.K. and M. Gupta, *Synthesis and surface engineering of iron oxide nanoparticles for biomedical applications.* Biomaterials, 2005. **26**(18): p. 3995-4021.
88. Malik, M.A., M.Y. Wani, and M.A. Hashim, *Microemulsion method: A novel route to synthesize organic and inorganic nanomaterials.* Arabian Journal of Chemistry, 2012. **5**(4): p. 397-417.
89. Lu, A.H., E.L. Salabas, and F. Schuth, *Magnetic nanoparticles: Synthesis, protection, functionalization, and application.* Angewandte Chemie-International Edition, 2007. **46**(8): p. 1222-1244.
90. Yin, B.S., et al., *Electrochemical synthesis of silver nanoparticles under protection of poly(N-vinylpyrrolidone).* Journal of Physical Chemistry B, 2003. **107**(34): p. 8898-8904.
91. Sajanlal, P.R., et al., *Anisotropic nanomaterials: structure, growth, assembly, and functions.* Nano Rev, 2011. **2**.
92. Lal, R.K.a.S., *Synthesis of Organic*

Nanoparticles and their

Applications in Drug Delivery

and Food Nanotechnology: A

Review. J Nanomater Mol Nanotechnol 2014, 3:4, 2014.
93. Prabhu, R.H., V.B. Patravale, and M.D. Joshi, *Polymeric nanoparticles for targeted treatment in oncology: current insights.* International Journal of Nanomedicine, 2015. **10**: p. 1001-1018.
94. Xu, W., P. Ling, and T. Zhang, *Polymeric micelles, a promising drug delivery system to enhance bioavailability of poorly water-soluble drugs.* J Drug Deliv, 2013. **2013**: p. 340315.
95. Kesharwani, P., K. Jain, and N.K. Jain, *Dendrimer as nanocarrier for drug delivery.* Progress in Polymer Science, 2014. **39**(2): p. 268-307.
96. Nanjwade, B.K., et al., *Dendrimers: Emerging polymers for drug-delivery systems.* European Journal of Pharmaceutical Sciences, 2009. **38**(3): p. 185-196.
97. Tian, W.D. and Y.Q. Ma, *Theoretical and computational studies of dendrimers as delivery vectors.* Chemical Society Reviews, 2013. **42**(2): p. 705-727.
98. Madaan, K., et al., *Dendrimers in drug delivery and targeting: Drug-dendrimer interactions and toxicity issues.* J Pharm Bioallied Sci, 2014. **6**(3): p. 139-50.
99. Stuart, M.A.C., et al., *Emerging applications of stimuli-responsive polymer materials.* Nature Materials, 2010. **9**(2): p. 101-113.
100. Cheng, R., et al., *Dual and multi-stimuli responsive polymeric nanoparticles for programmed site-specific drug delivery.* Biomaterials, 2013. **34**(14): p. 3647-3657.
101. Mura, S., J. Nicolas, and P. Couvreur, *Stimuli-responsive nanocarriers for drug delivery.* Nature Materials, 2013. **12**(11): p. 991-1003.
102. Gao, W.W., J.M. Chan, and O.C. Farokhzad, *pH-Responsive Nanoparticles for Drug Delivery.* Molecular Pharmaceutics, 2010. **7**(6): p. 1913-1920.
103. Colombo, P., et al., *Novel Platforms for Oral Drug Delivery.* Pharmaceutical Research, 2009. **26**(3): p. 601-611.
104. Lin, Y.H., et al., *Development of pH-responsive chitosan/heparin nanoparticles for stomach-specific anti-Helicobacter pylori therapy.* Biomaterials, 2009. **30**(19): p. 3332-3342.
105. Danhier, F., O. Feron, and V. Preat, *To exploit the tumor microenvironment: Passive and active tumor targeting of nanocarriers for anti-cancer drug delivery.* Journal of Controlled Release, 2010. **148**(2): p. 135-146.

106. Murphy, R.F., S. Powers, and C.R. Cantor, *Endosome Ph Measured in Single Cells by Dual Fluorescence Flow-Cytometry - Rapid Acidification of Insulin to Ph-6.* Journal of Cell Biology, 1984. **98**(5): p. 1757-1762.
107. Behr, J.P., *The proton sponge: A trick to enter cells the viruses did not exploit.* Chimia, 1997. **51**(1-2): p. 34-36.
108. Rozema, D.B., et al., *Dynamic PolyConjugates for targeted in vivo delivery of siRNA to hepatocytes.* Proceedings of the National Academy of Sciences of the United States of America, 2007. **104**(32): p. 12982-12987.
109. Aryal, S., C.M. Hu, and L. Zhang, *Polymer--cisplatin conjugate nanoparticles for acid-responsive drug delivery.* ACS Nano, 2010. **4**(1): p. 251-8.
110. Tagami, T., et al., *MRI monitoring of intratumoral drug delivery and prediction of the therapeutic effect with a multifunctional thermosensitive liposome.* Biomaterials, 2011. **32**(27): p. 6570-6578.
111. Zhang, X.Z., et al., *A novel thermo-responsive drug delivery system with positive controlled release.* International Journal of Pharmaceutics, 2002. **235**(1-2): p. 43-50.
112. Schroeder, A., et al., *Remotely activated protein-producing nanoparticles.* Nano Lett, 2012. **12**(6): p. 2685-9.
113. Xiao, Z.Y., et al., *DNA Self-Assembly of Targeted Near-Infrared-Responsive Gold Nanoparticles for Cancer Thermo-Chemotherapy.* Angewandte Chemie-International Edition, 2012. **51**(47): p. 11853-11857.
114. Ahmed, N., H. Fessi, and A. Elaissari, *Theranostic applications of nanoparticles in cancer.* Drug Discovery Today, 2012. **17**(17-18): p. 928-934.
115. Rhee, J.K., et al., *Glycol Chitosan-Based Fluorescent Theranostic Nanoagents for Cancer Therapy.* Marine Drugs, 2014. **12**(12): p. 6038-6057.
116. Liechty, W.B., et al., *Polymers for Drug Delivery Systems.* Annual Review of Chemical and Biomolecular Engineering, Vol 1, 2010. **1**: p. 149-173.
117. De Jong, W.H. and P.J. Borm, *Drug delivery and nanoparticles:applications and hazards.* Int J Nanomedicine, 2008. **3**(2): p. 133-49.
118. Fahmy, T.M., et al., *Targeted for drug delivery.* Materials Today, 2005. **8**(8): p. 18-26.
119. Bae, Y.H. and K. Park, *Targeted drug delivery to tumors: Myths, reality and possibility.* Journal of Controlled Release, 2011. **153**(3): p. 198-205.
120. Gabizon, A., et al., *Prolonged Circulation Time and Enhanced Accumulation in Malignant Exudates of Doxorubicin Encapsulated in Polyethylene-Glycol Coated Liposomes.* Cancer Research, 1994. **54**(4): p. 987-992.
121. Hans, M.L. and A.M. Lowman, *Biodegradable nanoparticles for drug delivery and targeting.* Current Opinion in Solid State & Materials Science, 2002. **6**(4): p. 319-327.
122. Anderson, J.M. and M.S. Shive, *Biodegradation and biocompatibility of PLA and PLGA microspheres.* Advanced Drug Delivery Reviews, 2012. **64**: p. 72-82.
123. Markovsky, E., et al., *Administration, distribution, metabolism and elimination of polymer therapeutics.* Journal of Controlled Release, 2012. **161**(2): p. 446-460.
124. Bertrand, N. and J.C. Leroux, *The journey of a drug-carrier in the body: an anatomo-physiological perspective.* J Control Release, 2012. **161**(2): p. 152-63.
125. Segal, E. and R. Satchi-Fainaro, *Design and development of polymer conjugates as anti-angiogenic agents.* Advanced Drug Delivery Reviews, 2009. **61**(13): p. 1159-1176.
126. Kumar, A., et al., *Innovative pharmaceutical development based on unique properties of nanoscale delivery formulation.* Nanoscale, 2013. **5**(18): p. 8307-8325.
127. Geng, Y., et al., *Shape effects of filaments versus spherical particles in flow and drug delivery.* Nature Nanotechnology, 2007. **2**(4): p. 249-255.

128. Duncan, R., *The dawning era of polymer therapeutics.* Nature Reviews Drug Discovery, 2003. **2**(5): p. 347-360.
129. Byrne, J.D., T. Betancourt, and L. Brannon-Peppas, *Active targeting schemes for nanoparticle systems in cancer therapeutics.* Advanced Drug Delivery Reviews, 2008. **60**(15): p. 1615-1626.
130. Mehvar, R., *Dextrans for targeted and sustained delivery of therapeutic and imaging agents.* Journal of Controlled Release, 2000. **69**(1): p. 1-25.
131. Bohrer, M.P., et al., *Influence of Molecular-Configuration on the Passage of Macromolecules across the Glomerular Capillary Wall.* Journal of General Physiology, 1979. **74**(5): p. 583-593.
132. Matsumura, Y. and H. Maeda, *A New Concept for Macromolecular Therapeutics in Cancer-Chemotherapy - Mechanism of Tumoritropic Accumulation of Proteins and the Antitumor Agent Smancs.* Cancer Research, 1986. **46**(12): p. 6387-6392.
133. Nune, S.K., et al., *Nanoparticles for biomedical imaging.* Expert Opinion on Drug Delivery, 2009. **6**(11): p. 1175-1194.
134. Weissleder, R., *Molecular imaging in cancer.* Science, 2006. **312**(5777): p. 1168-1171.
135. Wang, H.L., et al., *Diagnostic imaging and therapeutic application of nanoparticles targeting the liver.* Journal of Materials Chemistry B, 2015. **3**(6): p. 939-958.
136. Estelrich, J., M.J. Sanchez-Martin, and M.A. Busquets, *Nanoparticles in magnetic resonance imaging: from simple to dual contrast agents.* International Journal of Nanomedicine, 2015. **10**: p. 1727-1741.
137. Crewe, A.V., J. Wall, and J. Langmore, *Visibility of Single Atoms.* Science, 1970. **168**(3937): p. 1338-&.
138. Schmid, F.-X., *UV-visible Spectrophotometry.* John Wiley & Sons, Ltd,, 2001: p. Biological Macromolecules.
139. Lleres, D., S. Swift, and A.I. Lamond, *Detecting protein-protein interactions in vivo with FRET using multiphoton fluorescence lifetime imaging microscopy (FLIM).* Curr Protoc Cytom, 2007. **Chapter 12**: p. Unit12 10.
140. Peter TC So, C.Y.D., *Fluorescence Spectrophotometry.*
141. Teale, F.W.J., *Principles of Fluorescence Spectroscopy - Lakowicz,Jr.* Nature, 1984. **307**(5950): p. 486-486.
142. Schott, S.A.-. *Theory and Praxis of Capillary Viscometry-An Introduction.*
143. Berne, B.J. and R. Pecora, *Dynamic light scattering : with applications to chemistry, biology, and physics*. Dover ed. 2000, Mineola, N.Y.: Dover Publications. vii, 376 p.
144. Europe, N., *Zeta Potential.* p. Characterization Techniques.
145. Lyklema, J., *Fundamentals of interface and colloid science*. 2000, San Diego: Academic Press. v. <3 >.
146. Instruments, M., *ZetaSizer Nano series- Technical Note.*
147. Sze, A., et al., *Zeta-potential measurement using the Smoluchowski equation and the slope of the current-time relationship in electroosmotic flow.* Journal of Colloid and Interface Science, 2003. **261**(2): p. 402-410.
148. Technologies, C., *ARAGO Refractometer.*
149. Bandyopadhyay, S., et al., *Synthesis and in vitro cellular interactions of superparamagnetic iron nanoparticles with a crystalline gold shell.* Applied Surface Science, 2014. **316**: p. 171-178.
150. Landgraf, L., et al., *A plasma protein corona enhances the biocompatibility of Au@Fe3O4 Janus particles.* Biomaterials, 2015. **68**: p. 77-88.
151. Xanthos, D.N., et al., *Effects of peripheral inflammation on the blood-spinal cord barrier.* Molecular Pain, 2012. **8**.
152. Aldrich, S. *Fluorescein Sodium Salt*. Available from: http://www.sigmaaldrich.com/catalog/product/sial/f6377?lang=en&region=NO.

153. Mallappa, M.K., R. Kesarla, and S. Banakar, *Calcium Alginate-Neusilin US2 Nanocomposite Microbeads for Oral Sustained Drug Delivery of Poor Water Soluble Drug Aceclofenac Sodium.* J Drug Deliv, 2015. **2015**: p. 826981.
154. Charles-Navarro, D., et al., *Encapsulation and Release Characteristics of Glibenclamide Loaded Calcium-Alginate Beads.* Quimica Nova, 2010. **33**(7): p. 1435-1439.
155. Jorgensen, T.E., et al., *Influence of oligoguluronates on alginate gelation, kinetics, and polymer organization.* Biomacromolecules, 2007. **8**(8): p. 2388-2397.
156. Nilsson, S., *A Thermodynamic Analysis of Calcium Alginate Gel Formation in the Presence of Inert Electrolyte.* Biopolymers, 1992. **32**(10): p. 1311-1315.
157. Braccini, I. and S. Perez, *Molecular basis of C(2+)-induced gelation in alginates and pectins: the egg-box model revisited.* Biomacromolecules, 2001. **2**(4): p. 1089-96.
158. Blandino, A., M. Macias, and D. Cantero, *Formation of calcium alginate gel capsules: Influence of sodium alginate and CaCl2 concentration on gelation kinetics.* Journal of Bioscience and Bioengineering, 1999. **88**(6): p. 686-689.
159. Larsen, B.E., et al., *Rheological characterization of an injectable alginate gel system.* Bmc Biotechnology, 2015. **15**.
160. Hanaor, D., et al., *The effects of carboxylic acids on the aqueous dispersion and electrophoretic deposition of ZrO2.* Journal of the European Ceramic Society, 2012. **32**(1): p. 235-244.
161. Tenuta, T., et al., *Elution of Labile Fluorescent Dye from Nanoparticles during Biological Use.* Plos One, 2011. **6**(10).
162. Samanta, D., J.L. Meiser, and R.N. Zare, *Polypyrrole nanoparticles for tunable, pH-sensitive and sustained drug release.* Nanoscale, 2015. **7**(21): p. 9497-9504.
163. Swierczewska, M., S. Lee, and X.Y. Chen, *The design and application of fluorophore-gold nanoparticle activatable probes.* Physical Chemistry Chemical Physics, 2011. **13**(21): p. 9929-9941.
164. Dulkeith, E., et al., *Fluorescence quenching of dye molecules near gold nanoparticles: radiative and nonradiative effects.* Phys Rev Lett, 2002. **89**(20): p. 203002.
165. Centeno, A., F. Xie, and N. Alford, *Predicting the fluorescent enhancement rate by gold and silver nanospheres using finite-difference time-domain analysis.* Iet Nanobiotechnology, 2013. **7**(2): p. 50-58.
166. Su, Y.L., et al., *Targeted Mesoporous Iron Oxide Nanoparticles-Encapsulated Perfluorohexane and a Hydrophobic Drug for Deep Tumor Penetration and Therapy.* Theranostics, 2015. **5**(11): p. 1233-1248.
167. Sato, K., et al., *Loading and release of fluorescent dye from layer-by-layer film-coated magnetic particles in response to hydrogen peroxide.* Journal of Colloid and Interface Science, 2014. **432**: p. 92-97.

Appendix 1:

Solutions Investigated in UV-Vis Spectroscopy:

Sample name	**Volume of Alginate (µl)**	**Concentration of alginate (mg/ml)**	**Volume of CaCl2 solution (µl)**	**Concentration of Cacl2 (mg/ml)**
S**1**	2500	0.5	500	1
S2	1500	0.5	1500	1
S**3**	500	0.5	2500	1
S4	500	0.5	2500	7.35
S5	500	0.5	2500	14.7
S6	500	0.5	2500	29.4
S7	1500	0.5	1500	14.7
S8	1500	0.5	1500	29.4
S9	2500	0.5	500	14.7
S10	2500	0.5	500	29.4
S11	100	0.5	4900	29.4
S12	50	0.5	4950	29.4
S13	50	1	4950	14.7
S14	25	1	4975	1

Solutions investigated using Spectrophotometer

Sample name	Volume of Alginate (µl)	Concentration of alginate (mg/ml)	Volume of CaCl2 solution (µl)	Concentration of Cacl2 (mg/ml)
S15	100	0.25	2900	7.35
S16	100	0.75	2900	7.35
S17	100	0.25	2900	14.7
S18	100	0.75	2900	14.7
S19	100	0.25	2900	29.4
S20	100	0.75	2900	29.4
S21	100	0.50	2900	7.35
S23	100	1	2900	7.35
S24	100	0.50	2900	14.7
S25	100	1	2900	14.7
S26	100	0.5	2900	29.4
S27	100	1	2900	29.4
S29	100	8.84	2900	0.7
S30	100	8.84E-1	2900	0.7
S31	100	1.26 E-2	2900	1000
S32	100	1.26 E-3	2900	1000
S33	100	2.3	2900	1
S44	100	2.3 E-3	2900	1000
S45	100	1.3 E-1	2900	100
S46	100	2.5E-1	2900	200
S47	100	3.8E-1	2900	300
S48	100	1.26 E-4	2900	1000
S49	100	1.26 E-1	2900	1000
S50	100	3.8 E-3	2900	60

Solutions investigated by Ubbelohde Viscometer

Sample name	Volume of Alginate (µl)	Concentration of alginate (mg/ml)	Volume of CaCl2 solution (µl)	Concentration of Cacl2 (mg/ml)
S1	100	1	2900	7.35
S2	100	0.25	2900	29.4
S3	100	2.5E-1	2900	200
S4	100	3.8E-3	2900	300
S5	100	8.84E-1	2900	0.7
S6	100	8.84	2900	0.7
S7	100	1.26E-3	2900	1000
S8	100	1.26E-2	2900	1000
S9	100	2.3	2900	1
S11	100	1.26E-4	2900	1000
S12	100	3.8E-3	2900	60

Appendix 2

Refractive indices:

Water	1mg/ml Alg	29.4mg/ml Cacl2	14.7mg/ml Cacl2	0.7mg/ml Cacl2	1mg/ml Alginate+29.4Cacl2	1mg/ml alginate +14.7mg/ml	1mg/ml Alginate 7.35 cacl2
1.3301	1.3310	1.3352	1.3327	1.3314	1.3349	1.3326	1.3313

Division procedure of t/tW or tC/tA. 6 measurements were taken from Viscometer

Divided the 6 measurements by each other and their average value is used. **e.g: t/tw**

't' is the flow time of the solution having 6 measurements : t1, t2,...t6

' tW' is the flow time of water having 6 measurements : tW1, tW2...tW6

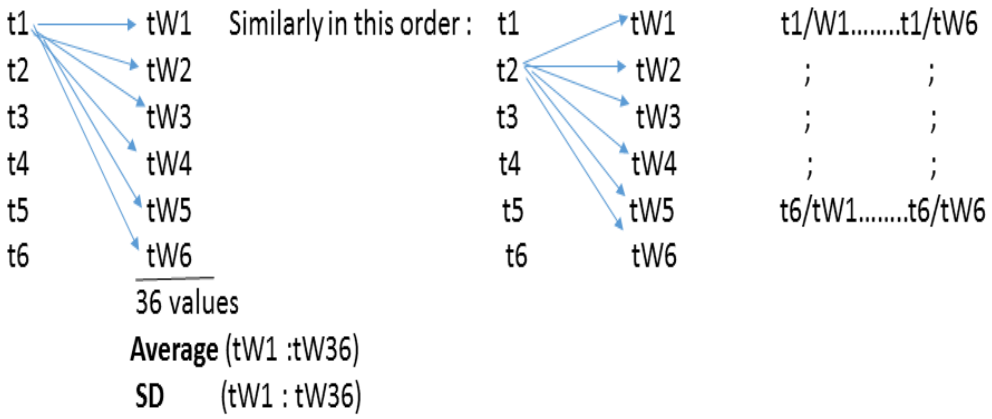

- 36 data points for each sample obtained. Their Average value is used.
- Calculated Standard Deviation

Appendix 3:

Measurement of moles of alginate and $CaCl_2$

1) **Finding moles of alginate by the following formula:**

$\frac{(volume\ ml \times concentration\ mg/ml)}{1000}$ = *x*, divide x by molecular weight of alginate i.e. 320000

$$= \frac{\boldsymbol{x}}{\mathbf{320000}}$$

2) Finding moles of $CaCl_2$ using following formula:

$$\frac{(\boldsymbol{volume\ ml \times concentration\ mg/ml})}{\mathbf{1000}} = \times$$

And divide the x value with molecular weight of **$CaCl_2$ which is 146.98**

$$= \frac{\boldsymbol{x}}{\mathbf{146.98}}$$

3) **Mole Ratio ($CaCl_2$ to alginate) =** $\frac{\boldsymbol{moles\ of\ CaCl2}}{\boldsymbol{moles\ of\ alginate}}$

Appendix 4

1) Dialysis tube experiment :

Calculation of percentage removal of dye after time:

$$\frac{\boldsymbol{Initial\ absorbance\ value(t0)\ -\ changed\ absorbance\ value(t1)}}{\boldsymbol{initial\ absorbance\ value(t0)}}\ \boldsymbol{x\ 100}$$

t0 denotes initial time , t1 denotes after dialysis time

2) Dye Loading at Fe@AU NPS :

Calculation of loading percentage at Fe@Au NPs:

Dye peak = Peak 1

Dyed Fe@Au peak = Peak 2

Calculate the area of both the peaks and divide:

$$\frac{\boldsymbol{Area\ of\ peak\ 2}}{\boldsymbol{Area\ of\ peak\ 1}} \times \boldsymbol{100}$$

3) Loading efficiencies :

a) Dyed NP + alginate curve (Without gelled dye peak)
b) Dyed NP + alginate + $CaCl_2$ curve (Gelled state peak)

Area under the curve for both ***(a)*** & ***(b)*** was calculated.

Formula:

$$\boldsymbol{Area\ of\ (a) - Area\ of\ (b) \div Area\ of\ (a)} \times 100$$

APPENDIX 5

Release behavaior in Microaggregate phase system:

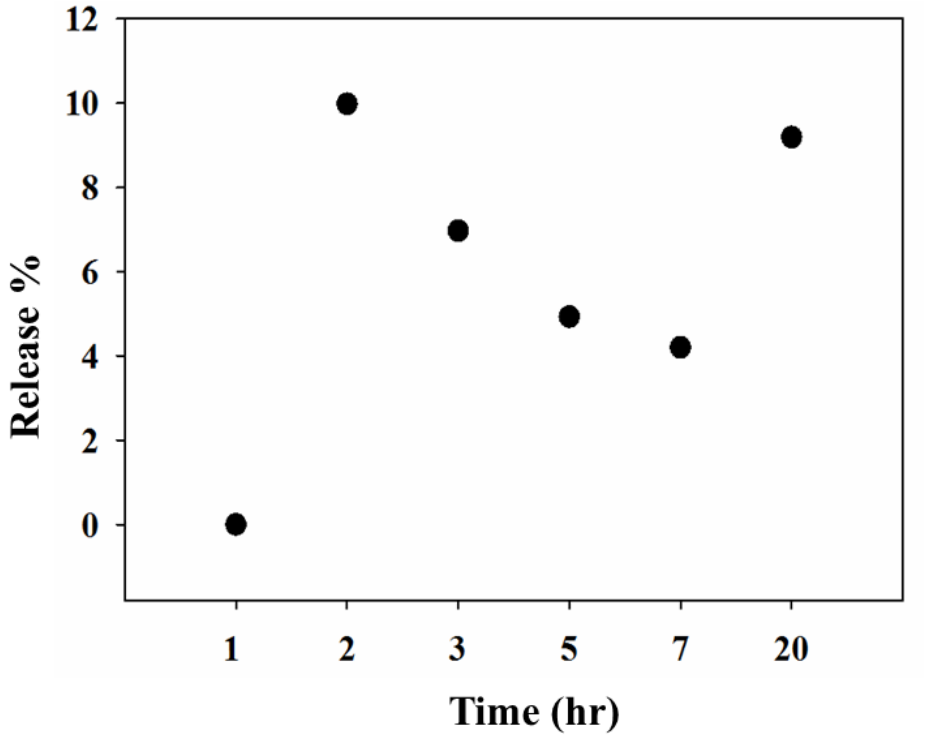

Figure 77: 1mg/ml dyed Fe@Au/alginate system at Micro aggregation phase. Release behavior

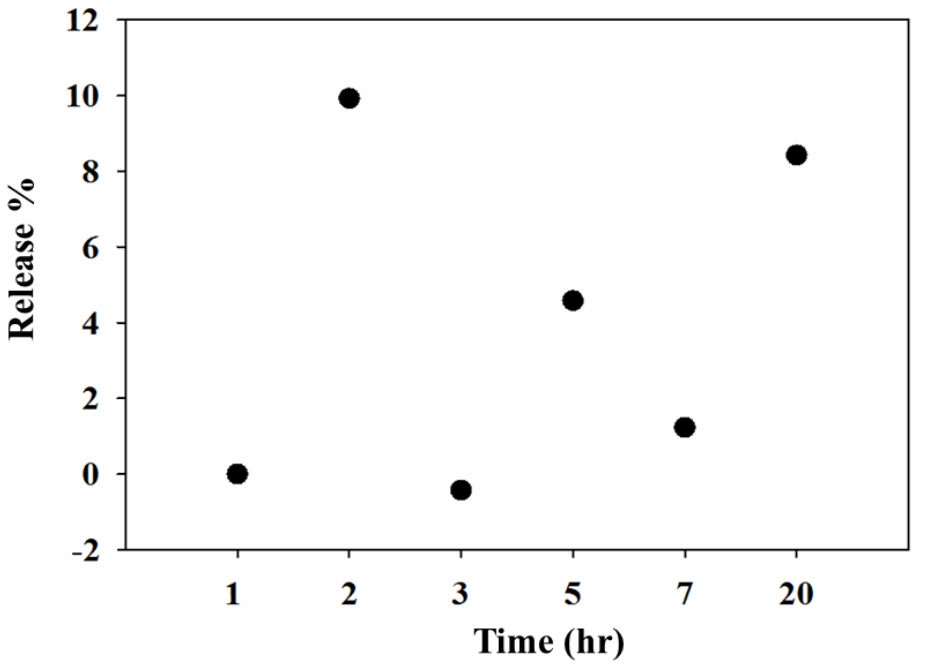

Figure 78: 2mg/ml dyed Fe@Au/alginate system at Micro-aggregation phase. Release behavior

Intermediate gelation phase Release behavior:

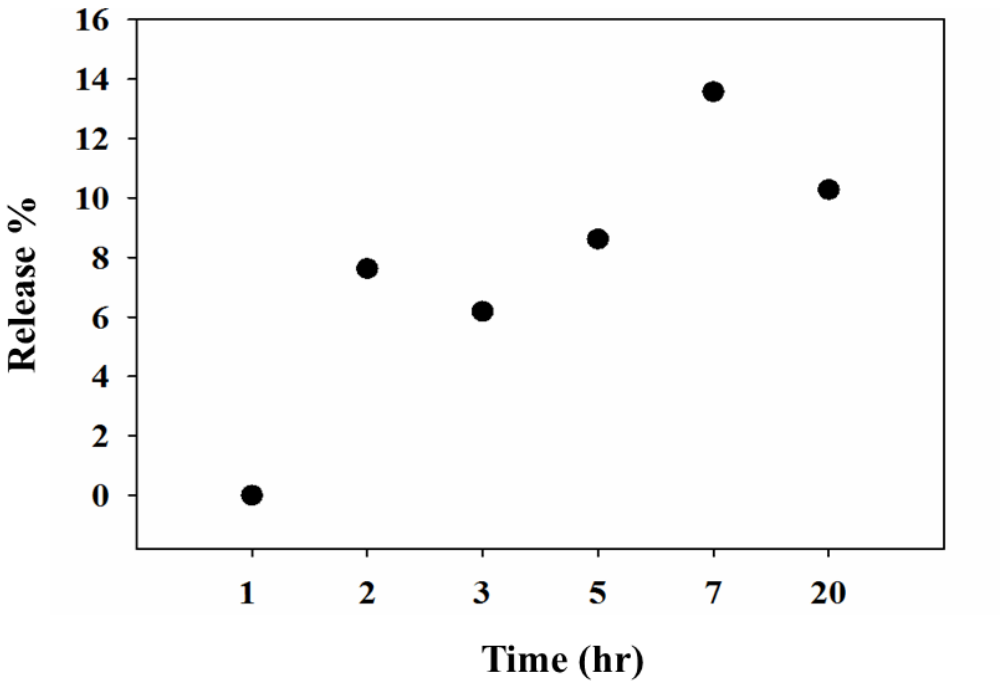

Figure 79 : 1mg/ml dyed Fe@Au/alginate system at Intermediate phase. Release behavior

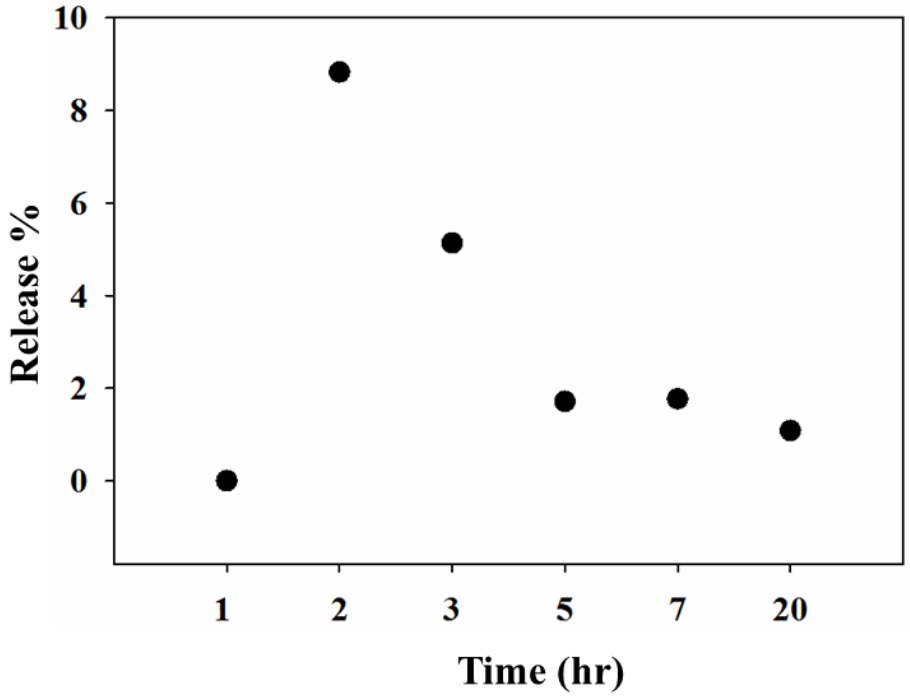

Figure 80 : 2mg/ml dyed Fe@Au/alginate system at Intermediate phase. Release behavior